

DTPH56 – 06 –T– 000023 - FINAL REPORT

EFFECT OF SURFACE PREPARATION ON RESIDUAL STRESSES IN MULTI-LAYER COATINGS AND THE CONSEQUENCES FOR DISBONDMENT FOLLOWING CONSTRUCTION DAMAGE AND EXPOSURE TO IN-SERVICE STRESS

SUBMITTED BY:

NOVA Chemicals Research & Technology Centre
2928 –16th Street NE, Calgary, Alberta, Canada, T2E 7K7

www.novachem.com

POC/PI: Dr. Bill Santos and Mr. Matthew Botros

Tel: (403) 250-0661, Fax: (403) 250-0633, Email: santosb@novachem.com

COLLABORATORS: Mr. Robert Worthingham (TransCanada Pipelines Ltd.)

&

Dr. Peter Singh (ShawCor Ltd.)

PUBLIC ABSTRACT

Underground pipelines are protected by a combination of cathodic protection and a protective coating. Multi-layer coatings offer protection against corrosion and from mechanical damage during construction or during service. Multi-layer coatings are widely used in Europe and other countries but have not been used as extensively in North America despite offering advantages in terms of combined corrosion and impact resistance.

The aim of this investigation is to improve the performance of multi-layer coatings through an understanding of the factors that affect the level of residual stress in the coating and ultimately, the consequences for coating disbondment. This report describes research to understand the effect of surface preparation and coating aging on the distribution of residual stress in plant applied HPCC and the consequences of in-service performance. Although it is known that the current manufacturing processes lead to the introduction of residual stress in multi-layer coatings, the magnitude of these stresses and the consequences for coating performance are unknown.

1.0 EXECUTIVE SUMMARY

This final report addresses Program Area 1. Coating Integrity in the PHMSA Advanced Coatings R&D Solicitation #DTPH56-06-BAA-0001.

Multi-layer coatings are widely used in Europe and other countries but have not been used as extensively in North America despite offering advantages in terms of combined corrosion and impact resistance. Part of this lack of market penetration is due to uncertainty in how these coatings will perform in service, especially whether the outer polyethylene (PE) layer will create shielding conditions if the coating disbonds. Although some information exists on the environmental aspects of multi-layer coating disbondment, from work on separate fusion bonded epoxy (FBE) and PE coatings and from work on multi-layer coatings in Europe and Canada, there is no information about the effect of residual and operating stresses on the coating and how this affects the probability or consequences of disbondment.

This investigation involves the determination of the effect of surface preparation on the distribution of residual stress in a plant applied three-layer coating and the consequences related to in-service performance. In particular, the stress-strain properties of the coatings will be compared with loads likely to occur during construction and from soil stress during service. This comparison will allow the probability of coating damage to be predicted, from which the potential for disbondment and the development of aggressive trapped water solutions can also be estimated.

This work will support a better understanding of multi-layer coating behaviour in service environments and provide direction for future development of coatings with improved performance. Together, these improvements should result in a more widespread use of these advanced pipeline coatings in North America, increasing pipeline integrity and safety. These advances will provide the basis for developing better industry standards for the manufacture of multi-layer coatings in order to provide reliable and predictable quality and coating performance.

This work brings together a team comprising a pipeline applicator (ShawCor Ltd.), a manufacturer of coating components (NOVA Chemicals Corp.), both of whom are active in developing new coating standards, a pipeline operator (TransCanada Pipelines), and a pipeline research organization (NOVA Chemicals Research & Technology Centre).

TABLE OF CONTENTS

PUBLIC ABSTRACT	2
EXECUTIVE SUMMARY	3
LIST OF TABLES	7
LIST OF FIGURES	7
LIST OF APPENDICIES	9
2.0 OBJECTIVE AND SCOPE	10
2.1 Impact on Public Safety	11
2.2 Main Deliverable and Benefit to Industry	11
3.0 INTRODUCTION	12
4.0 MULTI-LAYER COATINGS	16
4.1 Steel Pipe Surface	17
4.2 Chemical Surface Treatment	17
4.3 Multi-Layer Components	18
4.4 Multi-Layer Coating Standards	21
5.0 HIGH PERFORMANCE COMPOSITE COATING	22
5.1 HPCC Composition	23
6.0 GENERAL COATING DISBONDMENT MECHANISM	25
7.0 PREPARATION OF HPCC SAMPLES	27
7.1 Test Matrix	27
7.2 Application Process	29
7.3 Characterization of Surface Profiles Prior to Coating	29
7.4 Characterization of Coating Properties	30

8.0	RESULTS AND DISCUSSION	35
8.1	Discussion of Coating Physical Properties	35
8.2	Cathodic Disbondment Experimental Setup	40
8.2.1	Discussion of Cathodic Disbondment Tests	42
8.3	Introduction to Residual Stress Measurements	50
8.3.1	Hole-Drilling Method	51
8.3.2	Residual Stress Measurements on HPCC	54
8.4	Assessment of In-Service Coating Performance	59
8.4.1	In-Service Stresses – Laboratory Testing	59
8.4.2	In-Service Stresses – Field Experience	63
8.5	Comparison of Various Coating Property Measurements	65
9.0	CONCLUSIONS	68
10.0	RECOMMENDATIONS	73
11.0	REFERENCES	75
12.0	TABLES	80
13.0	FIGURES	95
14.0	APPENDICIES	130

LIST OF TABLES

Table 1 – Test Matrix of Tested Coating Physical Properties	80
Table 2 – Measured Profiles of Pipe Joints Subjected to Various Blast Profiles	81
Table 3 – Physical Property Data for HPCC, PE and FBE	82
Table 4 – Cathodic Disbondment Test Matrix	83
Table 5 – Cathodic Disbondment Measurements and Photographs	84
Table 6 – 28 Day HWS @ 75°C Test Results for HPCC Samples	93
Table 6a – CSA Z245.20-06 Adhesion Rating Criteria	93
Table 7 – Average Uniform Residual Stress in Tested Coatings	94
Table 8 – Average Change in Micro-strain as a Function of Depth	94
Table 9 – Average Cumulative Micro-strain Measured in Tested Coatings	94

LIST OF FIGURES

Figure 1 – ASTM Type VI Dog Bone Tensile Sample Specifications	95
Figure 2 – DSC Measurement for Standard HPCC Coating from 30" Pipe	96
Figure 3 – DSC Measurement from 1 year old HPCC Coated 36" Pipe	97
Figure 4 – DSC Measurement for a Lab Made Glass Cooled HPCC	98
Figure 5 – DSC Measurement for PE Air Cooled with Pressure	99
Figure 6 – DSC Measurement for PE Cooled at 30°C/min	100
Figure 7 – DSC Measurement for PE Standard Compression Molding	101
Figure 8 – DSC Measurement for Quench Cooled PE	102
Figure 9 – DSC Measurement for Lab-Made FBE	103
Figure 10 – Large Diameter CD Cell for Long-Term Testing	104
Figure 11 – Typical HPCC Coated Pipe Sample Section.....	104

Figure 12 – CD Experimental Configuration with Power Supply	105
Figure 13a – Picture of Cathodic Disbondment Experimental Configuration	106
Figure 13b – Cathodic Disbondment Testing for All Project Samples	107
Figure 14a - Cathodic Disbondment Experimental Setup	108
Figure 14b - Cathodic Disbondment Electrical Circuit Diagram	103
Figure 15a – Hot water Soaking Pre-treatment for CD Testing	109
Figure 15b – Hot Water Baths used for Hot Soaking Pre-treatment for CD Testing ...	109
Figure 16 – Current Response Recorded for Varying Surface Treatments during CD Tests Using 1 Year Old HPCC	110
Figure 17 – Current Response Recorded for Varying Surface Treatments during CD Tests Using New HPCC	111
Figure 18 – Current Response Recorded for Varying Surface Treatments during CD Tests Using Low Profile HPCC	112
Figure 19 – Current Response Recorded for Varying Surface Treatments during CD Tests Using High Profile HPCC	113
Figure 20 – Comparison of Current Response of No Pre-Treatment on Various HPCC Samples	114
Figure 21 – Comparison of Current Response of Hot Soaked Testing Treatment on Various HPCC Samples	115
Figure 22 – Comparison of Current Response of Impacted Surface Treatment on Various HPCC Samples	116
Figure 23 – Comparison of Current Response of Impacted and Hot Soaked Surface Treatment on Various HPCC Samples	117

Figure 24 – Comparison of CD Performance of 1 Year Old HPCC	118
Figure 25 – Comparison of CD Performance of New HPCC	119
Figure 26 – Comparison of CD Performance of Low Profile HPCC	120
Figure 27 – Comparison of CD Performance of High Profile HPCC	121
Figure 28 – Comparison of CD Performance of No Pre-Treatment Testing on Various HPCC Samples	122
Figure 29 – Comparison of Cathodic Disbondment Performance of Hot Soaked Testing Treatment on Various HPCC Samples	123
Figure 30 – Comparison of Cathodic Disbondment Performance of Impacted Surface Treatment on Various HPCC Samples	124
Figure 31 – Comparison of Cathodic Disbondment Performance of Impacted and Hot Soaked Surface Treatment on Various HPCC Samples	125
Figure 32 – Orientation of a Three-element Strain Gauge Rosette	126
Figure 33 – Residual Stress Measured on Varying Coating Surface Preparations (x-direction)	127
Figure 34 – Average Residual Stress Measured on Varying Coating Surface Preparations (y-direction)	128
Figure 35 – Relationship between Coating Disbondment of No Pre-Treatment Samples and Magnitude of Cumulative Micro-Strain	129

LIST OF APPENDICIES

APPENDIX 1 – Residual Stress Measurement Database on HPCC Samples	130
APPENDIX 2 – Shaw FBE Product Data Sheet	139
APPENDIX 3 – Shaw HPCC Product Data Sheet	141

2.0 OBJECTIVE AND SCOPE

This report is a first step in developing a research program aimed at increasing understanding of the development of coating stresses resulting from surface preparation, coating application procedures and environmental exposure conditions of the effects of these stresses on coating disbondment. Although it is known that the current manufacturing processes lead to the introduction of residual stress in multi-layer coatings, the magnitude of these stresses and the consequences for coating performance are unknown. Established techniques for determining the level of residual stress and stress-strain behavior (e.g., hole-drilling) were used to quantify the effect of different surface manufacturing processes on the mechanical properties of the coatings.

This information can then be used to optimize coating manufacturing and predict the effects of coating properties, residual stress on coating disbondment and performance in the field.

2.1 Impact on Public Safety

Public safety will be enhanced as a result of this research through the greater use of high-performance, multi-layer pipeline coatings and through improvements to the quality and performance of multi-layer, high performance composite coating (HPCC) and ultimately expanded to fusion bonded epoxy (FBE) coatings upon further research. A better understanding of the performance of these advanced coatings is expected to result in greater use of these coatings in North America and beyond.

2.2 Main Deliverable and Benefit to Industry

This research can be used to improve specifications for the manufacture and application of multi-layer coatings specifically to HPCC and ultimately upon further research expanded to include FBE. Together, these improvements should result in more widespread use of these advanced pipeline coatings in North America, increasing pipeline integrity and safety. Moreover, improvements to coating manufacturing and application procedures could be captured in various coating and pipeline standards.

3.0 INTRODUCTION

Regardless of coating system, buried pipelines are protected from external corrosion and stress corrosion cracking (SCC) by a combination of a protective coating and cathodic protection (CP). However, since coating defects and damage due to handling (wear and tear) are usually unavoidable, a full understanding of subsequent coating disbondment and its effects on pipeline integrity are essential.

Various coating systems have been used over the past 45 years and they have evolved with time and with innovation of new materials. Today, several coating systems are commonly used for pipelines: two layer polyethylene (2LPE), three layer polyethylene (3LPE), three layer polypropylene (3LPP), fusion bonded epoxy (FBE or Dual FBE), coal tar enamel (CTE), asphalt enamel and polyurethane (PUR). The different systems are specified by pipeline owners and consultants based on several factors, including short term cost, long term cost, captive usage, regional availability of the coating material, control on handling, transportation and installation of pipelines, and technical rationale [1].

3LPE coating is dominant worldwide with approximately 50% of the market share for onshore pipelines, with the exception of North America. The trend is increasing with a greater number of projects coated with 3LPE in China, India and the Middle East.

The increased acceptance of 3LPE is due to its broad operating temperature range from -45°C to +85°C and ability to withstand very rough handling and installation practices without damage to the coating. 3LPE systems consist of an epoxy primer, a grafted copolymer medium density (MDPE) adhesive to bond the epoxy primer with a high density polyethylene (HDPE) topcoat.

3LPP systems are recognized as excellent systems for offshore projects with elevated operating temperatures (0°C to +140°C) and extreme pipeline mechanical stresses. Recent projects in the North Sea, Africa, Gulf of Mexico and Arabian regions have set new standards for 3LPP coatings, which provide access to deeper gas and oil fields. 3LPP systems consist of an epoxy primer, a grafted copolymer PP adhesive to bond the epoxy primer with a PP topcoat. HDPE and PP based systems offer excellent mechanical protection and long term aging performance.

FBE is dominant in North America and in the United Kingdom. FBE has excellent adhesion to steel which provides long term corrosion resistance and protection of pipelines operating at moderate temperatures (-40°C to +85°C). FBE also provides resistance to cathodic disbondment which reduces the total cost of cathodic protection during pipeline operation. FBE is also applied as a dual layer product which provides tough physical properties that minimize damage during handling, transportation, installation and operation similar to 3LPE systems. Some pipeline owners have graduated from coal tar coating and urethane to Dual FBE due to environmental impact.

Coal tar and asphalt enamel are both still used in some countries. However, their use is declining due to health and environmental concerns.

SCC recommended practices written by the Canadian Energy Pipeline Association (CEPA), state of the art reviews (OPS/Baker report) and pipeline standards such as CSA Z662-03 (Oil and Gas Pipeline Systems) identify and require the following coating properties for pipeline applications:

1. A coating should electrically and physically isolate the environment from the pipe.
2. A coating should be compatible with CP (i.e., it should allow protection of the pipe by CP at coating defects).
3. A coating should resist under-film migration of moisture and maintain sufficient adhesion.
4. A coating should resist environmental degradation.
5. A coating should have sufficient strength to resist soil stress and mechanical damage during handling.
6. A coating should be sufficiently ductile to resist cracking.
7. Surface preparation prior to coating should reduce the steel's susceptibility to SCC.

FBE as well as multi-layer and composite coatings meet the above requirements. FBE external pipeline coatings are currently the most commonly used coatings for new pipeline construction in North America.

Introduced in the 1950's, FBE possesses a wide range of desirable attributes including high electrical resistance, low oxygen permeability, excellent adhesion and resistance to cathodic disbondment (CD), soil stress, penetration and abrasion.

However, limited high temperature performance, modest impact resistance and flexibility concerns can constrain some applications. Occurrences of blistering have been observed in the field. Environmental and physical damage (e.g. due to soil movement, the presence of rocks, or the effects of horizontal directional drilling) to the coating in service will increase the CP current requirements, but the pipe continues to be protected by CP where a loss of adhesion occurs. These field observations have led to the conclusion that the disbondment of FBE coatings does not present an integrity threat to a pipeline as long as CP is present on the line. No SCC failures have been reported for FBE coatings in over 40 years of experience.

Three-layer coatings provide excellent pipeline protection for small and large diameter pipelines with moderate operating temperatures. Some of the benefits of multi-layer coatings include the long term corrosion protection of FBE which, as mentioned previously, provides excellent adhesion to steel and protection of pipelines operating at moderate temperatures.

An added advantage of three-layer systems is the enhanced mechanical protection provided by the tough outer layer of polyethylene which protects pipelines during transportation and installation, thereby reducing costly repairs while also providing added in-ground protection against shear forces, chemicals and abrasive soil conditions that FBE-only systems can be susceptible [2-4]. By increasing the thickness of the polyethylene outer layer, multi-layer systems can provide a high level of mechanical protection across many diverse environments without requiring the use of costly select backfill. Currently, less than 15% of all pipeline coatings in North America consist of three-layer coatings. However, interest in multi-layer coatings is increasing as high performance coatings increases pipeline integrity and safety.

A typical three-layer coating comprises an inner layer of FBE, an inner adhesive or tie layer, and a low to high density polyethylene outer layer, thereby combining the advantages of epoxies and extruded polyethylene. The FBE coating is recognized for its excellent chemical resistance, good adhesion and interfacial properties. The polyethylene outer layer provides enhanced mechanical protection.

4.0 MULTI-LAYER COATINGS - GENERAL

Multi-layer coatings offer a means of countering the weakness of single layer coatings by combining materials in such a way to create a broader base of advantageous characteristics.

It is based on two principles which are: (i) optimization by combining favourable properties of different coating materials, and (ii) functional separation of performance such as corrosion protection and protection against mechanical damage.

Three layer side extruded coatings were originally developed in 1980's in Europe. The first coating of this kind did not use epoxy primer, they were designed usually as two layer systems and were susceptible to a phenomenon known as cathodic disbondment, causing runaway disbondment of the coating from the steel surface in the presence of holiday under cathodic protection conditions. This problem was corrected with the addition of an epoxy primer layer [5].

4.1 Steel Pipe Surface

The steel pipe surface must be prepared to near-white metal condition, or better, by using steel shot and steel grit, or a mixture of shot and grit. The preferred anchor pattern depth should not exceed 60 micrometers, but occasionally can be as deep as 100 micrometers, if it is compensated by higher FBE thickness.

4.2 Chemical Surface Treatment

Some pipeline owners specify use of chromate or phosphoric acid or combination of both, phosphoric acid and chromate rinse, after the abrasive steel blasting.

It is generally recognized that chromate treatments only benefit short term coating performance and do not improve long term coating performance. Phosphoric acid treatment improves long term coating performance by removing salt contamination and mildly etching the surface [6]. The benefits of using chemical surface treatment are well known in improving final properties of the product, but they can be categorized in two distinctive groups: (i) a physical benefit due to rinsing with liquid and therefore removing steel dust from the surface and (ii) a chemical benefit due to formation of crystalline network of phosphate or chromate on the surface, which activates the surface chemically and improves adhesion. The chemical benefit is especially visible in the wet testing, such as cathodic disbondment or hot water soak. The chemical surface treatment for multi-layer systems such as HPCC are similar to those used for FBE systems since the first layer applied to the pipe in HPCC is FBE.

4.3 Multi-Layer Components

Three layer pipeline coatings utilize a layer of FBE, a polyolefin outer layer and an adhesive tie layer. An initial layer of FBE is selected because of its excellent adhesion to steel and its cathodic disbondment resistance. This is achieved because of the strong polar molecular structure, which is also responsible for its high moisture absorption. FBE thickness selection and application temperature, including pipe pre-heat temperature, is the most important part of the successful three layer polyethylene final product.

Over last several years adhesive technology has developed and advanced from the early days of hot melt adhesives, based on ethylene-vinyl acetate (EVA), ethylene-acrylic acid (EAA) and ethylene-ethyl acrylate (EEA) through terpolymers to grafted polyethylenes. In most countries grafted polyethylenes are the widest used adhesives for the three layer coatings, as they provide the best overall properties for these systems. Adhesives needed for three layer coating systems are usually co-polymers of grafted polyethylene with active maleic anhydride or similar groups and are well known in most countries. Adhesives fulfill a dual purpose.

Firstly, adhesives bond chemically to the uncured groups in the epoxy powder and, providing that the FBE is not cured at the moment of contact with the adhesive, form a strong bond, which cannot be separated under a normal peel test. Secondly, the adhesive bonds physically to the outer polyethylene jacket by forming a chain entanglement between adhesive layer and polyethylene layer. There is a strong chemical affinity between the adhesive and polyethylene, i.e. over 95% of the adhesive consists of polyethylene, therefore the two layers bond together physically very well, especially in the molten state. Adhesive can be applied either by extrusion or by spray (in the powder form). Both systems differ dramatically in the property called melt flow index, which is a measure of viscosity of polyethylene, or, in other words, is a reflection of the polyethylene chains molecular mass.

The polyethylene layer is applied by side extrusion for large diameter pipe and by crosshead extrusion for smaller diameter pipes.

The polyethylene extruded on top of the adhesive can belong to several groups of density, molecular weight distribution and linearity. In the past, low density polyethylene was used extensively. Over the years, however, with new and improved polyethylene manufacturing processes, polyethylene density increased from approximately 0.925 to 0.945, as per ASTM D792, commonly used now. The respective merits of these two types of polyethylene are subject of many arguments. However, there is strong evidence that higher density polyethylene with narrower molecular weight distributions provide a much tougher coating with less mechanical damage, than its low density counterpart. There is a notable trend in the industry to switch to higher density polyethylene over last few years. Typically, however, there is a limit of density not exceeding 0.95, as above this value, polyethylene is more prone to environmental stress cracking.

The problem with extrusion on large diameter pipes with raised spiral or longitudinal welds is poor coverage of the welds especially where the profile is pronounced. There is a tendency to form voids at the weld neck area which produces pinholes and entraps water during the cooling stage. Rollers have been used to compress the molten polyethylene around the weld seam with some success in longitudinal welds. There is also a reduction of coating thickness at the top of the weld, which results in increased material usage to achieve the minimum required coating thickness. An advantage of using powder coatings is that they avoid these problems.

4.4 Multi-Layer Coating Standards

The three layer coatings are described in several national standards. The oldest and still most widely used is the German Standard DIN 30670. The French standard NFA 49-710 is also used to a lesser extent. The Canadian Standard CSA Z245.21 is gaining international acceptance over last few years, since it was first published in the early 1990's. There are significant differences between these national standards, not only in the properties, quality control, process or testing but also in the underlying philosophy of the respective standards. The biggest weakness of the DIN Standard is that it does not require the coating applicator to use an epoxy primer, it does not require cathodic disbondment testing and the specified peel adhesion value is set very low. The French NF Standard addresses many of the weaknesses of the DIN Standard and delves into a much higher level of detail in specifying the material selection and performance criteria [7].

The Canadian CSA Standard recommends that the polyethylene layer be two to three times thinner than specified in the DIN Standard. The rationale behind it is related to the fact that the Canadian Standard specifies HDPE, which is much more durable, than low density polyethylene (LDPE), used typically in Germany. Despite the lower coating thickness (1.5 mm CSA versus 3mm DIN), the resultant impact and damage resistances of both coatings are similar. In addition to these standards, there are many new three layer polyethylene standards being developed including the European EN standard, international ISO and American ASTM.

5.0 **HIGH PERFORMANCE COMPOSITE COATING**

High Performance Composite Coating (HPCC) was the multi-layer coating used for the majority of the research presented in this report. HPCC is considered an advanced composite system that represents the latest development in anti-corrosion systems. The product consists of fusion bonded epoxy, polyolefin adhesive and tough a polyethylene layer for a total coating thickness of approximately 0.8 to 1 mm. HPCC is designed to protect buried oil and gas pipelines in environments where mechanical protection, moisture and corrosion resistance and high operating performance characteristics are required.

Specifically, HPCC is a powder-coated, multi-component coating consisting of a FBE layer, a medium density polyethylene outer layer and a tie layer containing a chemically modified polyethylene adhesive. The tie layer is a blend of adhesive and FBE. This blend produces a physical interlocking of the components with no defined interface and single layer coating behaviour. The adhesive and polyethylene are similar to each other and intermingle easily to disperse any interface [8].

The composite coating components are applied in powder form using electrostatic powder coating techniques. The process provides versatility in customizing the thickness of the components of the coating system, as well as produces the composite system as described previously. A quenching process is used, minimizing the formation of voids and internal stresses.

The external polyethylene component of the composite coating does not exhibit the frozen-in-stresses that are typically seen in three layer systems. In three layer systems, the polyethylene layer is extruded and then wrapped over the pipe. This extrusion and stretching process can induce very high elongational stresses in the top layer that then become frozen in when the material is quenched. During storage and in service, these stresses can then act to produce shrinkage at the cutback area and can even result in disbondment at the FBE-steel interface. The polyethylene powder application in the Composite Coating does not involve any directional forces on the polyethylene material that would result in built-in stresses. There is no evidence that the composite coating suffers from the same disbondment failures as three layer systems that are becoming more widely used.

5.1 HPCC Composition

The thickness of the FBE component in HPCC has ranged from 100 μm to 400 μm . The FBE layer can be viewed partly as a corrosion coating and partly as an adhesion layer for the coating to steel interface. As an adhesion layer, thicknesses in the range of 50-72 μm have been used [3]. However, for a corrosion coating, the minimum thickness of 125 μm is recommended [8]. Optimization studies [9] have shown that a FBE primer thickness of 175 μm is a good base for corrosion resistance when used in conjunction with the powder polyolefin adhesive and polyethylene topcoat. Greater thicknesses of epoxy, above 250 μm , have been used in three layer coatings on some critical areas especially offshore pipelines.

Higher epoxy thickness increases the corrosion performance but this has to be balanced with increasing cost. The powdered adhesive component is used strictly as a functional “tie-layer” between the epoxy and the topcoat, and only a small amount of material is necessary to obtain good chemical bonding and melt blending of the components to form a composite material. Typically about 125-150 μm is used for the powder adhesive tailored for this technology.

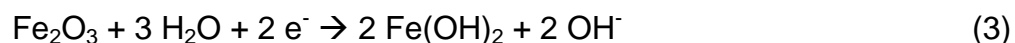
The polyethylene layer thickness is selected to withstand environmental conditions, especially impact during transportation and installation of pipe. Typical thicknesses can range from 500 μm to several millimeters. The polyethylene top layer serves several different functions: chemical and moisture barrier, mechanical protection and weather resistance.

Polyethylene thickness plays a role in overall corrosion performance of the coating; with slightly better cathodic disbondment performance with increasing thickness. However, at thicknesses above 1 mm, there is an increase in cathodic disbondment performance but it does not appear to be substantial as in the case of FBE [8]. The tendency has been to use thicknesses of up to 3 mm of LDPE, based on the supposition of fairly severe transportation and construction scenarios. However, recommendations are for lower thickness especially with medium and high density polyethylene, which have better impact resistance. Typical impact strength requirements for three-layer polyethylene are in the range of 5-7 J/mm [10].

6.0 GENERAL COATING DISBONDMENT MECHANISM

In the presence of a coating defect in a three-layer system, the controlling factors in the disbondment mechanism resemble those of FBE coatings, namely the generation and transport of hydroxyl ions to the disbonding front in parallel with the transport of cations. The main reason for differences in the disbondment mechanism of FBE and three-layer coatings pertains to the shielding of CP by the outer polyethylene layer in the three-layer coatings. Consequently, cathodic reactions that produce hydroxyl ions and increase the disbondment pH are limited and mostly restricted to the holiday site.

Widely accepted theory based on the increase in pH at the site of the holiday as a result of cathodic reactions is presented in the following mechanism [11]:



Reduction of hydrogen ions (Equation 1) quickly increases the pH and as the pH rises, the concentration of H^+ declines and the reaction becomes unfavorable. Equation 2 increases the pH through the reduction of oxygen from the solution. Intermediate species, such as peroxides, superoxides or hydroxyl radicals, have been suggested as possible agents of coating disbondment as well [6].

These species may form due to the increase in solution pH. The reduction of ferric oxide on the steel surface to form ferrous hydroxide according to Equation 3 can result in a high pH environment in the crevice area surrounding the holiday. Finally, water itself may be reduced and raise the local pH, as shown in Equation 4.

If FBE disbondment is predominantly controlled by the presence of hydroxyl ions in conjunction with an applied potential, it would appear that the disbondment area of three-layer coatings is most likely of limited size. A maximum disbondment radius of approximately 25-35 mm has been suggested by laboratory data [12]. A small disbondment would reduce the threat of SCC, since the crack length would not be able to grow sufficiently to result in fracture.

The European experience on the other hand has indicated large areas of disbondment for three-layer coatings [13]. Much of this disbondment was attributed to poor coating application. Aging of the coating, influenced by temperature, water, and/or oxygen can result in or enhance coating disbondment. However, in-service aging was found to have minimal effects on water and oxygen permeation in coating permeation tests.

7.0 PREPARATION OF HPCC SAMPLES

7.1 Test Matrix

Various physical coating properties, listed in Table 1, were measured through performing several standard and non-standard tests to help understand coating performance and relate mechanical properties to measured residual stress and disbondment data. Adhesion, impact, flexibility and cathodic disbondment (CD) tests were performed to provide insight into the propensity of coating disbondment as a function of pipe surface roughness and simulated service conditions. CD tests were only completed as single experiments and not replicated, therefore resultant trends or correlations are extrapolated from a small data set and future experimental replications are recommended to confirm the results and conclusions reported herein.

For the purpose of this study several pipeline coating samples with a three-layer composite coating, HPCC, provided by ShawCor Ltd. were used. Specifics on the preparation of the pipe surface and pipe coating samples are provided below:

- i. A three-layer coating produced by an electrostatic powder coating process for all three layers. The manufacturing process results in diffuse interlayer boundaries, minimal voids and, likely, no or low residual stresses with a total coating thickness of 0.8-1.0 mm.

-
- ii. Various surface preparation treatments are considered, with a focus of the effects of these treatments on the surface profile and residual stresses on the steel surface. Different blast media (1 low profile and 1 high profile) were used to produce different surface profiles and to impart different levels of compressive stresses to the steel. These stresses are desirable for preventing the initiation of SCC should a supportive environment develop on the pipe at a coating defect.

Following preparation of the samples, the coated samples were subjected to simulated service conditions in order to "age" or deteriorate the samples. This investigation considered different service stresses and different exposure conditions:

- i. Service stresses may consist of shear forces as a result of soil movement or impact damage during installation or excavation. High shear stresses are also experienced during horizontal directional drilling activities. Recent work on an impacted three-layer coating showed that the impact damage may extend beyond the actual impact site, thereby increasing the coating disbondment [14]. These service stresses are simulated by standard impact tests.
- ii. Coating permeation is increased by high temperature exposure to wet environments, and generally has a negative effect on coating disbondment [15].

7.2 Application Process

The application process for the composite coating consists of similar steps as required for FBE coating. The steel pipe is prepared by pre-warming in a hot water rinse, followed by abrasive blasting to achieve a near white metal finish and a specified anchor pattern. The pipe is then inspected for defects such as slivers, which can be removed by grinding. Phosphoric acid washing and deionized water rinsing is carried out followed by induction heating to the recommended powder application temperature. The three components are applied sequentially to the hot pipe in the same powder booth. After fusing and curing is completed, the pipe is cooled using both internal and external water quench. Finally, the coating is inspected, marked for identification, and tested for quality conformance.

7.3 Characterization of Surface Profiles Prior to Coating

Four Grade 483 Cat II pipe samples were prepared for coating with HPCC. Two samples were prepared with a standard blast profile using 100% GB25 grit. One was aged for a period of 1-year to study the effect of aging on HPCC. A sample was made with increased blast profile which was achieved by grit blasting with panabrasive GB18 grit. Finally, a low blast profile sample was prepared by subjecting the sample to half the blasting time and with reduced amperage (which is a measure of the amount of grit fed to the blasting units during profiling) as compared to the standard blasting procedure used with GB25.

The preparation of the low profile blasted sample to create a smoother pipe surface required several iterations before a surface roughness with a similar change in magnitude from the standard blast surface (as completed on the increased blast profile sample) could be achieved. The resultant surface roughness for each sample measured by laser profilometry is presented in Table 2. The surface roughness is reported in Rz and Peak Count. Rz refers to the average “peak to valley depth” or profile depth of the measured sample while peak count refers to the number of peaks per cm. The reported values represent an average of 4 measurements recorded in the sample region of the joint. ShawCor Ltd. was able to successfully create a significant difference in sample surface roughness when comparing the reduced profile to the increased profile pipe samples.

7.4 Characterization of Coating Properties

The HPCC coated pipe samples consisted of four joints of pipe prepared by ShawCor Ltd. Each joint was approximately 10 feet long. Each sample underwent a slightly different manufacturing condition. One sample was made with the standard blast profile, one with a low blast profile, and one with a high blast profile. The fourth sample had the standard HPCC blast profile but was manufactured and stored outdoors in Camrose, Alberta for approximately 1 year.

With these four different HPCC coating variations selected standard and non-standard tests were chosen to understand coating performance. The data provided from these tests were then used to understand if the magnitude of residual stress has an impact on HPCC coating performance.

In addition, standard and 1 year aged polymer samples were collected to understand the commercial polymer properties of plant applied HPCC. This data was compared to lab made HPCC to understand if any key coating property differences existed. These samples were also collected to analyze polymer property differences in commercial HPCC as a result of aging. In addition, 4 PE only samples prepared at different cooling rates were created in such a way to ensure that the cooling rate used for commercial polymer samples would fall within the PE sample range. This data was used to understand if the cooling rate of the coating was optimized to maximize the physical properties of the coating. Lastly, a free film FBE sample, with the same thickness as the commercial HPCC coating, was prepared to understand the performance contribution of this layer.

All four HPCC samples were sub-sectioned into appropriately sized test samples. All four pipe coated joints were cut into several 12" by 12" curved plate sub samples for standard test methods including cathodic disbondment tests. The sample plates were tested for holidays with a Tinker and Rasor Holiday detector set at 3400 V.

The specific samples tested were as follows:

1. Polymer sample from a standard HPCC coated on a 30" diameter pipe.
2. Polymer sample from a standard HPCC coated on a 36" diameter pipe. This pipe was coated with the HPCC coating 1 year before testing.
3. Lab made glass molded free film HPCC plaque sample.
4. PE compression molded sample (cooled 15°C/min).
5. PE compression molded sample that was air cooled under pressure. This was achieved by molding normally with heat and pressure on the heating cycle but turning the heating off during the cooling cycle (no forced convection cooling, ~1°C/min). The sample was then removed once the system was cooled to room temperature.
6. PE compression molded sample with a cooling rate of 30°C/min. This is achieved by molding with heat and hydraulic pressure normally during the heating cycle but using electrical controllers to control the cooling system to deliver the set cooling rate. The sample is complete once the system cools to room temperature.
7. PE compression molded sample was heated normally but cooled by submerging the sample in cold water. This is achieved by molding with heat and hydraulic pressure normally during the heating cycle then the sample is removed from the compression molder and subsequently submerged in water. The sample is complete once the system cools to room temperature.

-
8. Lab made glass molded FBE sample. FBE powder is poured into a mold with a glass bottom. The glass-powder-mold assembly is heated to properly cure the FBE. The system is allowed to cool to room temperature using natural convection.

All PE samples were made with the same proprietary grade of PE pipe coating resin. All of the above listed samples were tested for density, melt index (MI), tensile, and differential scanning calorimetry (DSC). The descriptions of these tests are described below:

- a) Density of all polymer samples was measured using a density column. Measurements are made by introducing a linear liquid density gradient inside a graduated glass cylinder. The density gradient is obtained by using a set of calibrated marker floats whose densities span the desired density range in equal intervals. Samples are placed in the column and sink until they reach a liquid level that matches their own density. The cylinder is graduated so the final position of the sample can be determined. The air temperature around the vessel must be maintained at 23°C to prevent the gradient from being affected by thermal convection. The testing conduct for this report was completed according to ASTM standard D1505-68.
- b) Melt index is a rheometric test performed on some plastics in which a measured amount of resin is melted and pushed through a defined orifice (0.0825") with a defined mass (2160g).

The amount of resin that is pushed through the orifice in a 10 minute period is defined as the melt index. This test gives a general indication of a resin's molecular weight. A higher melt index means that a larger amount of material has passed through the orifice. This usually indicates a polymer with lower molecular weight. A lower melt index usually indicates higher molecular weight polymer. MI results in this report for all resins used were tested to ASTM standard D2839.

- c) Tensile testing was conducted using ASTM standard D638 and a type IV dog bone as depicted in Figure 1. The tensile tests involved mounting of a dog bone sample into a hydraulic tensile testing machine that is able to fasten or grip both ends of the dog bone. The machine then applied a tensile load by separating at a constant velocity. Load cells in the tensile testing machine are then able to output load versus displacement data, which are then converted to a stress versus strain output.

- d) DSC was used to measure the percent crystallinity and melting points of all polymer samples. DSC is a thermoanalytical technique in which the difference in the amount of heat required to increase the temperature of a sample and a reference are measured as a function of temperature [16]. The main application of DSC is in studying phase transitions, such as melting or exothermic decompositions. These transitions involve energy changes or heat capacity changes that can be detected by DSC with great sensitivity.

As the coating sample undergoes an exothermic process like crystallization less heat is required to raise the sample temperature. By observing the difference in heat flow between the coating samples, a difference in material crystallinity can be determined.

MI, density and tensile data can be found in Table 3. The DSC data has been tabulated and presented in Figures 2-9.

8.0 RESULTS AND DISCUSSION

8.1 Discussion of Coating Physical Properties

The direct measurement of HPCC mechanical properties was not a trivial task. The difficulty with these measurements is that the thermoplastic and thermosetting microstructures of the material, and therefore mechanical properties, are defined by their molecular architectures (density, molecular weight, molecular weight distribution, co-monomer incorporation, etc.) and their heat histories.

The heat history of thermoplastic or thermoset will be affected by the specific heat transfer conditions present during the solidification of the thermoplastic or thermoset. In the case of coating a metal pipe with HPCC, the molten layers of PE, PE tie layer, and FBE on the outer surface of the pipe, cool under very specific conditions.

The molten layers release their heat to both the inside of the pipe (through the pipe wall) and to the air surrounding the external surface of the pipe. In addition, the commercial process of applying HPCC uses a water misting/deluging method to cool the coating more rapidly. Once the molten layers are solidified the microstructure of the various layers are set and define the coatings mechanical properties. Direct measurement of the mechanical properties of these solidified layers is essentially impossible because the coating is strongly bonded to the metal pipe surface and removal of the coating cannot be achieved without causing mechanical damage.

An attempt to infer the mechanical properties of HPCC using specific mechanical testing was completed. These tests were completed on various samples of HPCC, PE and FBE polymer to better understand the physical properties of these components. Through analysis of the data collected, the HPCC microstructure was inferred and therefore the mechanical properties. Six samples were tested to understand the mechanical properties of HPCC. Two samples were lab made FBE and HPCC. These samples were made by melting either all three HPCC components or just FBE alone into a thin film on a heated glass substrate. Due to the poor adhesion of glass with plastic films, the coatings are easily removed and tested mechanically.

In addition to these samples, four PE samples using a compression molding machine and different molding conditions were prepared. Specific molding conditions were chosen to provide various cooling rates that span the range of commercial HPCC coating cooling rates.

Compression molding is a process of applying heat and pressure to force polymer material to conform to the geometry of a mold. The cooling cycle is adjusted manually through a variety of methods. In the case of the samples tested, a rectangular 12" x 12" shaped mold of desired film thickness was used. Lab samples with an average HPCC coating with FBE at a thickness of 0.23 mm, PE tie layer at 0.15 mm and 0.51 mm of PE were used. The PE, FBE and HPCC samples were 0.51 mm, 0.23 mm, and 0.89 mm thick, respectively.

The tensile testing results are summarized in Table 3. A correlation between density and cooling rate is observed for the PE only samples. As the cooling rate of the molding is increased the density of the polymer is decreased. An explanation for this observation is that polymeric materials are comprised of long carbon chains that crystallize and pack together through a chain folding mechanism during solidification. During this solidification process, due to steric hindrance, the PE requires a longer time for the molecules to re-order themselves compared to other materials such as metals. The shorter the cooling period during solidification, in turn, results in less time that is available for the molecules to tightly pack, therefore, resulting in lower density polymer material.

Related to the cooling effect is the tensile yield strength of the PE samples. It is also observed in Table 3. As the density of the PE sample increases so does the yield strength of the material. Some interesting observations can be made by comparing these results to the lab made HPCC and FBE samples.

First, the overall tensile yield strength of the HPCC matches very closely to that of the air cooled PE sample. This is not surprising as the lab made HPCC was also air cooled during the molding process. Hence, both of these samples would have had slow cooling rates resulting in maximum yield strength. Secondly, both the air cooled PE and the HPCC samples have very similar yield strengths implying that the majority of the HPCC strength is derived from the PE layer and not the higher yield strength FBE material.

The elongation at yield of the HPCC, FBE and PE samples show some interesting differences. All of the PE samples have elongation at yield values in the 10-12% range depending on the cooling rate experienced by the sample. In general, the higher the cooling rate, the higher the elongation at yield. When referring to the lab made HPCC and FBE samples, their elongation at yield are surprisingly similar to each other. This would imply that the FBE component of the HPCC structure actually increases the stiffness but decreases ductility in the HPCC coating. This implication is supported by the measured ultimate elongation of all the samples. The PE samples are in the 936-1003% range compared to the 2% values measured for both the HPCC and FBE. The low values of ductility observed in the HPCC and FBE are likely a result of the FBE being a thermoset material. This material uses heat to increase the number of covalent bonds between molecules creating a ridged network of bonds that do not allow for a great deal deformation. When the stress/strain of these materials exceeds their limits, large amounts of the covalent bonds are torn apart causing a brittle catastrophic failure.

The chemical nature of the material does not allow for these bonds to be repaired through a second heating cycle.

DSC data for the lab prepared HPCC and FBE, the 4 PE samples and the two commercially prepared HPCC coatings can be found in Figures 2-9. The two commercially prepared HPCC samples were extracted from the ShawCor Ltd. plant applied HPCC coated pipes. The first sample was prepared from a recently coated 30" diameter pipe, while the second sample was taken from a one year old coated 36" diameter pipe. The DSC results for the PE samples in Figures 2-9, show that as the cooling rate of the samples is increased the percent crystallinity and enthalpy both decrease. This correlation is again, a result of the time needed for crystallization to occur during solidification. The faster the cooling rate, the less time that is available for large dense crystals to form. As a result, there is less energy stored in the material which will result in a lower enthalpy release when the material is re-melted during DSC. When comparing the DSC values of the commercial HPCC samples, taken from the 30" and 36" diameter pipes, to the four PE samples, the crystallinity and enthalpy values of the 30°C/min cooled PE sample aligns well with the commercial coatings. Meaning that, the commercially applied PE coating in the HPCC material is cooled relatively slowly. For this reason we can infer that these commercially applied HPCC coatings would likely have good overall strength. We can also infer good mechanical properties of the commercially applied HPCC based on the effect of cooling rate on tensile properties previously discussed in Table 3.

The same correlation is not apparent for the lab made glass cooled HPCC sample. The DSC numbers for this sample are difficult to decipher as the crystallinity numbers are very low despite having good tensile strength. Further work with these lab made HPCC samples must be conducted in order to ensure that they are truly a good representation of the commercial product from a microstructure/mechanical property perspective.

Finally, the DSC results for the FBE material shows that re-heating the material does not cause the FBE to melt but rather go through a softening phenomenon known as the glass transition temperature. This data establishes the point that FBE is a thermoset material which explains its lower ductility performance as compared to PE but appropriate for the purpose as a pipeline coating.

The melt index results summarized in Table 3 reveals that the PE material used was of a high melt index with a value close to 5. This is an appropriate value for a material to flow and melt sufficiently during the application phase of the coating, which would eliminate porosity and assist with adhesion to the tie layer.

8.2 Cathodic Disbondment Experimental Setup

Thirteen plates of each pipe coating variant, without holidays, were selected for various cathodic disbondment tests. The schedule for 3, 6 and 12 month tests for each coating sample is summarized in Table 4. Each plate was prepared with a 1/8" hole drilled for the cathodic connection to the test circuit.

The surface of the plate was then cleaned and a cylindrical acrylic test cell was centered on the holiday and adhered to the plate with silicon sealant. The cell diameter used was 15 cm to ensure that the size of a resultant disbondment would not be limited; hence the maximum disbondment radii possible for these tests were 7.5 cm. The coating area exposed to the water saturated commercially available screened/washed all purpose sand was $\sim 170 \text{ cm}^2$. Based on work completed by Payer on the effect of sand on coating disbondment [15], approximately 300 cm^3 of sterilized sand was added to the cell and spread out evenly. Deionized water was then added to fully saturate the sand and was periodically added throughout the duration of the tests to maintain saturation. The cells were covered with a Plexiglas[®] lid and left exposed to the atmosphere.

A graphite rod was used as the counter electrode as specified in Clause 10.8 of CSA Z245.20-06 / Z245.21-06 [10]. Pictures of the cathodic disbondment cells during setup are found in Figures 10-13b. The applied cathodic potential was controlled using a variable resistor and a power supply. The testing involved the use of a Keithley data acquisition (DAQ) unit connected to a variable resistor board, which set the potential for each cell. Current measurements were performed by measuring the potential across small 12-ohm resistors that were placed in the circuit between the counter electrode and the sample. The applied potential was periodically checked with a reference electrode and adjusted throughout the test. The potential for each cell was set to -3.0 V using a standard calomel electrode (SCE).

The variable resistor boards are powered by a 15 V power supply. Figures 14a and 14b show the experimental and electrical setup used for the cathodic disbondment tests.

Some of the coating samples were also subjected to a pretreatment process that was designed to qualitatively simulate field service. The first stage of the pretreatment process consisted of cooling the coated steel samples to -30° C for 24 hours and then impacting the coating with a 15.8 mm diameter ball according to Clause 12.12 in CSA Z245.20-06 / Z245.21-06 [10] at an energy of 3 Joules. This energy is sufficient to simulate rock damage but not sufficient to cause a holiday. The samples were examined for defects using a Tinker and Razor Holiday Detector at a high setting of 3400 V. These samples were then placed in a hot water bath at a temperature of 60° C, to simulate high operating temperature, for a period of 60 days, Figures 15a-b.

8.2.1 Discussion of Cathodic Disbondment Tests

Current measurements acquired during these experiments are summarized in Figures 16-23. The greatest average current was generally measured for the 1 year old HPCC coating as observed in Figures 16 and 20-23 and generally the lowest average currents were measured for the low profile coating sample, Figures 20-23.

Upon test completion, the saturated sand was removed from the cells and photographs were taken and are provided in Table 5. The disbondment area was measured as per Clause 12.13 in CSA Z245.20-06 [10].

Using a utility knife, radial cuts were made through the coating and the coating was chipped off between the radial cuts. There was a clear difference between the disbonded area in which the coating was removed easily and the edge of the disbondment, where the resistance to chipping became extremely high. The disbonded distance from the original holiday center along each cut was measured and these values were averaged. The resultant cathodic disbondment data is presented in Figures 24-31.

Each data point is reflective of only one experiment i.e. no repeat tests were carried out and therefore the authors believe that further testing should be performed to confirm the trends and correlations observed. In addition, the authors have observed wide ranges of uncertainty in controlled experiments with replicate tests in previous testing (at least $\pm 20\%$ for a given repeated CD disbondment result). Despite this, the project team attempted to maximize the test matrix to cover as many combinations as possible in the course of the present study and as a result subtle differences between sample performances may be difficult to discern.

When comparing Figures 24-27, the samples that underwent no pre-treatment prior to cathodic disbondment testing led to the lowest disbondment radius for each of the pipe sample treatments tested, i.e. 1 year old HPCC, “new” HPCC, Low Profile and High Profile, for 12 months which is echoed by the current measurements made in Figures 16-19.

The surface treatment which intuitively one would expect to be the most aggressive of all the scenarios tested, hot soaked + impacted, on average resulted in large disbondment radii, averaging approximately 50 mm, Figures 24-27, but only the “new” HPCC sample, as shown in Figure 25, resulted in the greatest disbondment radius for the impact + hot soak treatment. As for the hot soaked condition, two disbondments appear to have reached the cell wall, i.e. > 70 mm, Figures 24 and 27. However, the irregular trend observed in Figure 27 and the irregular disbondment shape, Table 5 (Page 91), could be due to non-uniform surface preparation and therefore should be replicated.

Figures 28-31 collect each specific surface treatment (i.e. no pre-treatment, hot soak, impacted and impacted + hot soak) and compare each of the surface sample preparations tested. On average, the low profile and “new” HPCC prepared surfaces performed the best, i.e. resulted in the lowest average disbondment radii. Also, the high blast profile prepared surface samples generally resulted in the largest average disbondment radius when compared to the standard and low blast samples with the only exception being in the no pre-treatment case, Figure 28.

When comparing these results to those in literature several insights can be made. First, it is known that surface cleanliness and roughness are the most important factors affecting coating adhesion [17]. Previous research by Varacalle et al [18], compared surface roughness produced by grit blasting steel using different blast abrasives.

The authors showed that sprayed liquid coatings on substrates roughened with steel grit (resulting in a rougher surface) exhibited superior bond strength to those prepared with conventional grit resulting in a smoother surface. The range in R_z measured by the authors, were in the range of 1.85 to 3.98 mils compared to values of 2.4 to 3.3 mils in this study, Table 2. In addition, Varacalle et al. [18] recorded peak counts, P_c , which is an indication of profile peak density, that were in the range of 100-185 peak/cm compared to a range of 20-22 peak/cm in this study. In both cases, the R_z and P_c values that were measured in this investigation were lower suggesting that, however opposite to findings by Varacalle et al, relatively minor changes in surface roughness in this study may have (recall these tests are based on single sample experiments with no replicates) influenced the bond strength between the FBE and steel substrate. This is indicated by the results attained from the CD disbondment tests, Figures 28-31, where the average disbondment radii are slightly different for the three surface roughness scenarios tested.

A possible explanation for the effect of surface roughness in this study could be attributed to the fact that HPCC coating layers are applied as powders which melt upon contact with the heated pipe. The implication here is that the melted FBE may not possess the same viscosity as other applied liquid coatings to flow into surface asperities of the substrate as easily as a liquid coating would (as in the case of a sprayed coating) which was investigated by Varacalle et al [18]. Since no liquid coatings were tested in this investigation, future testing should be completed to test this possibility.

Coating component viscosity may be responsible for the observation in this investigation of a less roughened surface leading to reduced coating disbondment as witnessed in the CD disbondment tests for what intuitively should be the most aggressive condition, impact + hot soak, Figure 31. A similar result was found with the 28-day hot water soak (HWS) adhesion test results performed at 75°C summarized in Tables 6 and 6a where the low blast treated surface possessed a superior average adhesion rating (CSA Rating: 2) than the high blast profile sample (CSA Ratings: 3). A broader spectrum of surface roughness values could be completed to determine what the optimum surface roughness is to achieve maximum FBE/substrate bond strength.

In relation to the issue of aging, the 1-year old HPCC coating generally resulted in the largest disbondment radius and greatest average measured current regardless of coating treatment or surface condition tested as seen in Figures 28-31 and Figures 20-23, respectively. Even in the case of the hot soak condition, Figure 29, the disbondment radius for the 1 year old HPCC appears to reach the cell limit, ~ 70 mm. These CD disbondment test results are supported by the 28-day HWS adhesion test results performed at 75°C summarized in Tables 6 and 6a. It is apparent that on average the 1-year coating was more easily removed with a CSA rating of 2 (less than 50% of the coating can be removed) as compared to the “new” HPCC coating with generally a CSA rating of 1 (coating cannot be removed cleanly). However, it is important to note that a CSA rating of 2 is still considered excellent as far as a new coating is concerned.

Overall, these limited results suggest that the age of the HPCC influences the amount of disbondment. The authors believe further experimental testing into the disbondment mechanism should be conducted to affirm these findings for HPCC and other multi-layer coating systems.

Reviewing the current response, Figures 16-23 and disbondment data, Figures 24-31 and comparing these results to previous literature studies several mechanistic points on the disbondment of HPCC can be claimed. Kamimura and Kishikawa [12] studied the mechanism of cathodic disbondment of a three-layer coating comprising an inner epoxy primer, a PE adhesive layer and an outer PE protective layer. The initial cause of disbondment was believed to be through reduction and dissolution of an interfacial oxide regardless of the fact that the steel surfaces were grit-blasted prior to coating.

Electrochemical reactions at the disbondment interface were supported by the transport of O_2 and H_2O through the coating and Na^+ ions and H_2O along the substrate-coating interface. Between the holiday and the perimeter of the disbonding coating, a potential gradient would exist, i.e., the location at which the disbondment is occurring. The potential at the holiday is controlled by the potentiostat or constant current device used to perform the CD test, in the case of this investigation, nominally $-3.0 V_{SCE}$. The potential will be less negative further into the crevice formed by the disbonding coating at the FBE-steel interface because of the iR drop caused by the geometrical restrictions presented by the disbondment.

The nature and rate of the cathodic electrochemical processes within the disbanded region will depend on the potential gradient within the disbondment and the rate of mass transport into and out of the crevice formed between the FBE and steel surface.

The electrochemical reduction of H_2O within the crevice will lead to an increase in pH, with the increase in the anion concentration balanced by the electrical migration of Na^+ ions into the crevice from the bulk solution. Dissolved O_2 will not diffuse into the crevice from the holiday because it is effectively consumed at the holiday itself. However, O_2 could diffuse to the disbanded interface through the coating. Water could also be transported into the disbondment crevice either via the holiday or through the coating [19]. The reduction of water will occur at a rate that is exponentially dependent on the potential ($-3.0 \text{ V}_{\text{SCE}}$ in this case) [20]. The transport of water into the crevice could become rate-limiting, especially if H_2 bubbles are generated and trapped under the disbanded coating.

In this investigation, for all the samples tested the disbondment of the HPCC occurred at the FBE/steel interface and not between the individual layers themselves. Several reasons have been previously proposed to account for the disbondment of FBE coatings, including the reduction of surface oxides, alkaline hydrolysis of the organic polymer, and the oxidative degradation of the polymer by superoxide and hydroxyl radicals formed during the reduction of O_2 [21, 22]. The epoxy-substrate bonding would be weakened by the reduction of surface oxides. The polymer would degrade by both the alkaline hydrolysis and oxidative degradation mechanisms, also seemingly weakening the epoxy-substrate interfacial bond.

The alkalinity necessary for hydrolysis could be produced by the electrochemical reduction of either O_2 or H_2O . The oxidative degradation mechanism specifically needs the presence of O_2 , and would not occur in the field under anaerobic conditions.

A potential gradient will exist away from the holiday under the disbonded coating for coatings that are shielding. The rate of OH^- generation by the reduction of O_2 and H_2O will be highest at the holiday and decrease further into the crevice. Therefore, the region of highest pH will also be at the holiday, decreasing further into the crevice. Hydroxide ions produced at the holiday will diffuse away though hindered by the presence of soil or sand, as reported by Payer [23], into the bulk solution and into the crevice to regions of lower pH. Transport of OH^- ions into the crevice can occur by diffusion and advection, the latter assisted by the enhancement of surface wetting with increasing pH [22]. The rate of oxide reduction will also diminish with distance into the crevice as the potential decreases.

O_2 will be consumed electrochemically at the holiday and will not diffuse into the crevice from the holiday, as discussed above. Nonetheless, O_2 could diffuse through the coating and could be electrochemically reduced in the crevice away from the holiday. With the possible exception of the diffusion of O_2 through the coating and reduction inside the crevice, all of the processes that lead to coating disbondment will occur at their highest rate at the holiday and diminish in rate further into the crevice.

The aforementioned studies provide mechanistic reasons for disbondment to occur, as observed in varying levels for the samples tested in this investigation as presented in Table 5 and Figures 24-31.

Considering that cathodic disbondment of FBE coatings can be attributed to the reduction of surface oxides, alkaline hydrolysis of the organic polymer, and the oxidative degradation of the polymer by superoxide and hydroxyl radicals, one could speculate that these processes were most prominent for the 1-year old HPCC and those samples subjected to hot soaking as observed in the disbondment data, Figures 24-31, due to the degradation of an already reduced FBE/substrate bond as compared to a “new” HPCC or a no pre-treatment subjected coating.

8.3 Introduction to Residual Stress Measurements

The major focus of the characterization work was on the ability to perform residual stress measurements and to determine the stress-strain properties of the HPCC coating. Residual stresses, which are internal and therefore locked-in are contained in materials that are produced by nearly every mechanical, chemical, and thermal process, either alone or in combination. As a result, most metallic or metallic oxide coatings are in a state of internal stress. The stresses in these coatings can be either compressive or tensile. It is generally recognized that compressive stresses in metallic or metallic oxide coatings are more favorable than tensile stresses because they increase resistance to fatigue failure. However, extremely high compressive stresses may cause either coating separation from the base metal or intracoating spalling. If a tensile stress leads to strain that exceeds the elastic limit of the coating, then it will cause cracking in the coating perpendicular to the direction of the stress.

Conversely, most polymeric coatings shrink during and after solidification due to chemical reaction, solvent evaporation, phase separation, or some combination thereof. Coating adhesion, however, prevents shrinkage from occurring freely; this frustration of in-plane shrinkage leads to a tensile stress in the plane of the coating [24]. At the same time, stress accumulates, which may be relaxed by processes such as molecular motion. The measured stress at any time is the result of the competition between stress buildup from frustrated shrinkage and stress relief from relaxation. Accumulation of stress is a problem because it can lead to defects such as cracks. Therefore, understanding the formation of residual stress in the coating is important to prevent the coating from peeling or cracking during service. Residual stresses have significant influence on the mechanical and physical properties of the coatings, particularly electrical resistivity, optical reflectance, fatigue and corrosion [25].

8.3.1 Hole-Drilling Method

The traditional hole-drilling method for measuring residual stresses involves drilling a shallow hole in the test specimen to a depth approximately equal to the hole diameter. Typical hole diameters range from 0.8 to 5.0 mm (0.030 – 0.200 in.). The removal of material by creating of the hole re-distributes the stresses in the material surrounding the hole. A specially designed three-element strain-gage, rosette, such as shown in Figure 32a [26], measures the associated partial strain relief.

The in-plane residual stresses that originally existed at the hole location can then be calculated from the measured strain reliefs using the method described in ASTM E 837-08 [27]. The ASTM standard also provides details of practical drilling procedures.

The partial strain relief measured by one of the three strain gages in the rosette is related to the principal in-plane residual stresses by:

$$\sigma_{max}, \sigma_{min} = \frac{\varepsilon_3 - \varepsilon_1}{4\bar{A}} \pm \frac{\sqrt{(\varepsilon_3 - \varepsilon_1)^2 + (\varepsilon_3 + \varepsilon_1 - 2\varepsilon_2)^2}}{4\bar{B}} \quad (5)$$

$$P = \frac{(\varepsilon_3 + \varepsilon_1)}{2}, Q = \frac{(\varepsilon_3 - \varepsilon_1)}{2}, T = \frac{(\varepsilon_3 + \varepsilon_1 - 2\varepsilon_2)}{2} \quad (6)$$

$$\text{where } \bar{A} = -\bar{a} \frac{(1+\nu)}{2E}, \bar{B} = \frac{-\bar{b}}{2E}$$

Where σ_{max} and σ_{min} are the maximum and minimum principal residual stresses.

\bar{A} and \bar{B} are calibration constants, the values of which depend on the specimen material properties, the rosette geometry, the hole diameter and the hole depth. ε_1 , ε_2 and ε_3 are the measured combination strains while the computed combination stresses are defined as P (isotropic (equi-biaxial) stress), Q (45° shear stress) and T (xy shear stress). \bar{a} and \bar{b} are dimensionless calibration coefficients. ASTM E 837-08 tabulates the calibration constants for the standard rosette pattern shown in Figure 32a-b [26].

The calibration coefficients \bar{A} and \bar{B} for hole drilling in a coated material differ from the standard values given in ASTM E 837-08. The actual values depend on the elastic properties of the coating and the substrate, the coating thickness, and the hole diameter and depth. These coefficients can be determined by either experimental calibrations [28] using known externally applied stresses or finite-element calculations [29].

Approximate values of \bar{A} and \bar{B} for thick coatings can be estimated from the values given in ASTM E 837-08. For this purpose, a “thick” coating is one that is at least 0.25 times the mean radius of the strain-gage rosette. For the smallest commercially available hole-drilling rosette, the mean radius is about 1.25 mm (0.050 in.). Therefore, the minimum acceptable coating thickness is about 0.3 mm (0.012 in.).

An approximate estimation of \bar{A} and \bar{B} , for a coated material is based on the observation that the hole-drilling method is most sensitive to the stresses closest to the specimen surface. Almost all of the measured strain relief is due to the stresses in the material within a depth of about 0.25 times the mean radius of the hole-drilling rosette.

Thus, a substrate coated to at least this depth is likely to behave similarly to a homogeneous thick specimen consisting only of coating material. Thus, \bar{A} and \bar{B} calibration constants for a “thick” coating are approximately equal to the ASTM tabulated values for a homogenous material with the elastic properties of the coating. For the purpose of this investigation the \bar{A} and \bar{B} constants were not changed throughout the hole-drilling process of the HPCC coating as the coating properties were generally related to the outer polyethylene layer.

8.3.2 Residual Stress Measurements on HPCC

As described in the previous section, conventional hole-drilling techniques were used to measure the amount of residual stress at different locations through the thickness of the composite coating.

The use of the hole-drilling technique to measure the residual stress in HPCC is an approach that is extremely novel since measurements on such “soft” materials are very difficult to capture. Initially, there was some concern that the residual stress fluctuations may be too large for this method and the depth at which one could obtain meaningful data was unknown. The fact that HPCC material was inherently a low modulus material complicated the measurement. The Young’s modulus and Poisson’s ratio used for the purpose of the calculations for the residual stress measurements on HPCC was equivalent to that of the PE layer, where 400 MPa and 0.4 were used, respectively.

The possibility existed that the magnitude of stress relief would be below the detection limit of the technique. This is not typically a concern with metals, metal coatings or metal oxide coatings because the magnitude to the stress relief is much higher due to the high modulus of the material.

An initial testing protocol was designed with the use of expertise supplied by an external contractor, Proto Manufacturing, which specializes in performing residual stress measurements on various materials.

Residual stress measurements were made on the four intact pipe ring sample conditions plus a “zero” stress compression molded sample used to benchmark the coating measurements on the rings.

Four intact pipe rings, each representing one of the surface preparations, (i.e. standard, low profile, high profile and standard 1-year old) were drilled in five different circumferential locations. The five test locations on the pipe ring were chosen so that they did not coincide with the spiral weld on the ring. An additional complexity was the fact that the HPCC coated pipe rings possessed a surface that was quite textured, i.e. similar to that of an orange peel. The surface texture led to initial measurements that were found to be quite variable and inconsistent when comparing measurements that were taken in a surface region defined as a “valley” versus a coating surface region defined as a “peak” (referring to the peaks and valleys of the textured coating). Valley measurements were problematic since insufficient material thickness existed to complete a full depth analysis of the coating.

Conversely, measurements made on “peak” coating regions resulted in complete and consistent measurements. Considering this observation, subsequent residual stress measurements were restricted to surface “peak” locations on the HPCC coating. Through the use of an attached micrometer to the hole drilling apparatus, an EA62RE drill bit was systematically stepped down at 0.005 inch (0.127 mm) increments to a total depth of 0.030 inches (0.762 mm), approximately 75 - 85% of the total coating thickness, in order to measure the coating strain as a function of depth.

With the ultimate depth measured being 0.030 in., the residual stress measurements that were taken were generally related to the polyethylene layer. Some venturing into the underlying tie-layer (which is essentially 95% or more polyethylene based) or even penetration into the upper limits of the FBE layer was possible, given the fact that the total HPCC coating thickness can range from 0.035 to 0.039 in. (0.89 to 1.0 mm).

The entire residual stress measurement data set attained can be found in Appendix 1, including stresses measured in the x- and y- direction (S_x and S_y), shear stress (T_{xy}), maximum and minimum principal stress (S_{max} and S_{min}), maximum shear stress and beta (angle from the gage axis to the maximum principal stress direction). A summary of this data can be found in Table 7, as an average uniform residual stress. An indication that the hole drilling technique is sensitive to changes in shear stress within the coating is based on the observation that there is a change in the beta angle as a function of depth, Appendix 1.

A plot of the data measured in the circumferential (hoop) x-direction (S_x) and tangential (longitudinal) y-direction (S_y) are presented as a function of coating depth for each pipe condition tested in Figures 33 and 34. The data used to plot these figures was extracted from Appendix 1 where the average error on each measurement is ~ 5%. According to the contractor, Proto Manufacturing, the difference between the stress values attained for each coating condition type presented in Figures 33 and 34 are considered significantly different as the measurements were highly reproducible and reliable.

It is apparent from both plots that the “zero” compression plaque which was manufactured to provide a “zero” residual stress benchmark for these measurements possessed the lowest residual stress. This result further validates the use of this technique to measure residual stress in non-metallic coatings.

The 1-year old HPCC standard surface coating sample generally resulted in the lowest residual stress as compared to the other coating surface treatments. This is not an entirely surprising observation as the polyethylene layer, which is approximately 0.8 mm thick, is a viscoelastic material, that will stress relax over time. The 1-year old HPCC pipe was stored outdoors where it would have experienced increased direct sunlight hours and summer temperatures during storage resulting in further and faster relaxation compared to the newly manufactured standard HPCC.

However, a second factor may have influenced the resultant residual stress measurements. The fact that the pipe used for the 1-year old HPCC had a larger diameter (36”) than the pipe material used to coat the other sample conditions (30”), may have changed the coating physical properties (i.e. crystallinity), even though the coating mill does attempt to control the pipe temperature by altering the pipe line speed. This is considered an important factor since the cooling rate of the pipe material during the coating application process is influenced by the geometry of the pipe, specifically the surface area, A_s , to volume, V , ratio by the following relation using the lumped capacitance method [30]:

$$\frac{T-T_{\infty}}{T_i-T_{\infty}} = \exp \left[- \left(\frac{hA_s}{\rho V c} \right) t \right] \quad (7)$$

Where T_i and T_{∞} are the initial and final temperatures, h is the heat transfer, ρ the density of the material, c is the conductivity and t , the cooling time. This relation is used to determine the time dependence of the temperature distribution within a solid during a transient process (i.e. cooling). The relation shown by Equation 7 suggests that it would take a pipe of larger diameter longer to cool. In this case, the 36" diameter pipe would take ~15% longer to cool than the 30" diameter pipe at the same line speed feed, which would theoretically allow the applied coating to solidify more slowly resulting in lower internal residual stresses. However, in reality, the difference in cooling time is expected to be less than 15% since the coating mill adjusts line speed feed rates according to pipe diameter.

Finally, the greatest residual stress values were observed on the low blast profile sample followed by the high blast and standard new HPCC samples. These results though limited do follow previous observations made by Kellner [31], who concluded that steel substrates with a ground finish leading to a considerably lower surface profile showed higher shear rates than samples with a shot blasted surface.

The use of the hole-drilling method to identify residual stresses in varying layers of coating, specifically HPCC, encountered some issues.

Specifically, there existed some non-uniformity in the thickness of the coating, therefore, not all the hole-drill measurements ventured through all three coating layers when considering the maximum drill depth was 0.0300 in (0.762 mm).

However, when reviewing the micro-strain data and calculating the change in delta micro-strain as a function of stepwise ingress into the coating, Table 8, there is a decrease in the magnitude of delta micro-strain, as you approach the hole-drill limit for some of the coating samples tested. These limited results would suggest that the drill has entered the region dominated by FBE since it is a much less ductile material than PE (i.e. FBE is not expected to relax as easily as PE). Therefore, though this trend was not observed with all the coating samples tested (for reasons mentioned), it is appropriate to consider the hole-drilling technique as a possible tool to identify residual stresses within varying layers of a coating.

8.4 Assessment of In-Service Coating Performance

8.4.1 In-Service Stresses – Laboratory Testing

The prediction of soil stress effects on coatings have been determined by burial of coating samples in large soil boxes or by more convenient laboratory methods [32] and apparatus [33]. Extensive testing has shown that the behaviour in the ground or in soil boxes is directly related to the ability of the coating to resist shear forces exerted by soil movement. This property can be directly measured by a determination of the amount or rate of shear of a sample when subjected to a known shear stress.

A buried pipeline experiences various types of soil stress and magnitude depending on burial depth, soil type, soil compaction, wet and dry, freeze and thaw cycles, seismic activity, operating temperature, pipe size, etc. These stresses can be categorized into four categories [34, 35]:

1. Axial stress due to pipeline expansion and contraction.
2. Static load due to soil and pipe weight.
3. Circumferential stress due to pipeline lateral movement at bends.
4. Stress applied in a random direction due to soil swelling and shrinkage (particularly important in clay soils during wet and dry cycles).

The magnitude of the stress on the pipeline depends on the ability of the soil to adhere to the coating and subsequently the stress transfer function between the soil and the coating. The calculation of soil forces on buried pipelines was first reported by Marston [36] in 1929 and modified by Spangler [37] in 1938. In 1986, Davis et al [38] calculated the distribution of forces generated by soil on a pipeline and compared it to a finite element analysis calculation. Essentially, when the coating strength is less than the stresses introduced by the soil, the coating will fail.

A review of the technical literature was performed to quantify in-service stresses due to soil stresses through laboratory testing of various coatings. Andrenacci et al [34] tested several multi-layer coating systems including 2LPE, 3LPE and FBE to evaluate their resistance to soil stress due to thermal changes in the pipeline with the use of a soil box apparatus. The authors concluded that the most critical properties of a coating's ability to resist soil stress are the cohesive strength and adhesive strength. Specifically, coatings with high cohesive and adhesive strengths like FBE and 3LPE showed excellent resistance to disbondment, wrinkling, tearing, shifting and abrasion while subjected to a longitudinal pipe movement test under a constant static load of 1400 kg to mimic 6 foot burial at both 23°C and 60°C. Only minor scratches in these coatings were observed after 500 cycles at 23°C and 250 cycles at 60°C. These results suggest that a PE outer layer is sufficiently adequate to withstand soil stresses when properly adhered to coating under-layers.

The viscoelastic behaviour of thick-walled MDPE pipe was also investigated by Hamouda et al. [39], to characterize the nonlinear time-dependent response of semi-crystalline thermoplastic material to creep deformation. Stress-strain behaviour was found to be high nonlinear and dependent on both strain and strain rate with resultant yield stress values slightly above 12 MPa. This value is slightly less than those recounted in this report for PE subjected to various cooling methods, Table 3, where yield strengths ranged from 18.6 MPa to 21.1 MPa.

In addition to laboratory experiments, various models have been developed to predict and quantify these sources of loads on pipe. In recent times, finite element (FE) modeling has been used to understand damage mechanisms of acrylic-steel (soft coat on hard substrate) and polyurethane-polypropylene (hard coat on soft substrate) [40]. The modeled scratch mechanisms are shown to be correlated with the material properties and the corresponding stress fields, which are related to the geometry of the scratch tip and coating thickness. The authors were able to propose a quantitative evaluation methodology by combining the ASTM scratch test method and FE modeling. These scratch results were based on materials that possessed a yield stress ratio of coating to substrate of 0.33 and 2.08, respectively [40].

In HPCC, the yield stress ratios are 0.29 (PE : FBE) and 0.24 (FBE : steel), considering the PE layer is the outer layer and FBE is considered well adhered to the steel substrate it is possible that the scratch mechanisms proposed for the acrylic-steel scenario could be loosely applied to the PE:FBE layers in HPCC. Unfortunately, the magnitude of the yield strength of acrylic and steel are ~5X the yield strength of MDPE and FBE. This is important since it was found that nearly 40 MPa of damage strength was required to cause delamination in the acrylic-steel example. It is apparent that the yield strength of both the coating and substrate play a role in scratch formation mechanisms observed in this research. A similar FE approach could be performed with multi-layer coatings like HPCC to observe potential disbondment mechanisms.

8.4.2 In-Service Stresses – Field Experience

Information from field experience was obtained from TransCanada Pipeline (TCPL) databases and construction records. In general, TCPL has not experienced any disbondment related to HPCC coating which has been tested in this report. In addition, as part of this investigation no report was discovered, as part of a literature review, that discussed field observed overall disbondment failure of FBE coating. However, information was provided by TCPL personnel that have identified disbondment failures with PE-based coatings which were likely due to soil stress related issues.

In literature, several authors [41-43] have specified some factors that lead to in-field disbondment of PE-based systems which include:

- i. Incomplete surface preparation
- ii. No or improper use of chromate pre-treatment to condition steel substrate
- iii. Use of inadequate type of FBE and/or PE
- iv. Inappropriate application temperatures for FBE
- v. Water absorption observed mainly in coating cutback areas

The CSA requirement for the peel strength value of coatings is 150N but according to data provided by ShawCor Ltd., related to one of their PE coating products, Yellow Jacket®, has shown peel strength values in the range of 400 - 500N.

Therefore, when referring to CSA Z245.20-06 / Z245.21-06 [10], Section 12.4 Peel Adhesion, a minimum peeling load of 15.3 kg (Peel Strength = 150N) to 50.9 kg (Peel Strength = 500N) is calculated. Therefore, HPCC has withstood in-service stresses imposed by soil stresses up to a peeling load of at least 50.9 kg since no reports of disbondment have been reported. It is important to note that historically peel tests on HPCC are not completed because the PE layer does not undergo sustained peel [8]. In addition, related shear tests also have shown no movement even at high temperatures. Shear failure, when it occurs, only does so within the weaker PE outer layer and only at temperatures above its softening point. Previous tensile testing performed on HPCC has resulted in no failure at the FBE/steel interface where shear strengths in excess of 17 MPa were typically obtained [8].

Field effects of pulling pipe during horizontal directional drill (HDD) pipe emplacement have been published by Polak et al [44]. The field test results of strain gage instrumented PE pipes were investigated. The test program involved 200 mm (8 inch) diameter pipe, standard dimension ratio (SDR) 17 and 150 mm (6 inch) diameter, SDR 11, high density and medium density PE pipes pulled along 90 m and 177 m bore paths. The pipes were instrumented with strain gages to measure both flexural and axial deformations with time and along the bore path. Pulling loads of 10-20 kN were used while strains of 0.2% were measured for the MDPE pipe. The authors concluded that extruded PE pipes are well suited for HDD construction since they allow reduction of the pulling loads on the pipe due to their low flexural stiffness.

The large pulling loads experienced by the extruded PE pipe during their research, would be expected to be too high for a multi-layer coated pipe system such as 3LPE since expected peel strengths are of the order of up to 500 N as reported earlier.

8.5 Comparison of Various Coating Property Measurements

In this section, the mechanical properties and coating residual stress measured in Sections 8.1 and 8.3.2 are compared with the results of the CD tests used to characterize the coatings in Section 8.2.1 and the surface profiles measured in Section 7.3.

The magnitude of the residual stress in the circumferential (hoop) direction as shown in Figure 33 and Table 7, can influence the adhesive strength of the coating by affecting how tightly bound the coating is to the substrate in a manner that can be described as an elastic band being stretched over the circumference of the pipe. Tensile stresses which are indicated by positive stress values as seen in Table 7 would be expected in such a scenario. The lowest value of S_x is found for the standard 1 year old HPCC as compared to the other pipe surface treatments.

This is an intriguing result as the CD disbondment tests for the 1 year old HPCC with no pre-treatment, Figure 28, resulted in the largest average disbondment radii. The limited data suggests that there is an inverse correlation between the circumferential residual stress, S_x , and the amount of coating disbondment.

This trend is also apparent for the balance of samples tested; Table 9, which summarizes the average cumulative micro-strain ($\mu\epsilon$), measured. When analyzing, the magnitude of total cumulative $\mu\epsilon$ at a depth of 0.0300 in., there exists a steady increase in magnitude from Standard 1-Year < Standard < High Blast Profile < Low Blast Profile. This trend is inversely related to the CD disbondment data for the no pre-treatment samples, Figure 28, where the average disbondment for a no pre-treatment surface increases from Low Blast Profile < High Blast Profile < Standard < Standard 1-Year. This relationship is presented in Figure 35.

By incorporating the effect of surface roughness to the combination of the residual stress and CD disbondment data, one notices that the smoother surface (low profile) sample results in the greatest coating bond strength. A similar trend is shown with the 28-day hot water soak (HWS) adhesion test results performed at 75°C summarized in Tables 6 and 6a where the low blast treated surface possessed a superior average adhesion rating (CSA Rating: 2) than the high blast sample (CSA Ratings: 3).

This trend is only applicable to the surface roughness extremes used in this investigation as anomalies are identified in the disbondment results attained for the standard profile (roughness) samples, Figures 28 and 29, which do not fall in between the low and high blast profile samples. Completion of future sample replicates could elucidate some of these observations and anomalies. In addition, only three surface roughness profiles were tested and further replicates would be useful to determine whether there is value in optimizing for surface roughness.

As mentioned earlier, the low profile surface disbondment result could be attributed to the fact that HPCC coating is applied as a powder and may not possess the same flow characteristics as a liquid coating when melted to fill surface asperities of the substrate as easily, where a greater number of asperities would exist on a surface with enhanced roughness. The implication of this scenario would be that more air gaps would form or remain between the coating and substrate after application on a rougher surface as compared to a smoother surface. A further investigation into the coating/substrate interface is required to confirm this scenario.

Once confirmed one would expect that the rate at which ions Na^+ , OH^- or molecules of O_2 and H_2O , as previously discussed, could penetrate into the FBE / steel substrate interface would be affected. The realization that “gaps” could exist between the FBE and steel as the steel surface roughness increases is intriguing along with the implication that lower residual stress may predict the extent of coating disbondment.

Although some work has been done on the environmental aspects of coating disbondment, little is known about the effect of residual stresses remaining from the manufacturing process. For example, there is little information on the impact of surface preparation techniques, coating application, and environmental exposure conditions on the time-dependent mechanical properties of the coating, the resulting stresses in the coating and at the interlayer and coating/steel interfaces. The presence of residual coating stresses, environmental exposure or impact damage during construction may contribute greatly to disbondment of the coating.

This investigation has resulted in the realization that further research is required to complete a greater understanding of the role of inherent and/or applied stresses on coating disbondment, ultimately, leading to identifying improved methodologies for surface preparation and coating application. This will only be achieved through the completion of a much larger experimental research program with the same strict controls that were applied in these experiments but with more attention to understanding the normal variability that is expected with coated pipe supplied by a coating mill. Only then will complete insights, when related to construction damage, into evaluating the impact damage on the long-term integrity of a pipeline be plausible.

9.0 CONCLUSIONS

This investigation has served as an initial step into determining the effect of surface preparation on the distribution of residual stress in a plant applied three-layer coating. The three-layer system used was HPPC, produced by an electrostatic powder coating process for all three layers. Various surface preparation treatments were considered, with a focus of the effects of these treatments on the surface profile and residual stresses on the steel surface. Different blast media (1 low profile, 1 standard profile, and 1 high profile) were used to produce different surface profiles and to impart different levels of compressive stresses to the steel though not quantified. Following preparation of the samples, the coated samples were subjected to simulated service conditions in order to "age" or deteriorate the samples through impacting and hot soaking the coating samples.

Information from field experience obtained from TransCanada Pipeline (TCPL) databases and construction records show that no disbondment related issues have been experienced with HPCC applied coatings. An extensive literature survey also resulted in no report of worldwide overall disbonding failure of FBE coatings. However, the literature review identified several PE (2LPE and 3LPE) coating issues that have been observed which were linked to either improper application, surface preparation issues or disbondment failures likely due to soil stress related issues [41-43].

The major focus of the characterization work was on the ability to perform residual stress measurements and to determine the stress-strain properties of the HPCC coating. The use of the hole-drilling technique to measure the residual stress in HPCC is an approach that is extremely novel and considered successful for this application. Further measurements on other coating systems specifically, PE (2LPE, 3LPE) and FBE are required to identify stresses that may be indigenous to a particular coating type which could ultimately contribute to the overall stress measured in a three-layer system like HPCC.

The following section highlights some of the findings related to specific HPCC properties and measurements made during this investigation:

A. Physical Properties of HPCC

- i. The direct measurement of mechanical properties was difficult since HPCC contains thermoplastic and thermosetting microstructures, therefore mechanical properties, are defined by their molecular architectures (density, molecular weight, molecular weight distribution, co-monomer incorporation, etc.) and their heat histories.
- ii. HPCC mechanical strength is derived from the PE layer and not the higher yield strength FBE material.
- iii. The FBE component of the HPCC structure increases the stiffness but decreases ductility in the HPCC coating with respect to the PE component.
- iv. The crystallinity and enthalpy values attained from DSC analysis of HPCC show that commercially applied HPCC coatings would likely have good overall strength since they are similar to values attained for PE cooled at 30°C/min.
- v. Commercially applied HPCC possesses good mechanical properties based on the effect of cooling rate on tensile properties as presented in Table 3.
- vi. The melt index results summarized in Table 3 shows that the PE material used in HPCC is of a high melt index with a value close to 5.

As a result, this material would be expected to flow and melt well during the application phase of the coating. This would eliminate porosity and help with adhesion to the tie layer. However, further research into how the viscosity of liquids affects the flow into surface asperities is required to compare powder vs. liquid applied coatings.

B. Effect of Surface Preparation and Aging on Cathodic Disbondment

Results provided by the CD data suggest that the adhesion of the FBE layer to the steel substrate is affected by both the surface roughness of the substrate and the age of the coating:

- i. The low profile surface tested in this investigation resulted in the least amount of disbondment, Table 5 and Figures 28-31, and provided better adhesion which was supported by the 28-day HWS adhesion tests, Table 6. A broader range of surface roughness samples could be investigated to determine an optimum surface roughness.
- ii. The 1-year old HPCC consistently resulted in the largest average disbondment radii regardless of surface treatment or profile. The speculation provided for this observation include that the material may have relaxed over the storage time exposed to various weather conditions and also that this coating was applied to a 36" diameter coating versus a 30" diameter coating.

As discussed in Section 8.3.2, the size of the pipe could influence the cooling rate and time for the coating to set (even though the coating mill attempts to compensate for this by pipe line feed speed) thereby possibly affecting the overall coating properties, though subsequent DSC measurements were not able to detect any significant differences in coating crystallinity. Further testing may be worthwhile to determine the impact of pipe diameter on coating crystallinity and disbondment.

C. Residual Stress Technique and Measurements

The residual stress measurements taken were reproducible and significant. The “zero” compression plaque provided an appropriate baseline for validating the technique. The measurements performed on the pipe coating samples were mostly related to the polyethylene layer with some venturing into the underlying tie-layer and on occasion reaching the upper limits of the FBE layer as described in Section 8.3.2.

- i. The 1-year aged standard surface coating sample resulted in the lowest residual stress as compared to the other HPCC surface treatments.
- ii. The greatest residual stress values were observed on the low blast profile sample followed by the high blast and standard new HPCC samples.

-
- iii. The hole-drilling method to identify residual stresses in the varying layers of HPCC is considered a viable option. The sensitivity of this technique towards identifying varying layers was demonstrated by the decrease in the magnitude of delta micro-strain as the drill approached the hole-drill depth limit suggesting a transition from a PE dominated tie-layer into a FBE dominated region, Table 9.

10.0 **RECOMMENDATIONS**

Based upon the findings of this study, the following is recommended:

1. An investigation to determine what amount of residual stress would be detrimental to coating adhesion (as a function of coating type for example extruded or powder applied).
2. Similar comparisons using other coating types such as 2LPE, 3LPE, FBE and PE tape to measure residual stress would be beneficial to determine the implication of residual stress on coating disbondment. In addition, residual stress measurements on other coatings i.e. PE only, FBE only should be completed to determine if the magnitude of the stress in the coating adjacent to the substrate is also a function of coating type and layer depth.
3. Determine the effect of surface roughness on residual stress in the PE layer and at what point does it become detrimental to the long term coating performance.

-
4. Perform a similar investigation with an increased number of residual stress measurements to ensure statistics are significant between varying surface preparations as a function of depth into the coating.
 5. Repeat residual stress measurements in HPCC to greater depths and with a greater sample size to confirm/validate initial results where the change in delta micro-strain occurs when approaching the FBE layer. This would address any concerns related to the use of residual stress measurements in identifying specific layers within multi-layer coatings.
 6. Using residual stress measurements to compare coating surface “peak” versus “valley” locations whereby determining the effect of varying layer thickness on the residual stress and ultimately coating disbondment.
 7. Supplementary CD test replicates are required to confirm the results in this investigation and complement research in future studies related to recommendations 1-3.

These recommendations if completed would result in a clearer understanding of the performance of multi-layer coatings and lead to some modifications to coating manufacturing and application procedures which could be captured in various international coating and pipeline standards.

11.0 REFERENCES

1. Dasgupta C., Developments in Steel Pipelines Coating Systems, Pipelines International Magazine, 2009.
2. Alexander, M., High Temperature Performance of Three-Layer Epoxy / Polyethylene Coatings, Paper No. 0575, Corrosion 91, NACE International, 1991.
3. Connelly G., Gaillard G., et al, Three Layer Pipe Coatings for Elevated Temperatures, Pipeline Industry, p. 53, 1990.
4. Gaillard G., Connelly G., three-layer Polyolefin Pipe Coatings, U.K. Corrosion, 1987.
5. Haimbl J.G., Geiser J., Polyethylene Coatings in Europe. A Look Back on 30 Years of Experience, Prevention of Pipeline Corrosion Conference, Pipeline and Gas Industry, Houston, 1995.
6. Kehr J.A., Fusion Bonded Epoxy (FBE) – A Foundation for Pipeline Corrosion Protection, NACE Press, Houston, TX., 2003.
7. Alexander, M., Three Layer Epoxy/Polyethylene Side Extruded Coatings for Pipe for High Temperature, Garneau Inc., ASME 1998.
8. Singh P., R. Worthingham, et al, New Developments in High Performance Coatings, Proc. 2005 16th International Conference on Pipeline, Paphos, Cyprus, Paper No. 55-66, 2005.
9. Shaw Pipe Protection Limited, Internal Report, RD9217.

-
10. CSA Z245.20-06 / CSA Z245.21-06, "External Fusion bonded epoxy Coating for Steel Pipe / External Polyethylene Coating for Pipe," Canadian Standard Association, Etobicoke, ON, 2006.
 11. Been J., Given R., Ikeda-Cameron K., Factors Affecting the Rate and Extent of Disbondment of FBE Coatings, Paper No. 05138, Corrosion 05, NACE International, 2005.
 12. Kamimura, T., H. Kishikawa, Mechanism of Cathodic Disbonding of Three-Layer Polyethylene-Coated Steel Pipe, Corrosion, Vol. 54, No. 12, pp. 979-987, 1998.
 13. Argent, C., D. Norman, Fitness for Purpose Issues Relating to FBE and Three Layer PE Coatings, Paper No. 05034, Corrosion 05, NACE International, 2005.
 14. Been J., R. Given, R. Worthingham, Performance Testing of a Multi-Component Powder Coating System, Proc. 2006 International Pipeline Conference, Calgary, AB, Paper No. IPC2006-10443, 2006.
 15. Payer, J.H., I. Song, B. Trautman, J.J. Perdomo, R.E. Rodriguez, K.M. Fink, Interrelationships Among Coatings, Cathodic Protection and Corrosion of Pipelines, Research Topical Symposium, Corrosion 97, NACE International, 1997.
 16. Wunderlich, B. (1990). Thermal Analysis. New York: Academic Press. pp. 137-140.
 17. Engineering and Design – Thermal Spraying: New Construction and Maintenance, Engineer Manual EM 1110-2-3401, U.S. Army Corps of Engineers, 1999.

-
18. Varacalle D.J., Guillen D.P., Effect of Grit-Blasting on Substrate Roughness and Coating Adhesion, J. Therm. Spray Tech., Vol. 15 (3), p.348, 2006.

 19. Meyer, M., X. Campagnolle, F. Coeuille, and M.E.R. Shanahan, Impact of Aging Processes on Anticorrosion Properties of Thick Polymer Coatings for Steel, "In" Corrosion Modeling for Assessing the Conditions of Oil and Gas Pipelines, (F. King and J.A. Beavers, Eds.), NACE International, Houston, TX, p. 93, 2004.

 20. Cheng, Y. and F. King, Temperature Dependent Corrosion Rates in Salt Slough Environments – Electrochemical Aspects. NOVA Research & Technology Centre Report, NRTC-01532, 2001.

 21. Gervasio, D., I. Song, and J.H. Payer, Determination of the Oxygen Reduction Products on ASTM A516 Steel during Cathodic Protection. J. Appl. Electrochem. 28, 979-992, 1998.

 22. Rodriguez, R.E., B.L. Trautman, and J.H. Payer, Influencing Factors in Cathodic Disbondment of Fusion Bonded Epoxy Coatings. Corrosion 00, NACE International, Paper No. 00166, 2000.

 23. Payer, J.H., Cathodic Disbondment of Pipeline Coatings under Realistic Field Conditions, PRCI Report, Contract PR-75-9609, 2001.

 24. Francis, L.F., Development and Measurement of Stress in Polymer Coatings, J. Mat. Sci., Vol. 37 (22), 2002.

 25. Sue J.A., Schajer G.S., "Stress Determination in Coatings", In: Totten G., Howes M., Inoue T. (Eds.), Handbook of Residual Stress and Deformation of Steel, ASM International, 2002, p. 118.

-
26. Jerry Lord, The NPL Materials Centre, BCA Structural Materials Workshop – September 2000.
 27. “Determining Residual Stresses by the Hole-Drilling Strain-Gage Method”, E 837-08 Annual Book of ASTM Standards, ASTM.
 28. “Measurements of Residual Stresses by Hole-Drilling Strain-Gage Method”, TN503-4, Measurements Group, Wendell, NC, 1993.
 29. Schajer G.S., J. Eng. Mater. Technol. (Trans. ASME), Vol. 103 (No. 2), 1981, p 157.
 30. Incropera F.P. and DeWitt D.P., Introduction to Heat Transfer, 3rd Ed., 1996, p 212.
 31. Kellner J.D., Shear Strength Testing of Pipeline Coatings and Soil Stress, Paper No. 199, Corrosion 96, NACE International, 1996.
 32. Kellner J.D., Laboratory Evaluation of the Effect of Soil Stress on Anti-Corrosion Pipeline Coatings, Paper No. 282, Corrosion 85, NACE International, 1985.
 33. Kellner, J.D., Soil Stress Apparatus, USA 4,483,197, 1984.
 34. Andrenacci A. and Wong D.T., Simulation of Coating Behaviour in Buried Service Environment, Paper No. 07020, Corrosion 07, NACE International, 2007.
 35. B.C. Yen et al., Measurements of Soil Anchoring Effect on Protector Coatings for Heated Pipelines”, Oil and Gas Journal, 1985, p 63.
 36. Marston A., The Theory of External Loads on Closed Conduits in the Light of the Latest Experiments, Proc. 9th Annual Meeting, Highway Research Board, 1929.

-
37. Spangler M.G., Horizontal Pressures on Retaining Walls Due to Concentrated Surface Loads, Iowa Eng. Exp. Sta. Bull., 140, 1938, p. 79.
 38. Davis J.A. et al, Interaction Between Soil and Coatings on Buried Pipelines, Proc. 26th Australasian Corrosion Association, Adelaide, Australia, 1986.
 39. Hamouda H.B.H et al, Viscoplastic Behaviour of a Medium Density Polyethylene (MDPE): Constitutive Equations Based on Double Nonlinear Deformation Model, Int. J. Plasticity, 23, 1307-1327, 2007.
 40. Jiang H., Browning R., et al, Mechanical Modeling of Scratch Behavior of Polymeric Coatings on Hard and Soft Substrates, Tribol. Lett., Springer Netherlands, 2009.
 41. D. Norman, Are We Protecting Our Assets?, 15th International Pipeline Protection Conference, Bedfordshire, U.K.: BHR, 2003.
 42. Nazarbeygi A.E., Moeini A.R., Three-Layer Polyethylene Coating Performance in Iran, Materials Performance, NACE International, p.32, 2009.
 43. Argent C.J. and Norman D., Three Layer Polyolefin Coatings: Fulfilling Their Potential, Corrosion 06, NACE International, Paper No. 56, 2006.
 44. Polak, M.A., Duyvestyn, G., Knight, M., "Experimental Strain Analysis for Polyethylene Pipes Installed by Horizontal Directional Drilling, Tunnelling and Underground Space Technology 19, p. 205, 2004.

12.0 TABLES

Table 1 – Test Matrix of Tested Coating Physical Properties

Sample	Standard and Non-Standard Tests							
	Impact Test	Adhesion	Flexibility	Hole Drilling Residual Stress	CD Disbondment 3.0V CP, Saturated Sandy Soil - 3, 6, & 12months			
					No pre-treatment	Impacted	Hot soaked	Both impacted & Hot soaked
Standard HPCC	X	X	X	X	X	X	X	X
Low Amperage Blast Profile HPCC	X	X	X	X	X	X	X	X
High Blast Profile HPCC	X	X	X	X	X	X	X	X
1 year Outdoor Aged HPCC	X	X	X	X	X	X	X	X

Table 2 - Measured Profiles of Pipe Joints Subjected to Various Blast Profiles

Sample ID	Profile	Conditions	Rz (mils)	Peak Count (peak/cm)
US DOT – 001	Standard	Standard	2.8	21
US DOT - 002	Reduced	Unit #1 Only	2.4	20
US DOT -003	Increased	½ Drum of GB18 added to Unit #2	3.3	22

Table 3 – Physical Property Data for HPCC, PE and FBE

Sample	Density (g/cm ³)	Tensile Yield Strength (MPa)	Std Dev of Tensile Strength (MPa)	Elongation at Yield (%)	Std Dev Elongation at Yield (MPa)	Melt Index (g/10 min)	Ultimate Tensile Strength (MPa)	Std Dev of Ultimate Tensile Strength (MPa)	Ultimate Elongation (%)	Std Dev of Ultimate Elongation (%)
Fusion Bond Epoxy	>1	64.9	5	2	0	N/A	64.9	5	2	0
Glass Cooled HPCC	1.0692	23.7	5.9	2	0	N/A	23.7	5.9	2	0
PE Air Cooled with Pressure (~1°C/min)	0.9544	21.1	0.4	10	0	4.97	23.2	0.7	936	44
PE 30°C/min cooling with pressure	0.9509	18.6	0.1	10	1	4.59	26	1	1003	72
PE Standard Compression Molding (15°C/min)	0.9478	17.7	0.1	12	1	4.91	26	2	970	66
PE Quench Cool	0.9457	15.6	0.2	12	1	4.88	26.7	1.5	961	75

Table 4 – Cathodic Disbondment Testing Schedule

Station 1	Station 2	Station 3	Station 4	Station 5	Station 6	Station 7	Station 8	Station 9	Station 10		
12 months IM	6 month IM	3 months IM	12 months	6 month	3 month	1 month	3 month	6 month	12 month		
		3 months IM & HS			6 month IM & HS	3 month HS				1 month	3 month IM
						6 month HS				1 month CSA	
	6 month HS	6 month IM & HS		1 month CSA			3 month HS			6 month HS	
				6 month IM & HS	1 month CSA						
					6 month HS	1 month CSA					
Station 11	Station 12	Station 13	Station 14	Station 15	Station 16	Station 17	Station 18	Station 19	Station 20		
12 month HS	6 month IM	12 month IM	12 month IM & HS	3 month	3 month	6 month	6 month IM	6 month	6 month IM		
				3 month IM	3 month IM						
	6 month IM & HS			3 months IM & HS	3 months IM & HS	6 month HS	6 month IM & HS			6 month HS	6 month IM & HS
				3 month HS	3 month HS						
Station 21	Station 22	Station 23	Station 24	Station 25	Station 26	Station 27	Station 28	Station 29	Station 30		
12 month HS	12 month IM & HS	12 month	12 month IM	12 month HS	12 month IM & HS	12 month	12 month IM	12 month HS	12 month IM & HS		
Old HPCC											
New HPCC											
High Profile											
Low Profile											

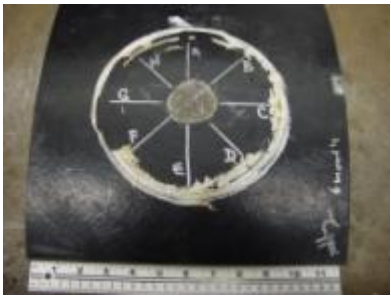
Table 5 – Cathodic Disbondment Measurements and Photographs

Sample Name	Cathodic Disbondment Locations								Images
	A	B	C	D	E	F	G	H	
1 year old HPCC, 1 month	17	16	17.5	18	18.5	17	15	18	
1 year old HPCC 3months	22	20	20	19	21.5	23	22	23	
1 year old HPCC, Impacted 3 months	19	20	20	20	20	20	20	20	
1 year old HPCC, 6 months	37	35	34	35	35	37	37	40	
1 year old HPCC impacted, 6 months	31	32	32	31	32	32	30.5	30	

Sample	Cathodic Disbondment Locations								
	A	B	C	D	E	F	G	H	
New HPCC 1 month	6	6	5	6	7	5	5	5	
New HPCC 3 months	19	16	21	22	22.5	21	19	19	
New HPCC, 3 months impacted	22	24	20	21	23	23	24	22	
New HPCC, 6 months	31	26	27	26	29	27	29	29	
New HPCC Impacted 6 months	34	28	29	28	26	30	32	34	

Sample	Cathodic Disbondment Locations								
	A	B	C	D	E	F	G	H	
#3, 3 months	22	23	23	21	21	23	21	22	
#2, 3 month	12	15	20	18	14	15	15	11	
1 yr old HPCC Hot soaked 3 months	70	82	75	67	64	55	54	54	
1 yr old HPCC HS + Impacted 3 months	45	35	33	33	54	60	63	62	
#3 Impacted 3 months	24	24	26	25	26	23	24	23	

Sample	Cathodic Disbondment Locations								
	A	B	C	D	E	F	G	H	
#3 3 months	22	17	10	11	24	29	31	29	

#2 6 months	24	28	30	25	21	22	20	19	
#3 Impacted 6 months	21	24	24	25	25	23	23	21	
#2 Impacted 6 months	17	19	17	15	15	20	19	18	
#2 3 months (supposed to be 1 month)	16	19	20	20	19	19	22	21	

Sample	Cathodic Disbondment Locations								
	A	B	C	D	E	F	G	H	
1 year old HPCC HS 6 months (turned into 3 months)	34	35	40	42	36	34	32	33	
1 year old HPCC, HS and Impacted 6 months (turned into 3 months)	32	28	29	26	32	28	31	39	
#3 1 month	12	11	11	10	8	8	10	11	
#2 1 month	12	12	11	11	9	9	10	10	
New HPCC HS and Impacted 3 month	20	23	21	19	20	20	19	21	

Sample	Cathodic Disbondment Locations								
	A	B	C	D	E	F	G	H	
1 year old HPCC 12 month	44	41	51	54	51	38	37	38	
1 year old HPCC Impacted 12 month	51	47	40	39	66	59	57	54	
Low profile #2 Hot soaked 3 month	27	25	23	25	28	28	29	28	
1 year old HPCC HS and Impacted 12 months	76	78	45	3	38	53	63	78	
1 year old HPCC Hot soaked 12 months	63	74	74	70	64	66	68	71	

Sample	Cathodic Disbondment Locations								
	A	B	C	D	E	F	G	H	
#3 HS and Impacted 3 months	19	19	19	17	20	23	67	61	
New HPCC Impacted 12 months	25	27	29	35	40	43	37	29	
New HPCC 12 months	32	30	23	24	28	30	27	30	
Low profile #2 HS and Impacted 3 month	20	20	20	20	19	20	19	19	
New HPCC HS and Impacted 6 month	47	45	37	34	46	44	45	38	

Sample	Cathodic Disbondment Locations								
	A	B	C	D	E	F	G	H	
New HPCC Hot soaked 6 month	46	31	32	34	22	22	29	36	
New HPCC Hot soaked 3 month	17	18	18	20	18	15	16	17	
#3 Hot soaked 3 month	75	76	58	80	26	57	60	32	
#3 12 Month	21	20	24	28	31	27	20	21	
#2 Impacted 12 month	30	32	35	40	38	36	18	17	

Sample	Cathodic Disbondment Locations								
	A	B	C	D	E	F	G	H	
#3 HS and Impacted 6 month	46	42	56	44	46	36	40	40	
#2 12 month	22	25	26	24	22	19	20	19	
#3 Impacted 12 month	40	36	35	36	45	50	43	40	
#2 HS and Impacted 6 month	27	26	30	27	19	17	19	21	

Table 6 – 28 day HWS @ 75°C Test Results for HPCC Samples

Sample #	CSA Acceptance Criteria	Standard Surface (1 Year)	Standard Surface (New)	Low Blast	High Blast
1	Rating of 1-3	Rating of 2	Rating of 1	Rating of 2	Rating of 2
2		Rating of 2	Rating of 2	Rating of 2	Rating of 3
3		Rating of 2	Rating of 1	Rating of 2	Rating of 3
4		Rating of 2			

Table 6a – CSA Z245.20-06 Adhesion Rating Criteria

CSA Rating	Description
1	Coating cannot be removed cleanly
2	Less than 50% of the coating can be removed
3	More than 50% of the coating can be removed, but the coating demonstrates a definite resistance to the levering action
4	The coating can be easily removed in strips or large chips
5	The coating can be completely removed as a single piece.

Table 7 – Average Uniform Residual Stress in Tested Coatings

Sample	S _x (ksi)	S _y (ksi)	T _{xy} (ksi)	S _{max} (ksi)
Standard	+0.218 ±0.063	+0.075 ±0.026	-0.248 ±0.010	+0.425 ±0.093
Low Blast	+0.461 ±0.047	+0.334 ±0.081	-0.034 ±0.004	+0.502 ±0.032
High Blast	+0.286 ±0.046	+0.266 ±0.064	-0.075 ±0.017	+0.413 ±0.033
Standard - 1 year	+0.160 ±0.025	+0.163 ±0.092	+0.054 ±0.055	+0.225 ±0.034
"Zero" Compression	+0.069 ±0.006	-0.020 ±0.063	-0.018 ±0.046	+0.111 ±0.038

Table 8 – Average Change in Micro-strain as a Function of Depth

COATING REGION	STANDARD SURFACE	LOW BLAST PROFILE	HIGH BLAST PROFILE	STANDARD SURFACE - 1 YR	"ZERO" COMPRESSION PLAQUE
0.0000 - 0.0050	-103	-55	-102	-36	-9
0.0005 - 0.0100	-77	-194	-187	-49	-17
0.0100 - 0.0150	-170	-181	-165	-99	-2
0.0150 - 0.0200	-42	-177	-128	-75	-32
0.0200 - 0.0250	-30	-137	-91	-21	-12
0.0250 - 0.0300	-45	-108	-12	-51	-9

Table 9 – Average Cumulative Micro-strain Measured in Tested Coatings

Depth (in.)	STANDARD SURFACE	LOW BLAST PROFILE	HIGH BLAST PROFILE	STANDARD SURFACE - 1 YR	"ZERO" COMPRESSION PLAQUE
0.0000	0	0	0	0	0
0.0050	-103	-55	-102	-36	-9
0.0100	-180	-249	-289	-85	-26
0.0150	-350	-430	-454	-184	-28
0.0200	-392	-607	-582	-259	-60
0.0250	-422	-744	-673	-280	-72
0.0300	-467	-852	-685	-331	-81

13.0 FIGURES

Figure 1 – ASTM Type VI Dog Bone Tensile Sample Specifications

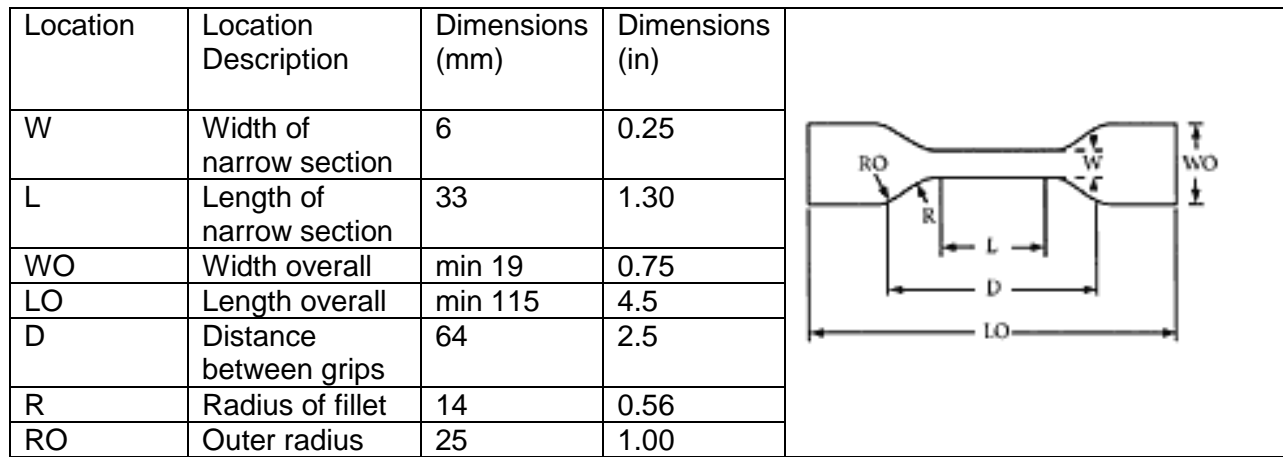


Figure 2 – DSC Measurement for Standard HPCC Coating from 30" Diameter Pipe

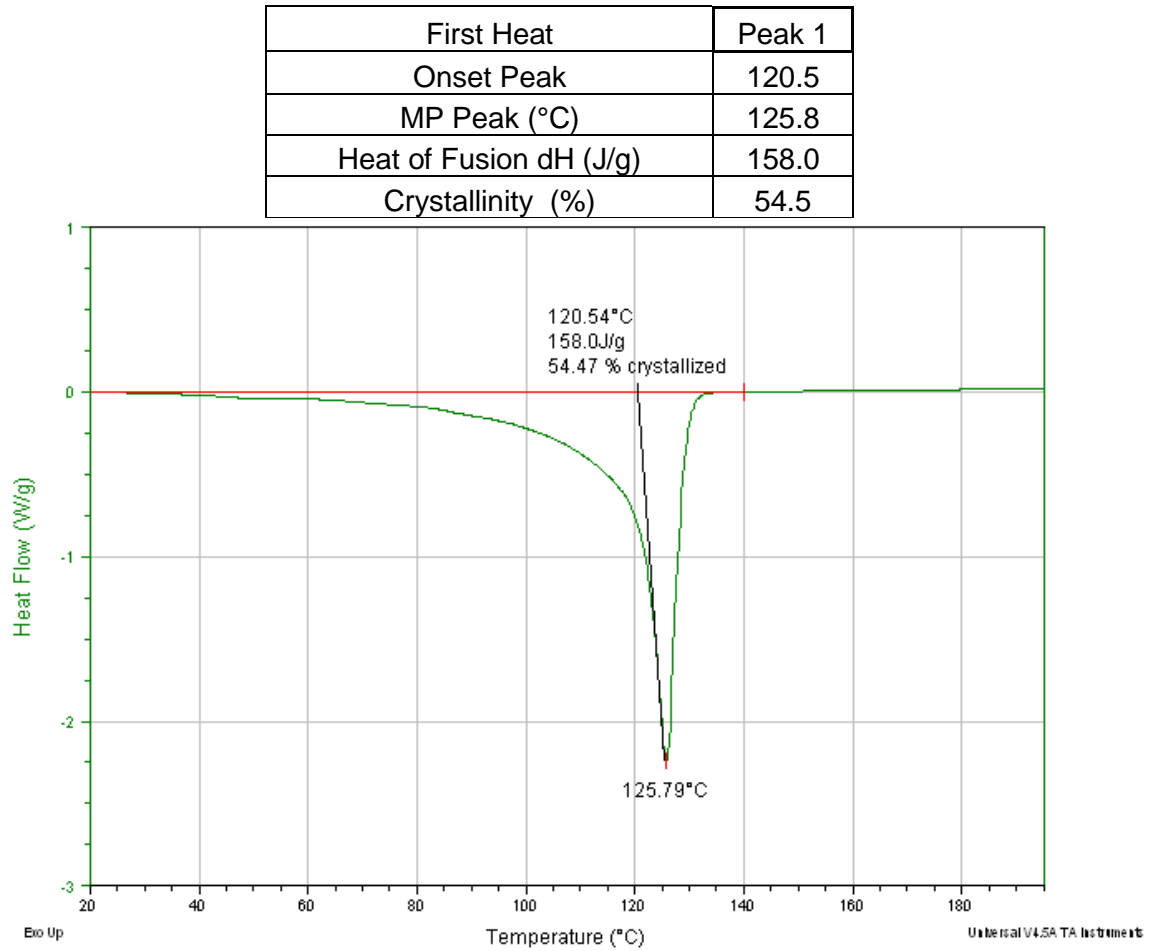


Figure 3 – DSC Measurement from 1 year old HPCC Coated 36" Diameter Pipe

First Heat	Peak 1
Onset Peak	118.6
MP Peak (°C)	125.9
Heat of Fusion dH (J/g)	158.0
Crystallinity (%)	54.5

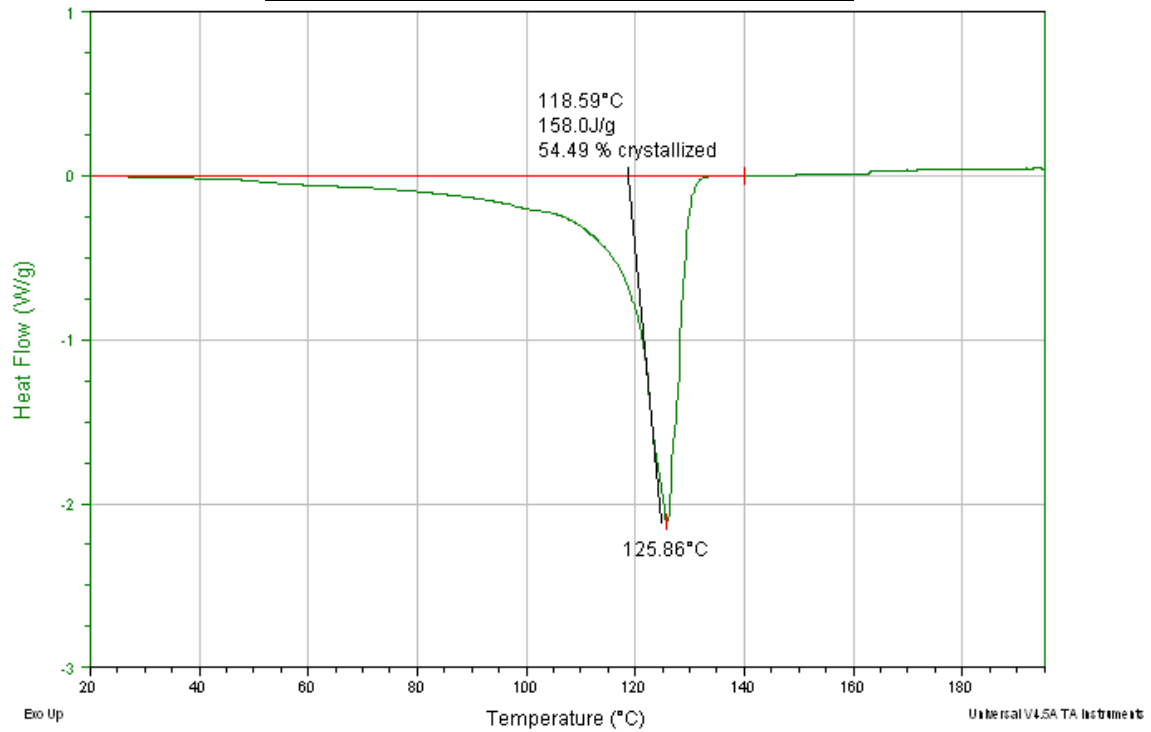


Figure 4 – DSC Measurement for a Lab Made Glass Cooled HPCC

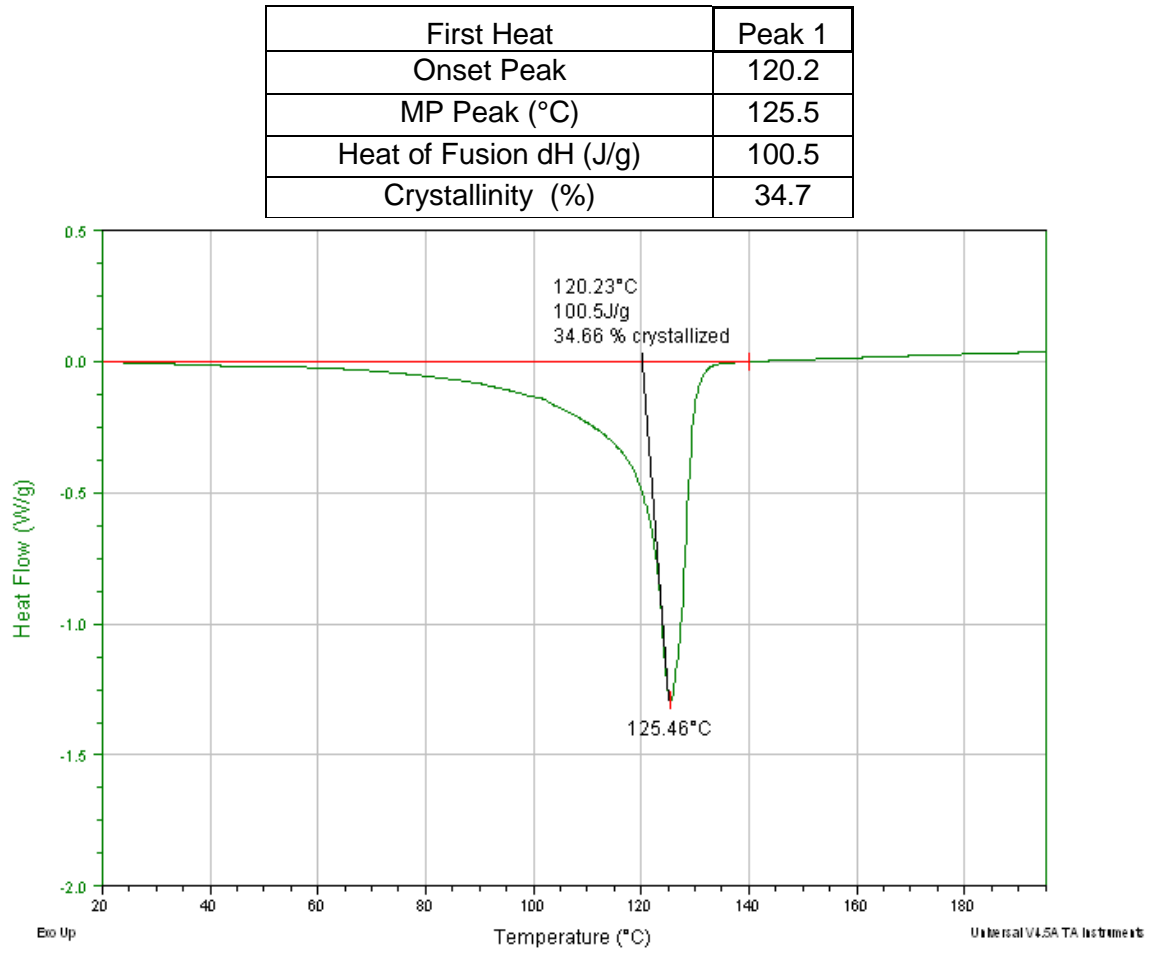


Figure 5 – DSC Measurement for PE Air Cooled with Pressure

First Heat	Peak 1
Onset Peak	123.4
MP Peak (°C)	130.4
Heat of Fusion dH (J/g)	170.4
Crystallinity (%)	58.8

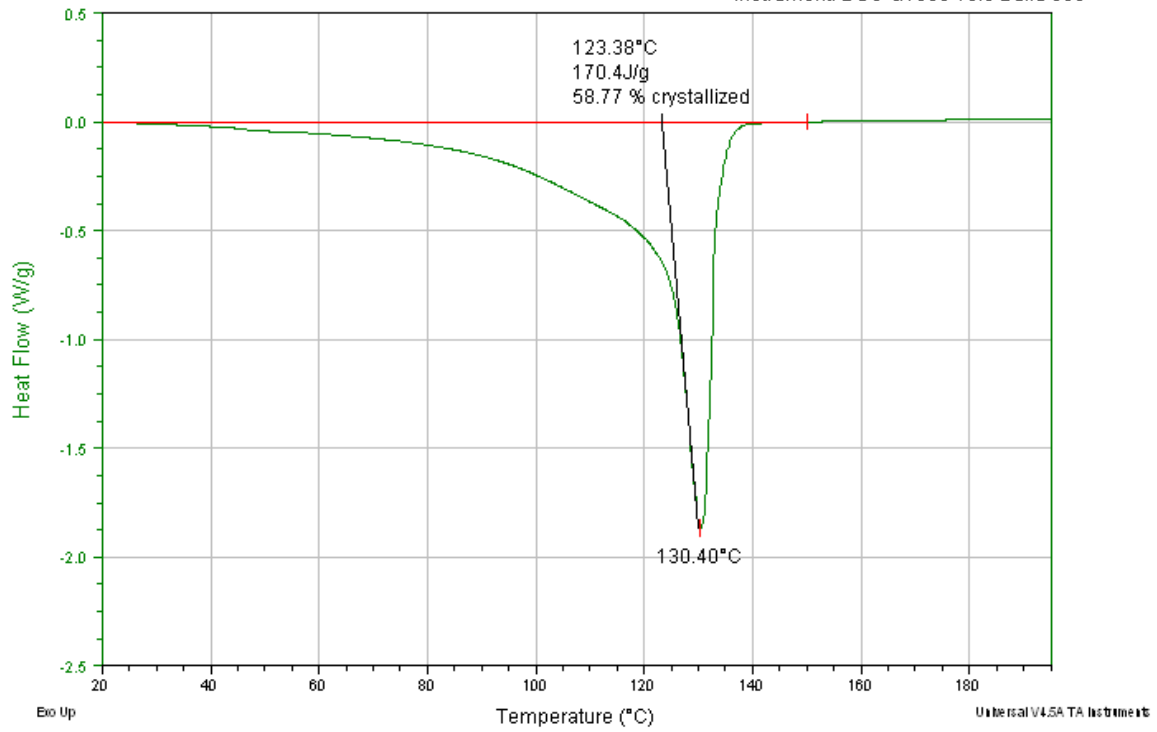


Figure 6 – DSC Measurement for PE Cooled at 30°C/min

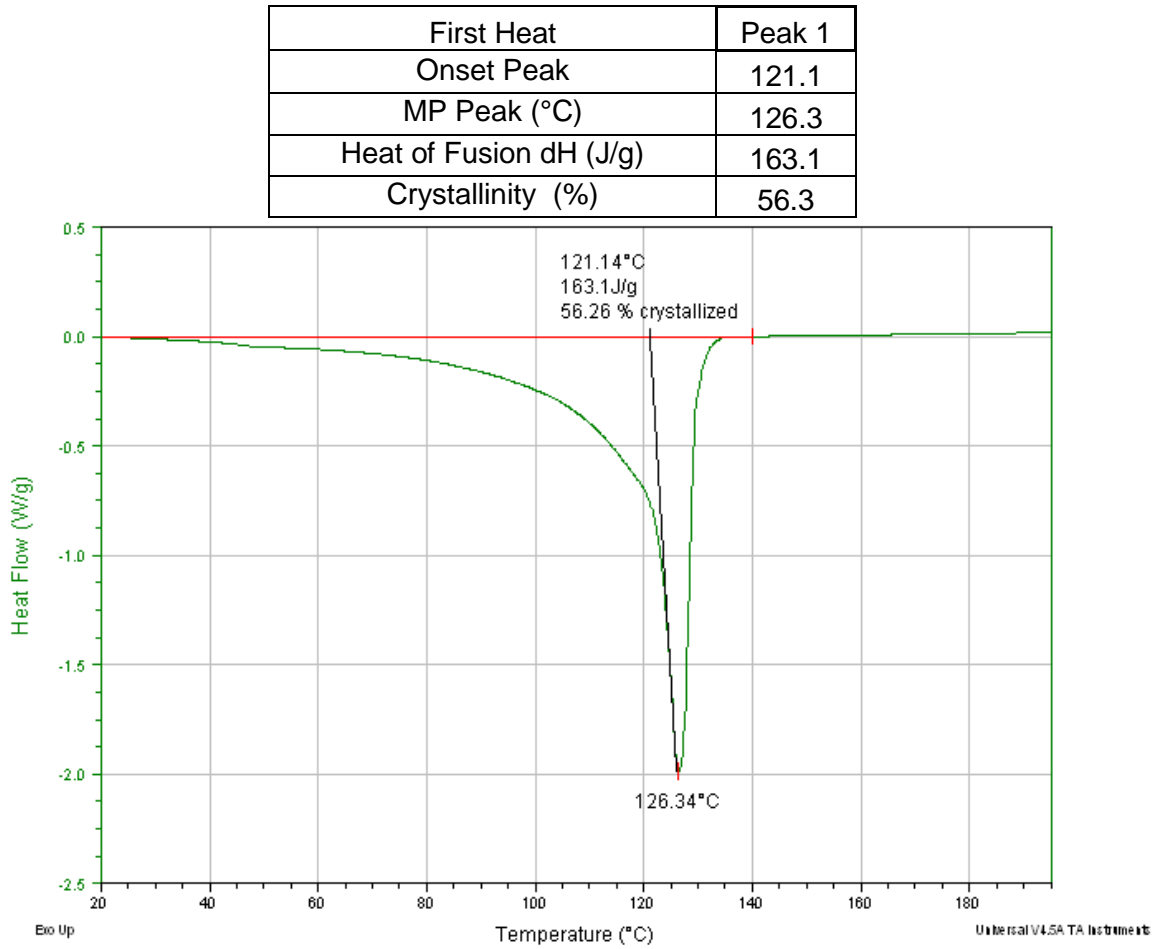


Figure 7 – DSC Measurement for PE Standard Compression Molding

First Heat	Peak 1
Onset Peak	119.4
MP Peak (°C)	126.0
Heat of Fusion dH (J/g)	158.8
Crystallinity (%)	54.8

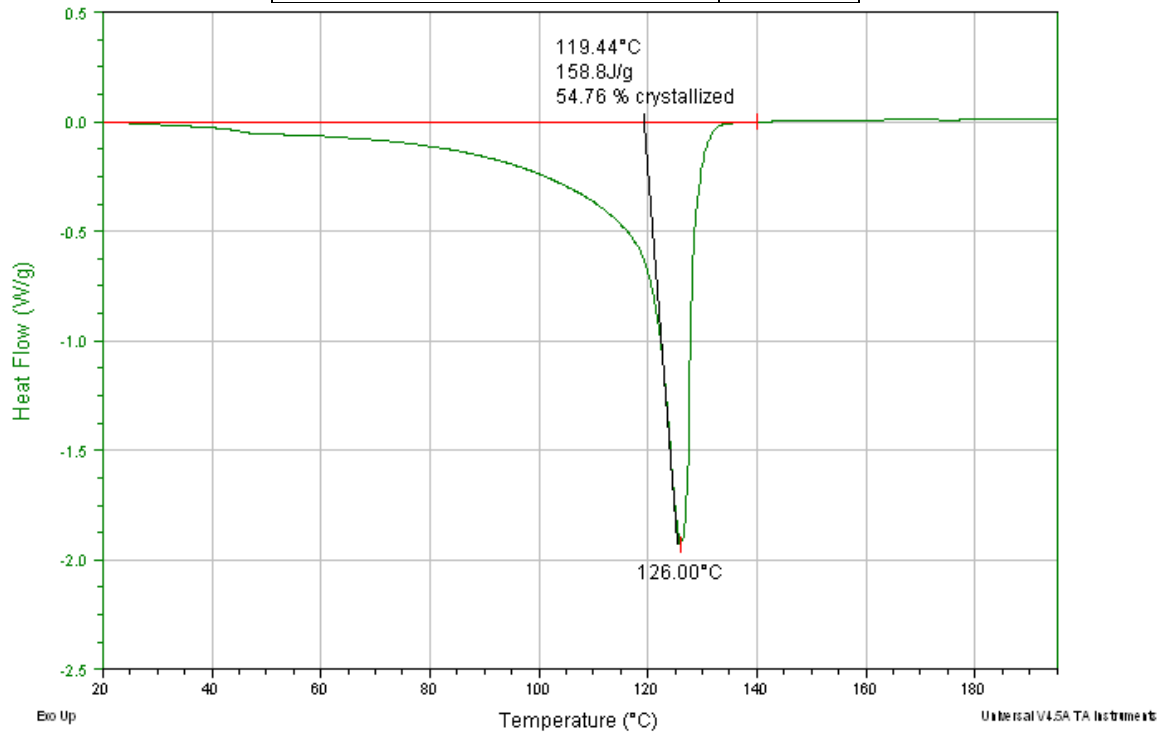


Figure 8 – DSC Measurement for Quench Cooled PE

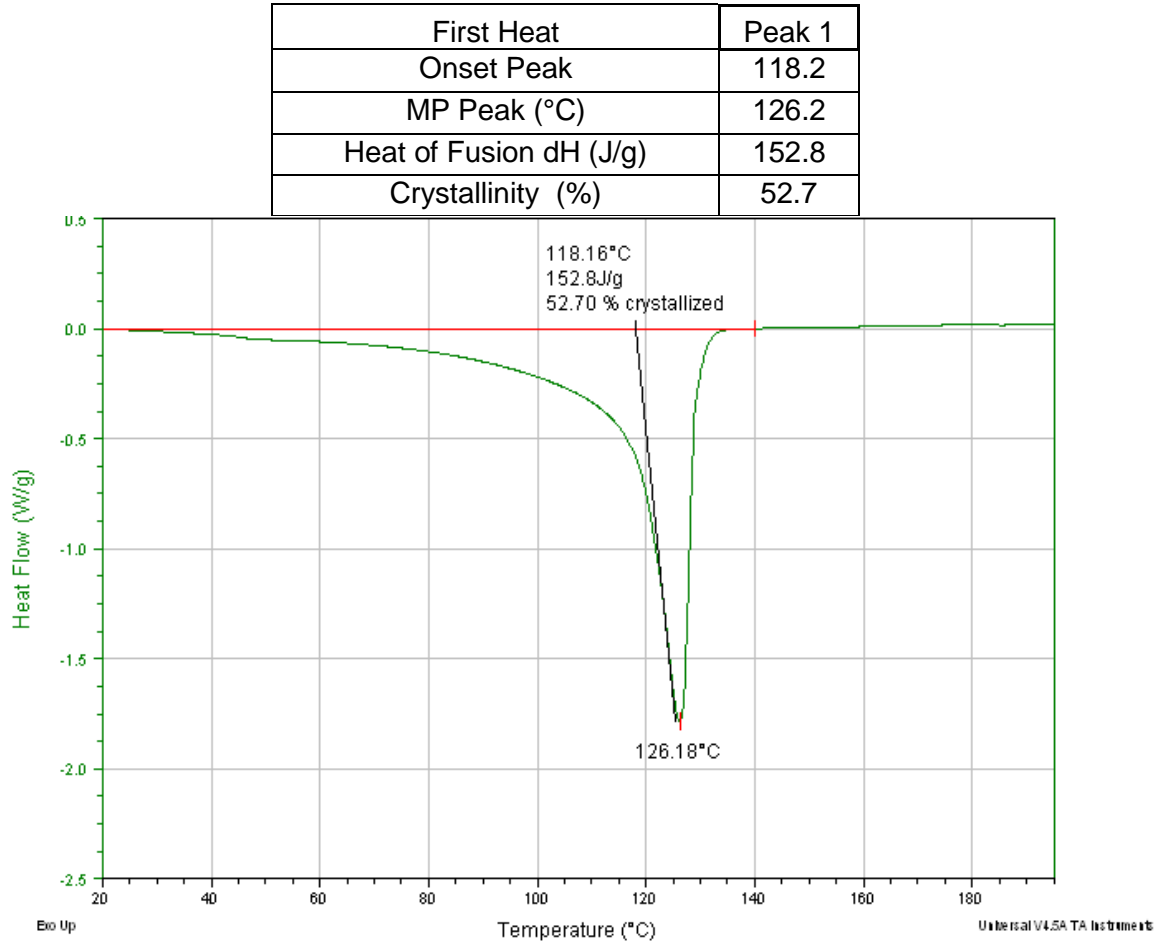


Figure 9 – DSC Measurement for Lab-Made FBE

First Heat	Peak 1	Peak 2
Onset temperature (°C)	71.8	100.5
Inflection point (°C)	74.4	104.8
End Temperature (°C)	80.7	106.3
Crystallinity (%)	N/A	N/A
MP Peak (°C)	N/A	N/A
Delta Cp [J/(g·°C)]	0.084	0.15

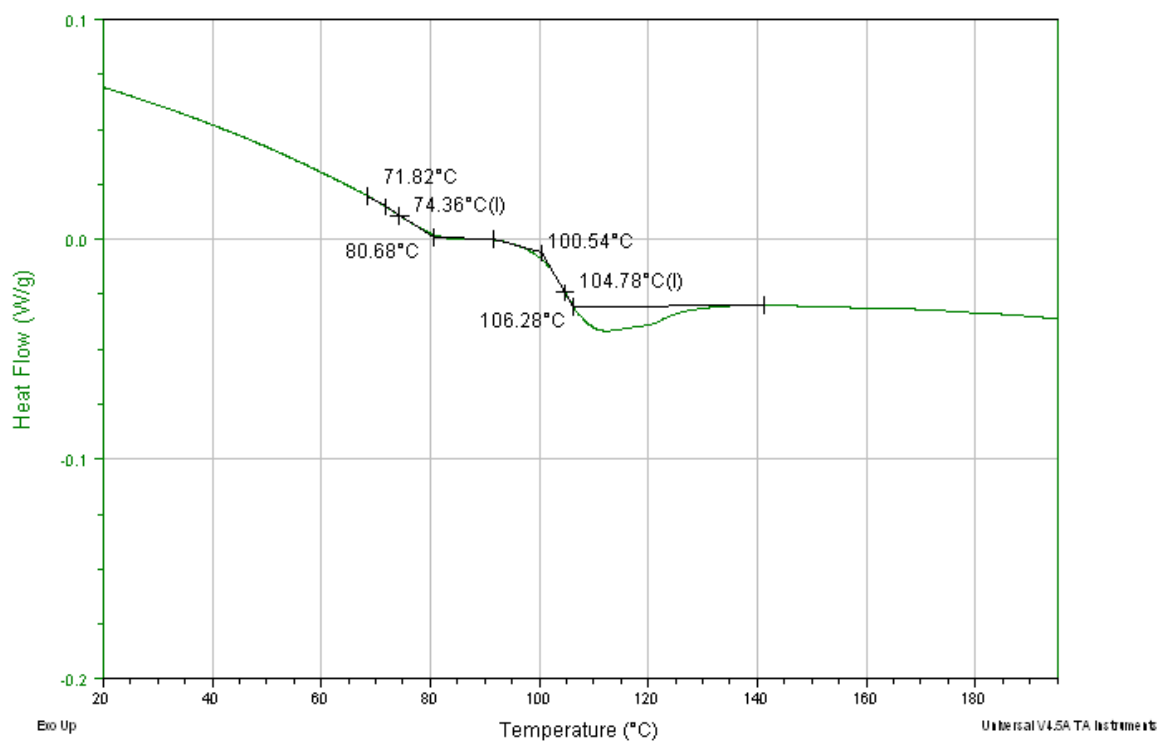


Figure 10 – Large Diameter CD Cell for Long-Term Testing



Figure 11 – Typical HPCC Coated Pipe Sample Section



Figure 12 – CD Experimental Configuration with Power Supply

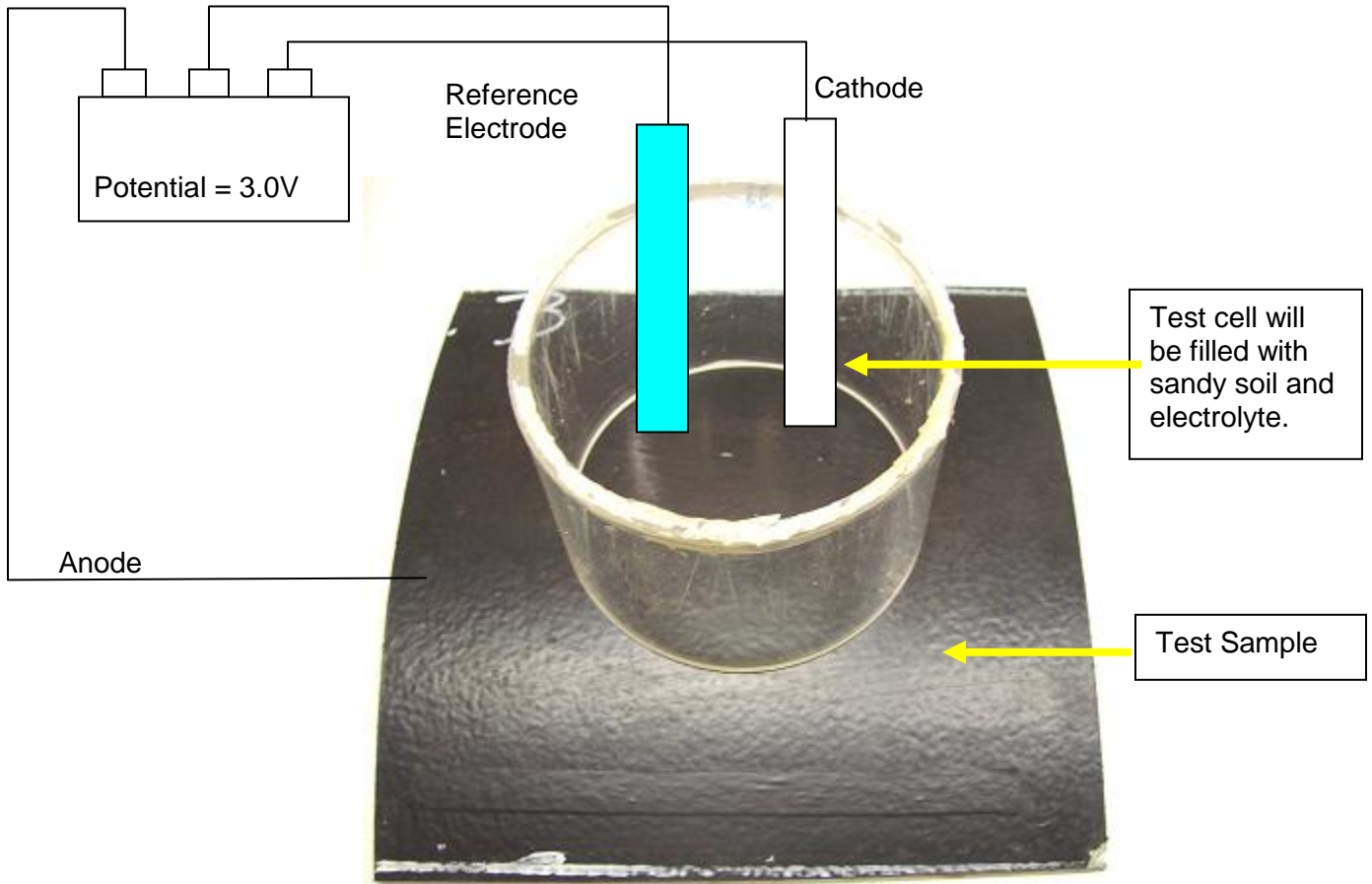


Figure 13a – Picture of Cathodic Disbondment Experimental Configuration



Figure 13b – Cathodic Disbondment Testing for All Project Samples



Figure 14a - Cathodic Disbondment Experimental Setup

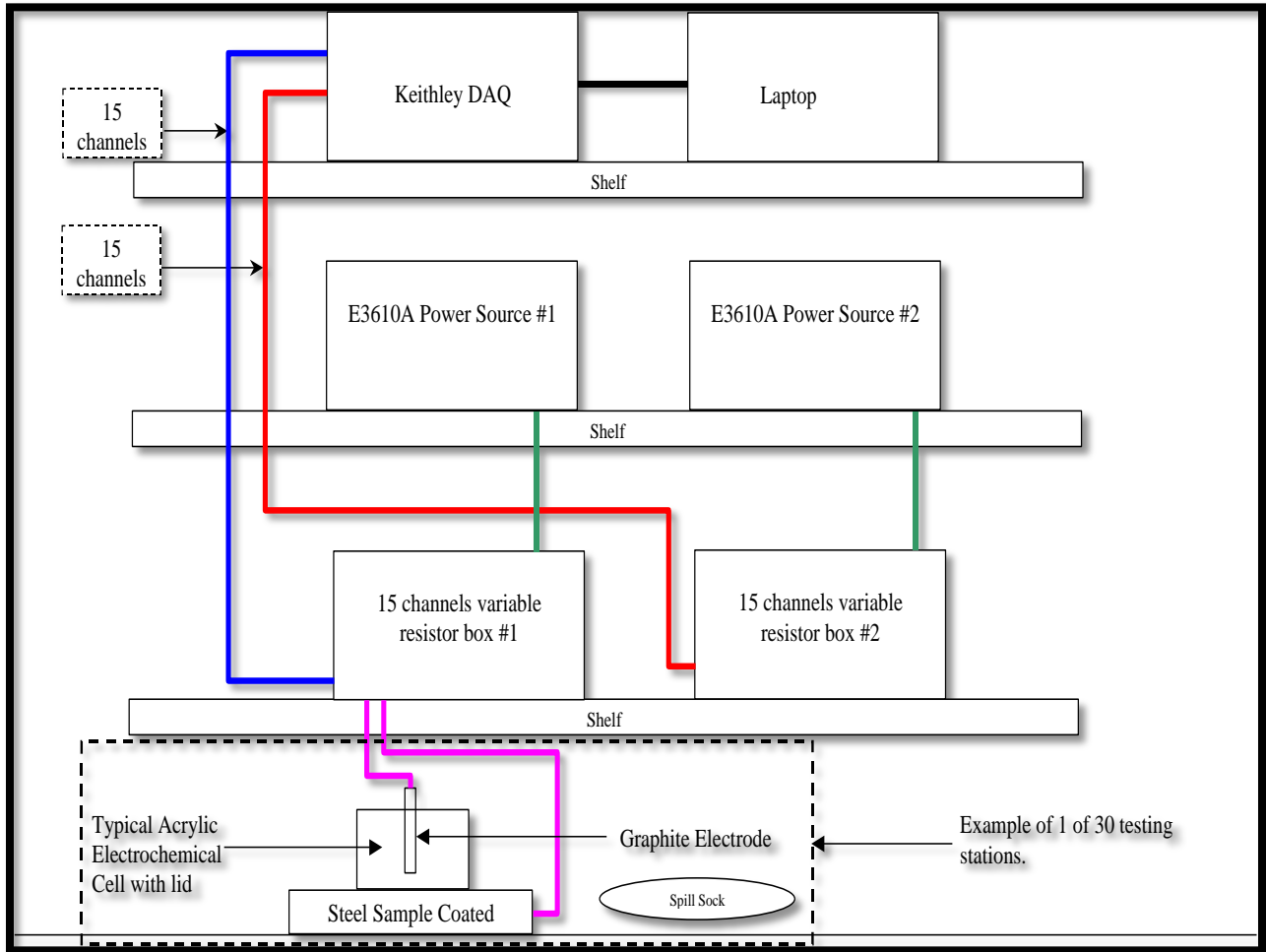


Figure 14b - Cathodic Disbondment Electrical Circuit Diagram

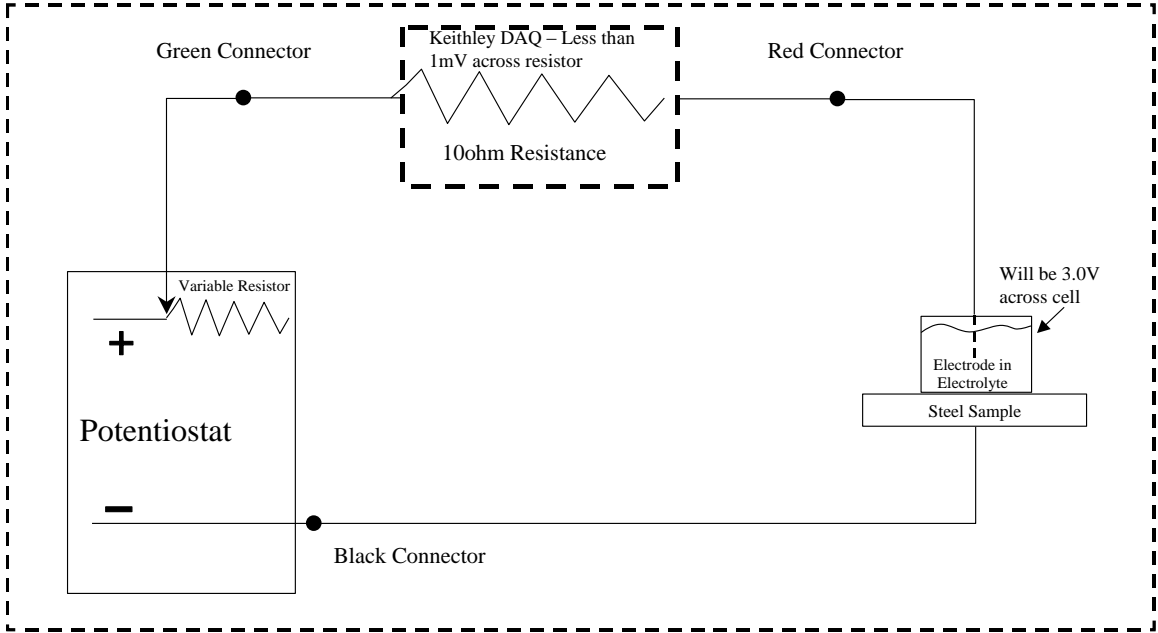


Figure 15a – Hot water Soaking Pre-treatment for CD Testing

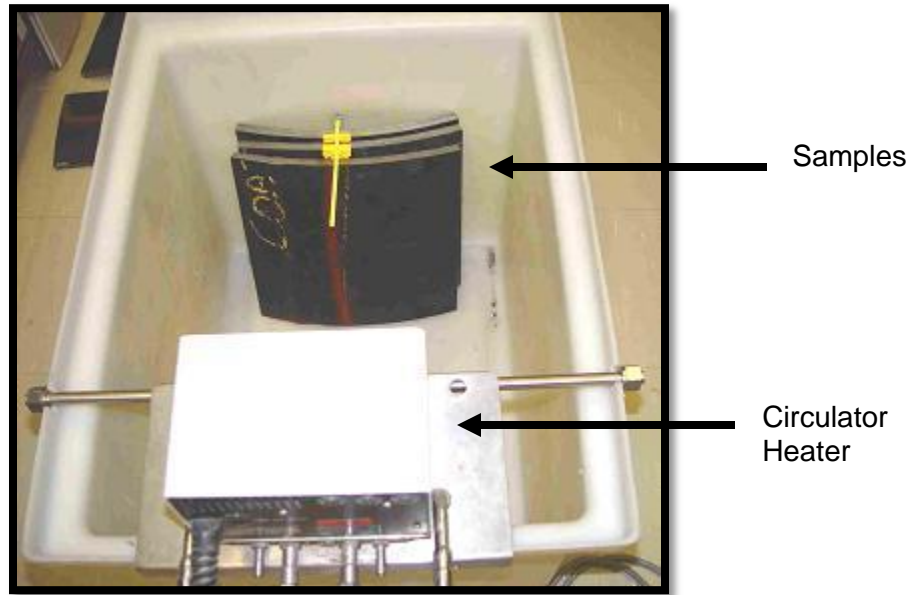


Figure 15b – Hot Water Baths used for Hot Soaking Pre-treatment for CD Testing

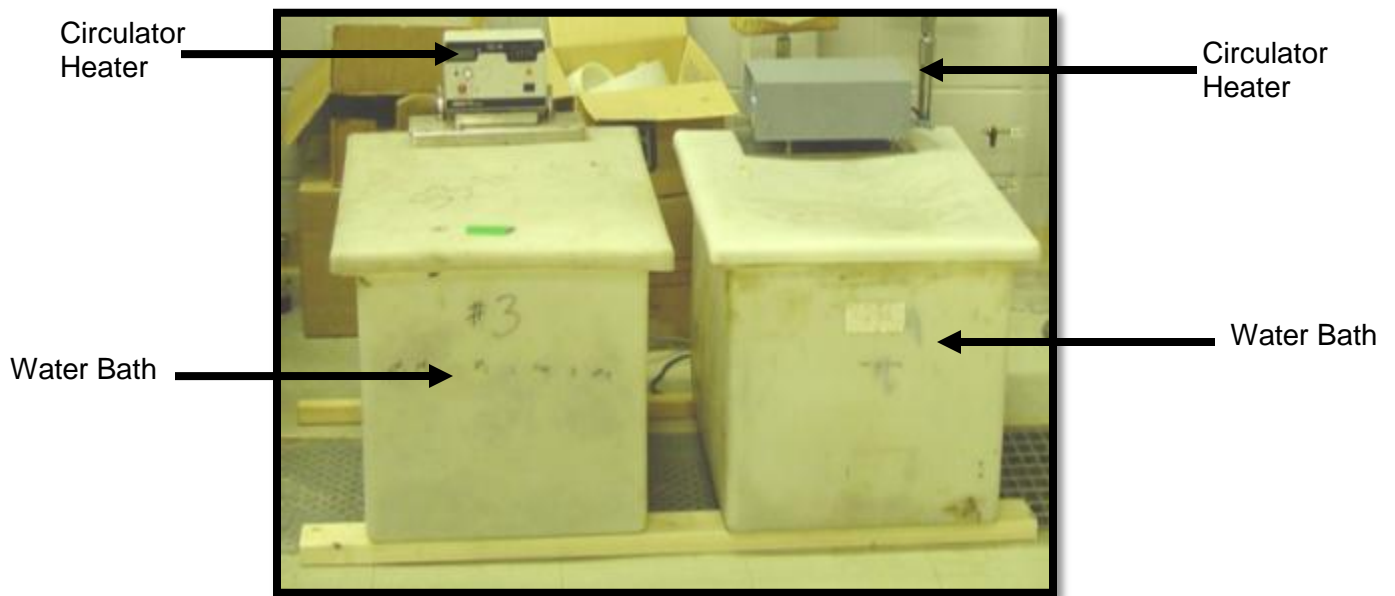


Figure 16 – Current Response Recorded for Varying Surface Treatments during CD Tests Using 1 Year Old HPCC

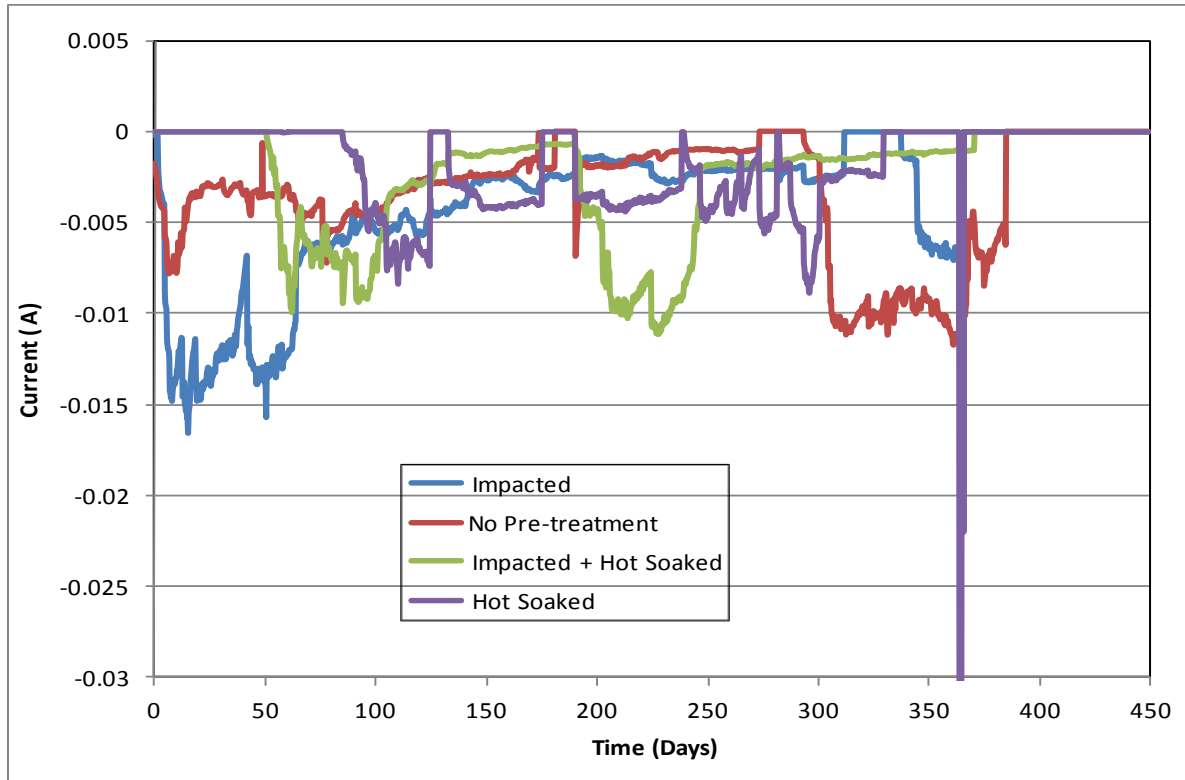


Figure 17 – Current Response Recorded for Varying Surface Treatments during CD Tests Using New HPCC

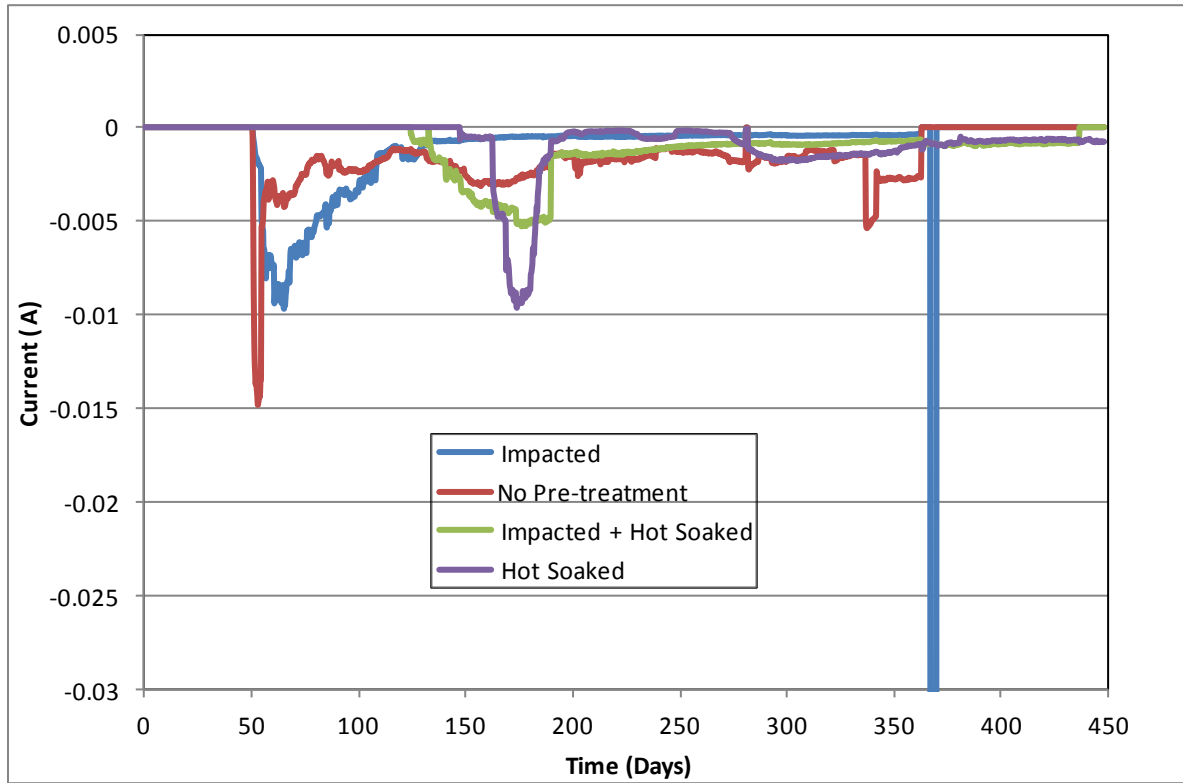


Figure 18 – Current Response Recorded for Varying Surface Treatments during CD Tests Using Low Profile HPCC

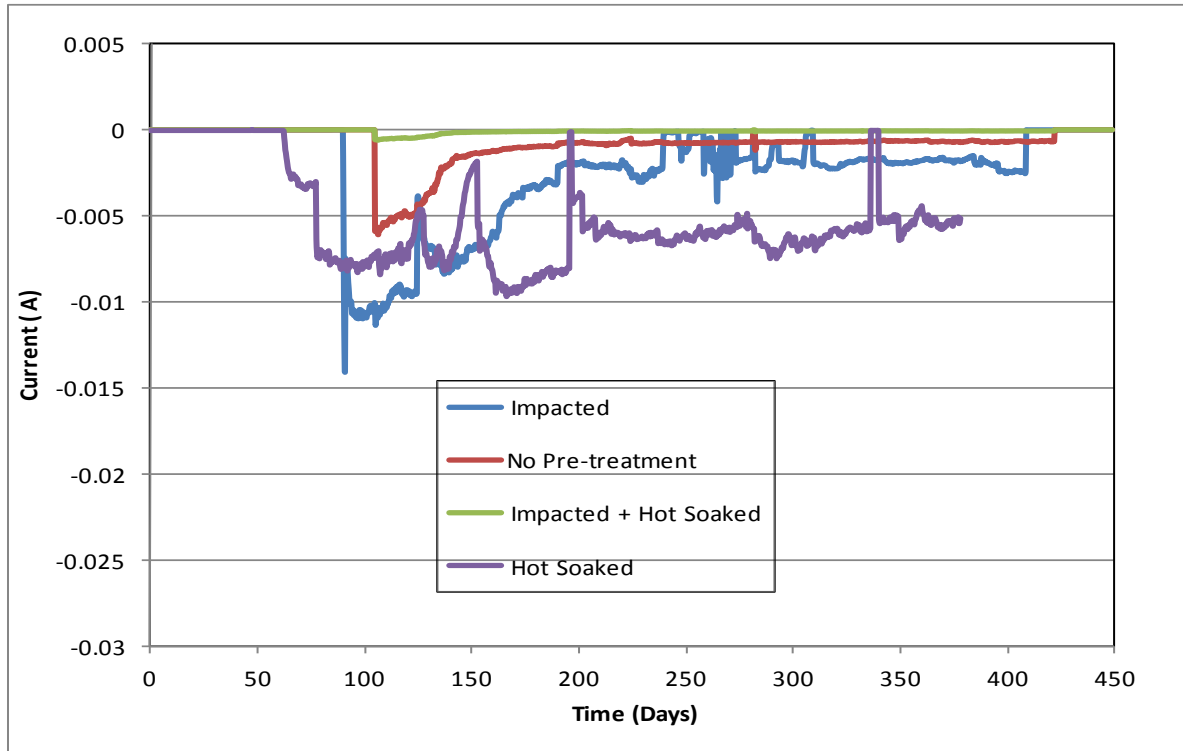


Figure 19 – Current Response Recorded for Varying Surface Treatments during CD Tests Using High Profile HPCC

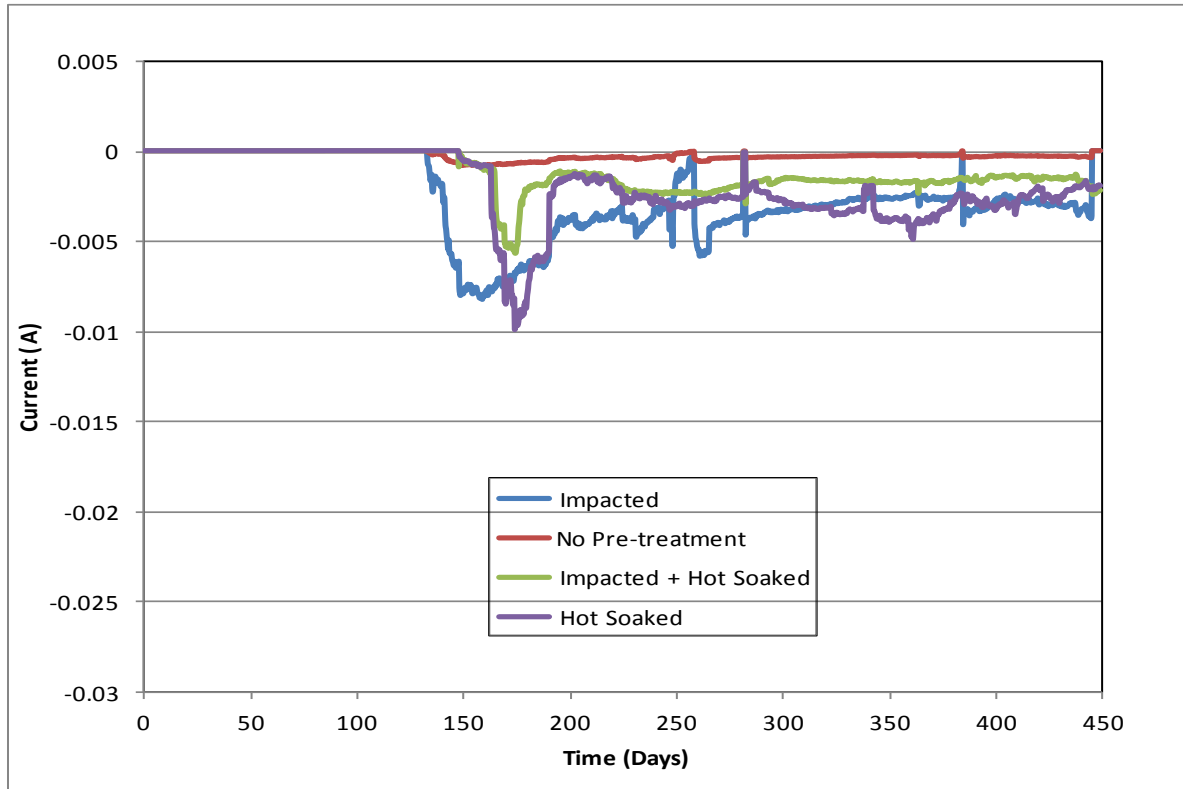


Figure 20 – Comparison of Current Response of No Pre-Treatment on Various HPCC Samples

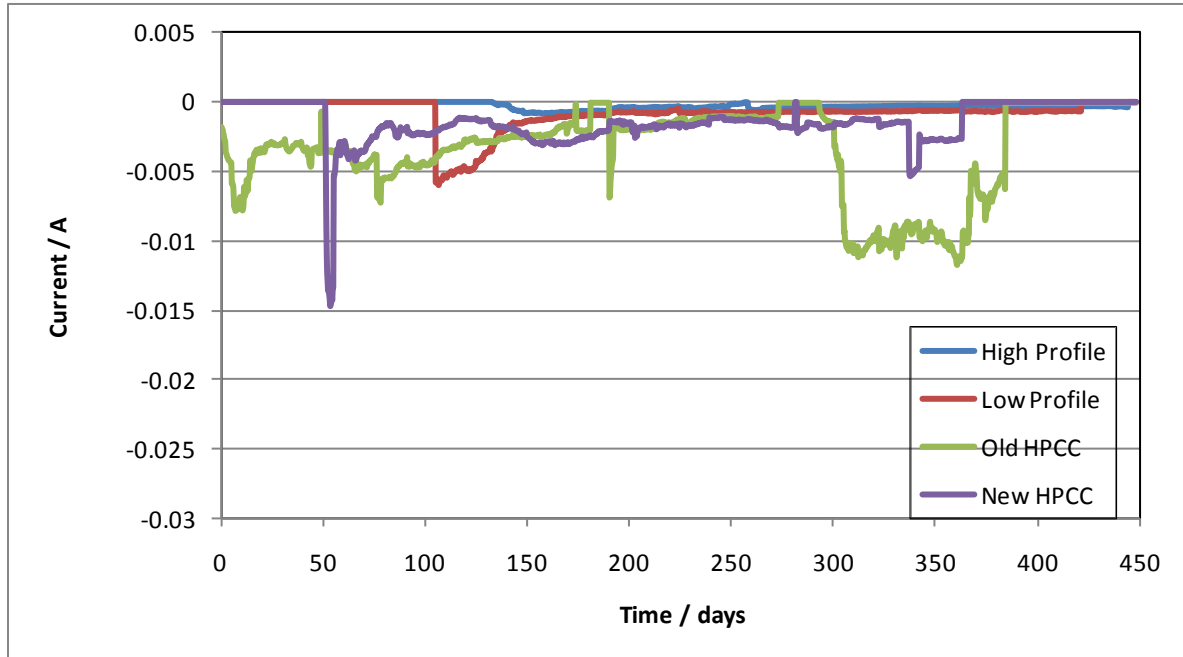


Figure 21 – Comparison of Current Response of Hot Soaked Testing Treatment on Various HPCC Samples

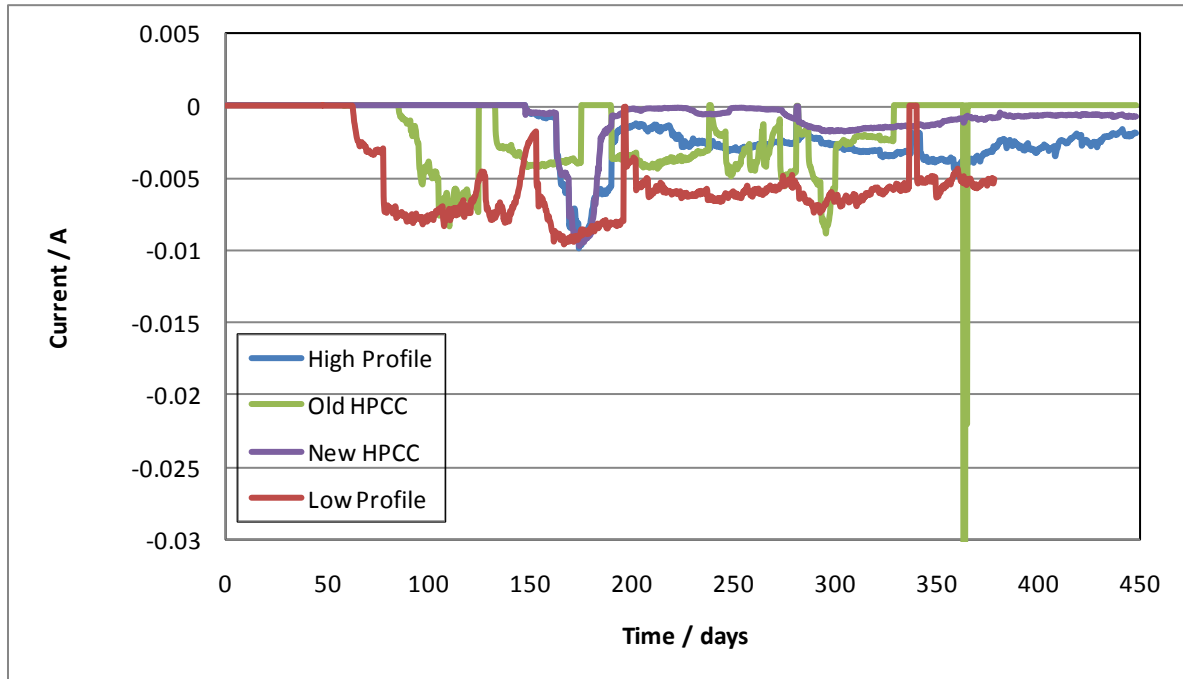


Figure 22 – Comparison of Current Response of Impacted Surface Treatment on Various HPCC Samples

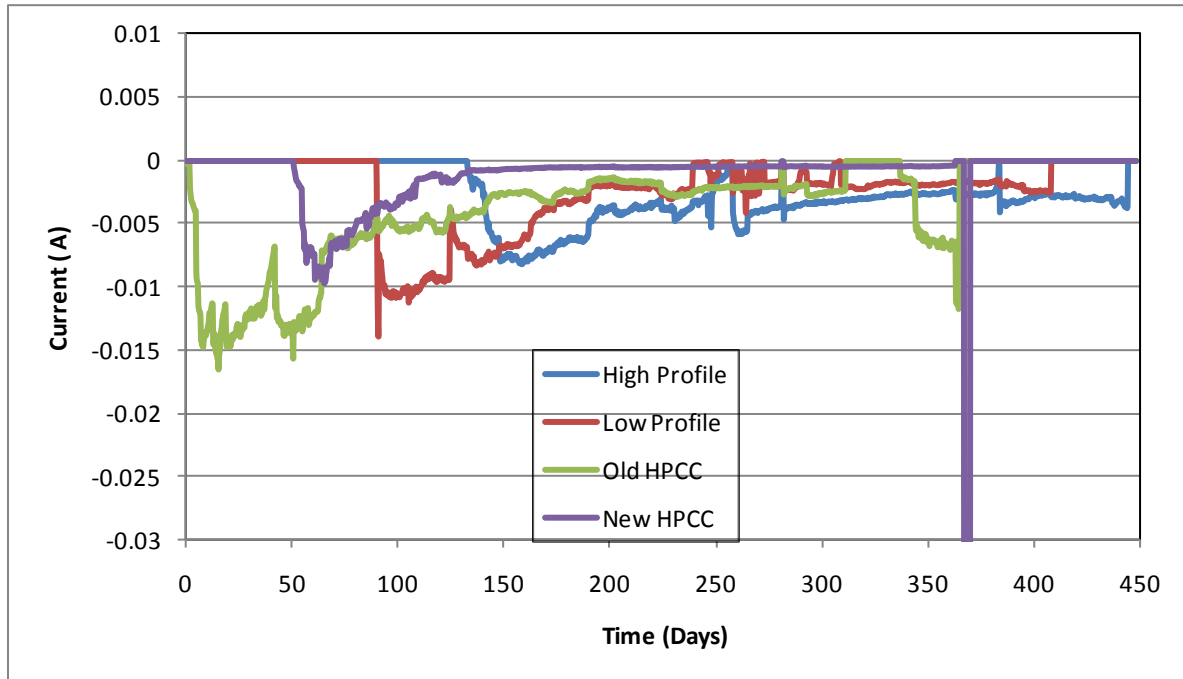


Figure 23 – Comparison of Current Response of Impacted and Hot Soaked Surface Treatment on Various HPCC Samples

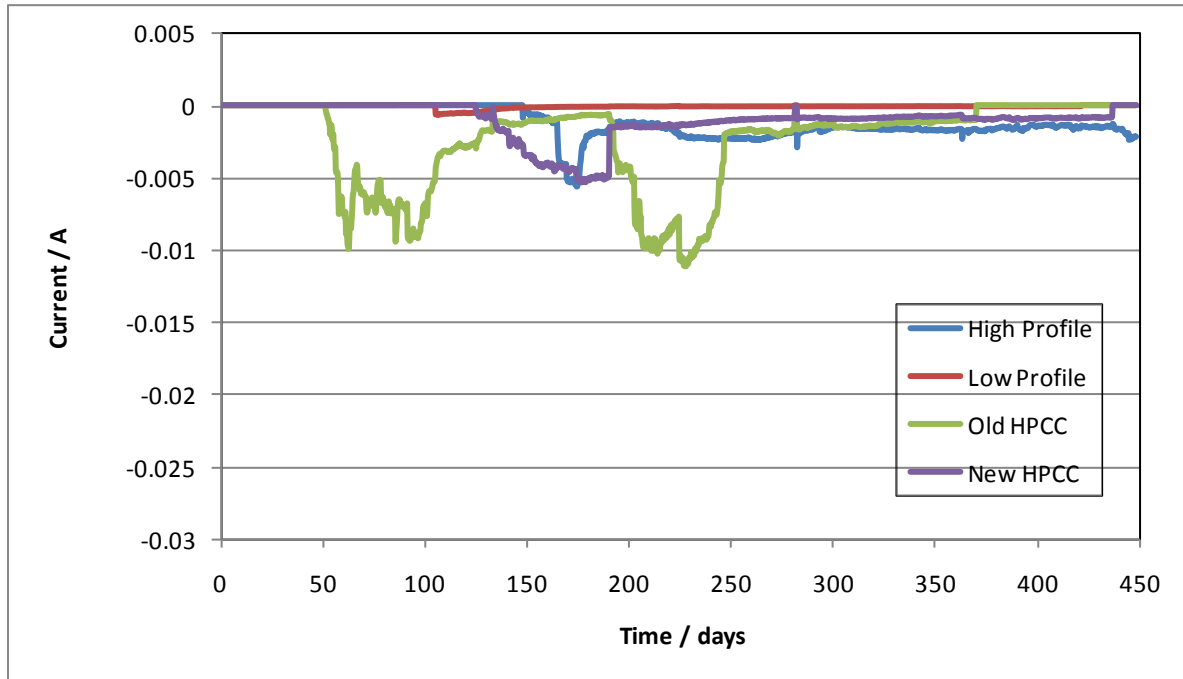


Figure 24 – Comparison of CD Performance of 1 Year Old HPCC

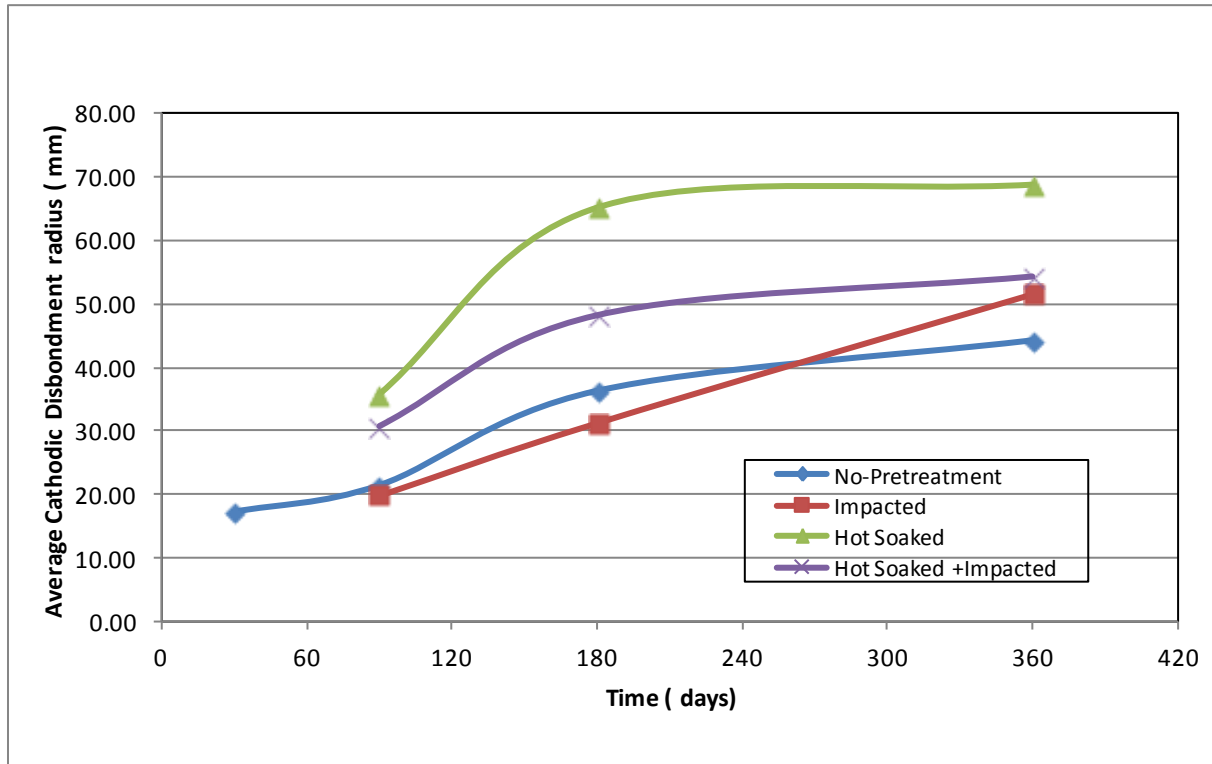


Figure 25 – Comparison of CD Performance of New HPCC

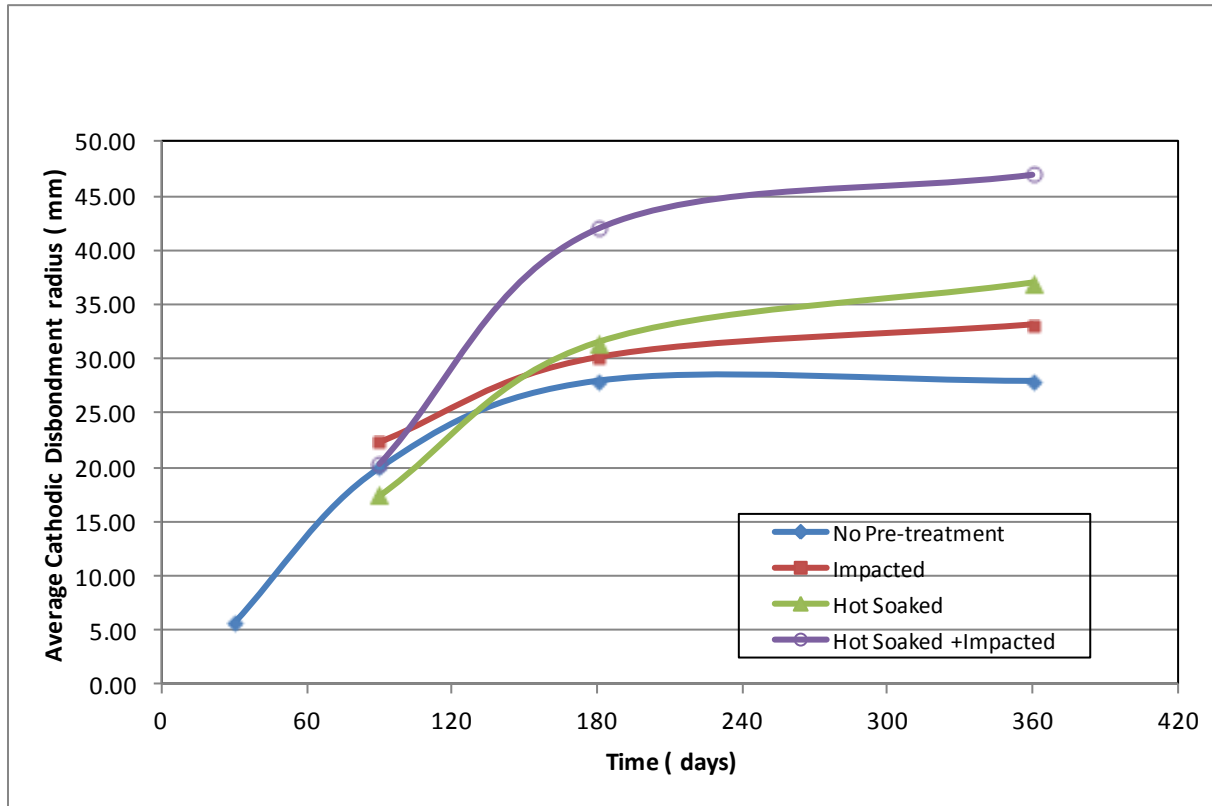


Figure 26 – Comparison of CD Performance of Low Profile HPCC

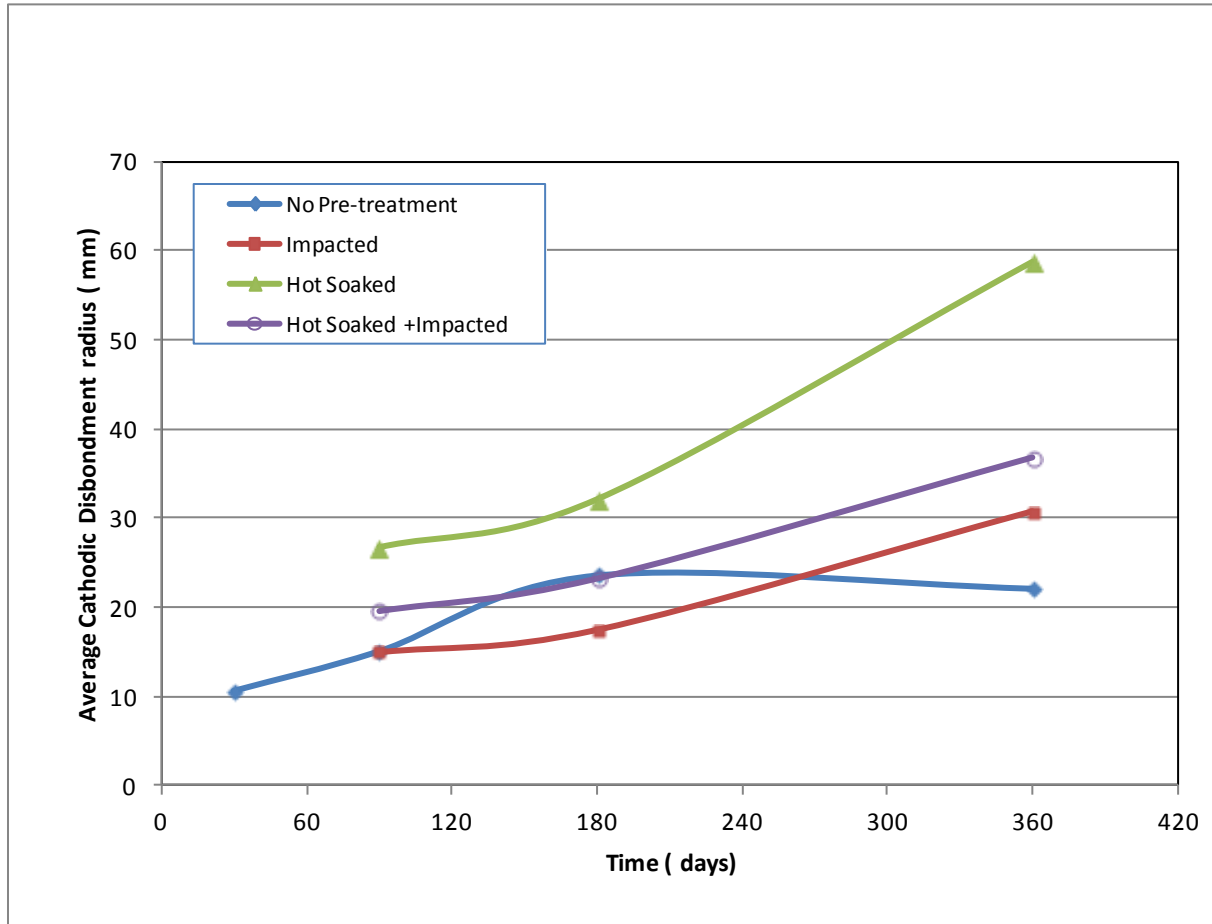


Figure 27 – Comparison of CD Performance of High Profile HPCC

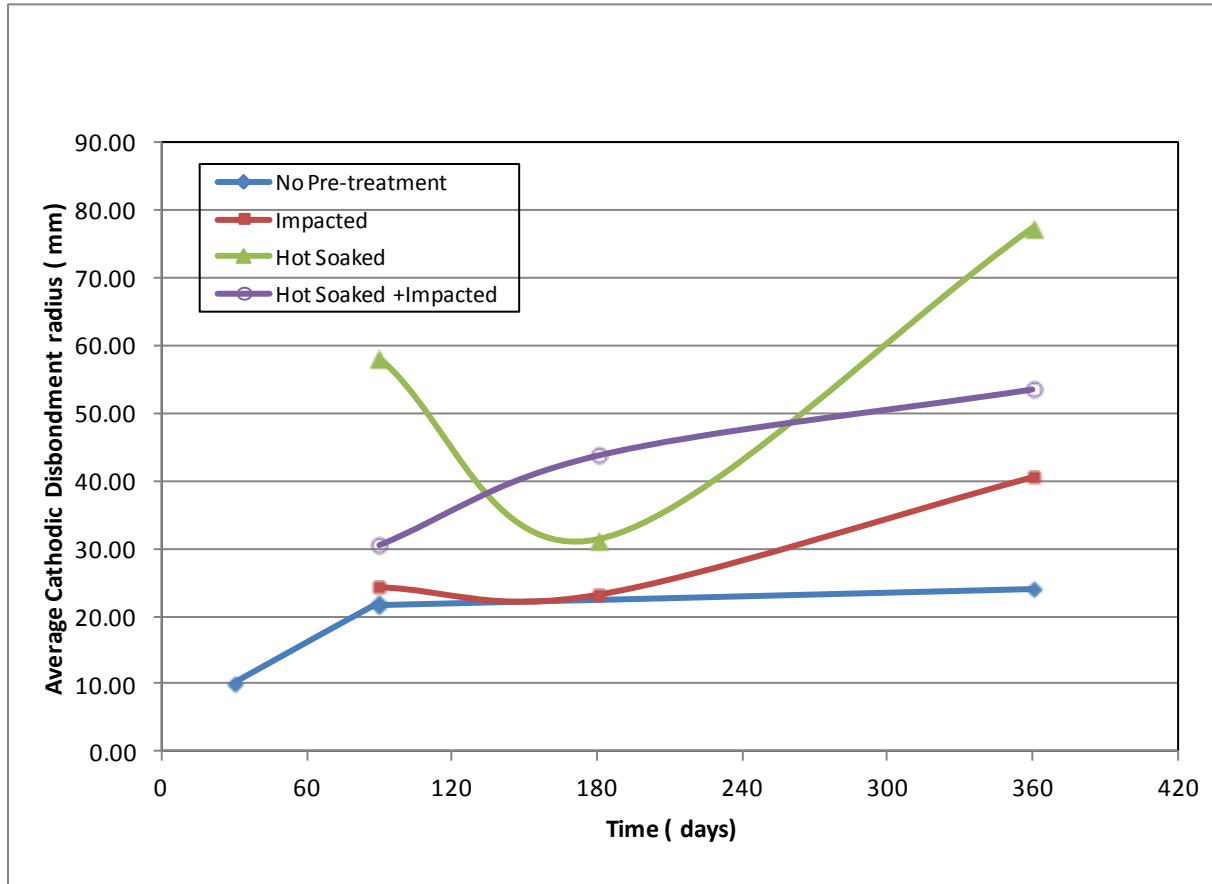


Figure 28 – Comparison of CD Performance of No Pre-Treatment Testing on Various HPCC Samples

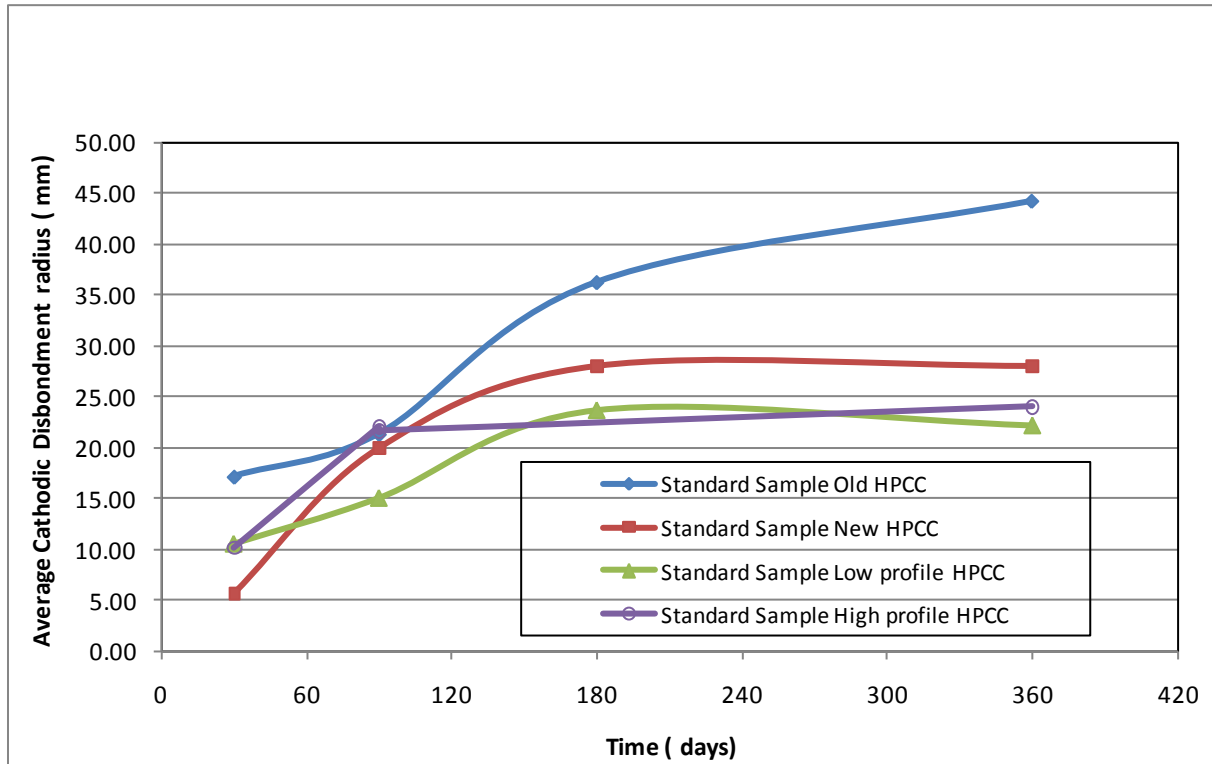


Figure 29 – Comparison of Cathodic Disbondment Performance of Hot Soaked Testing Treatment on Various HPCC Samples

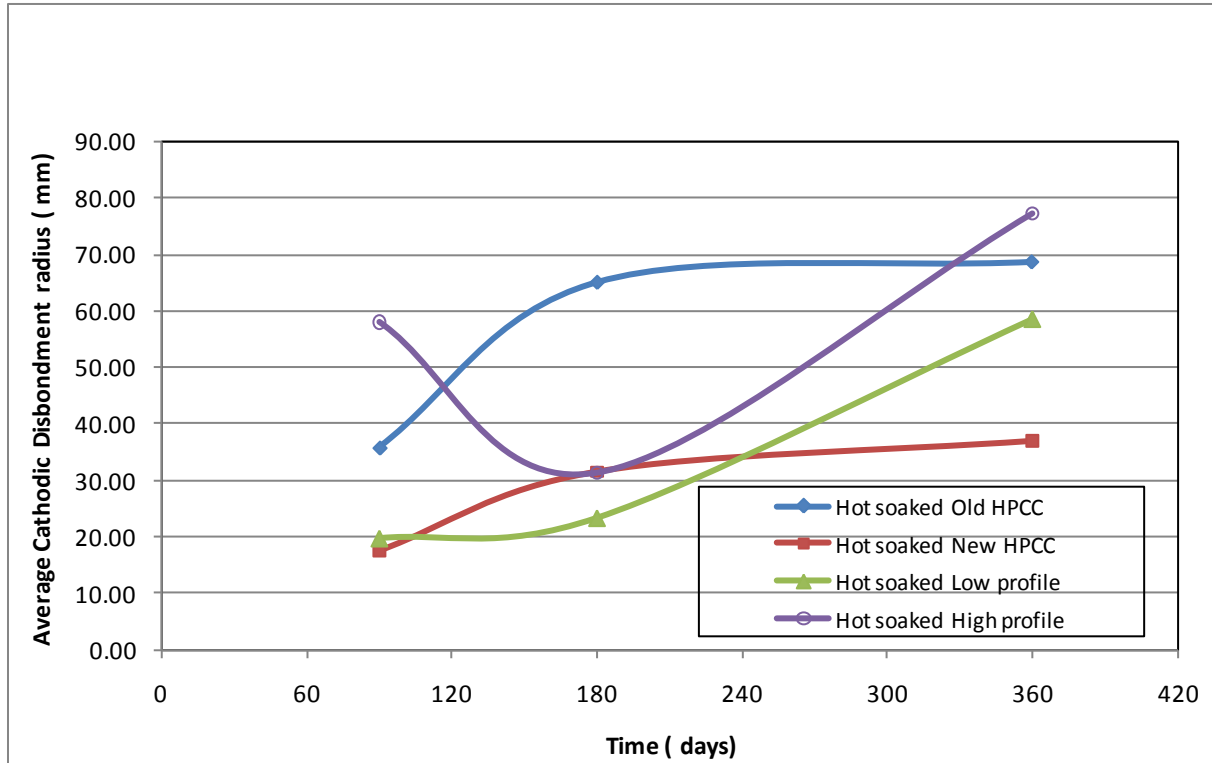


Figure 30 – Comparison of Cathodic Disbondment Performance of Impacted Surface Treatment on Various HPCC Samples

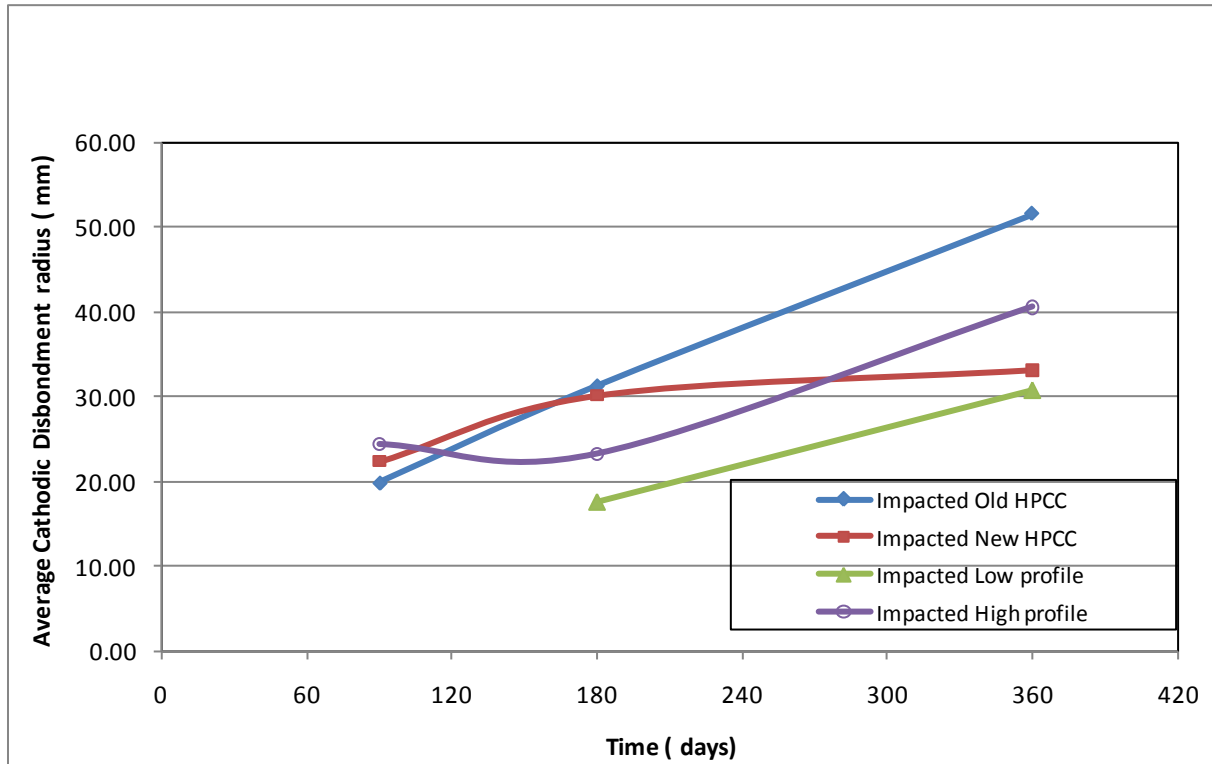


Figure 31 – Comparison of Cathodic Disbondment Performance of Impacted and Hot Soaked Surface Treatment on Various HPCC Samples

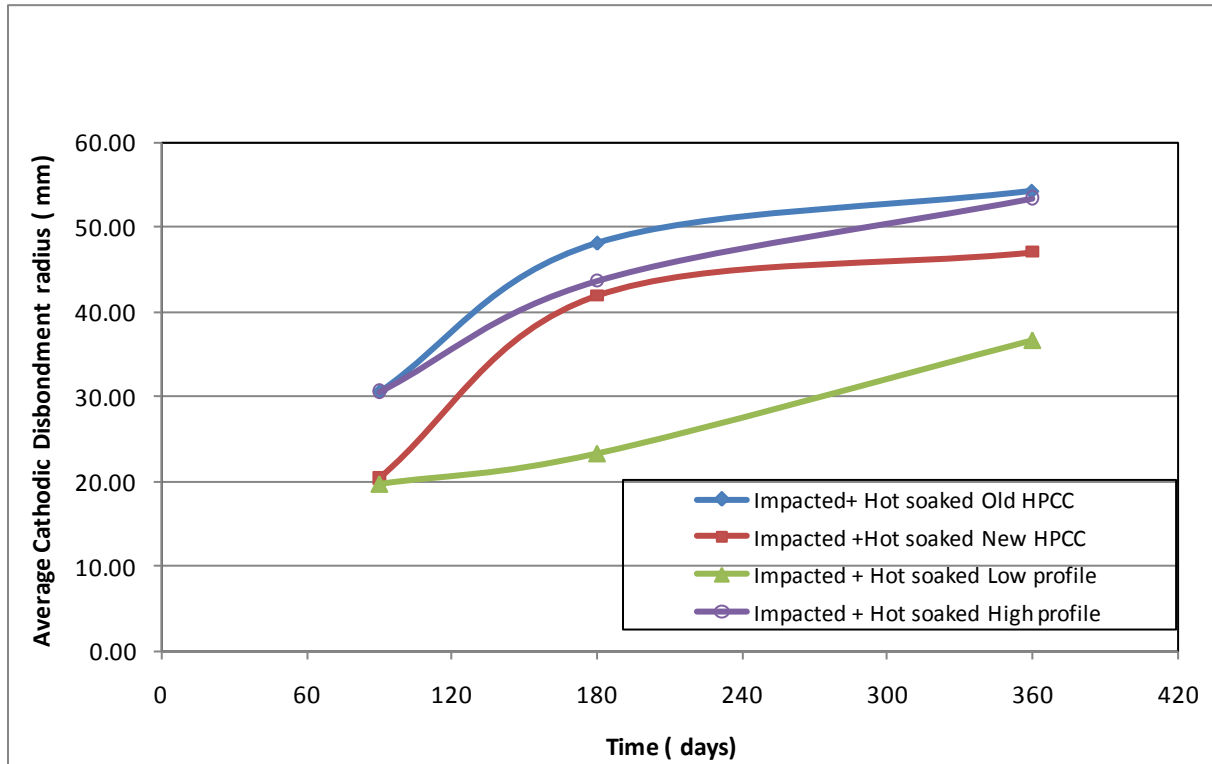


Figure 32 – Orientation of a Three-element Strain Gauge Rosette

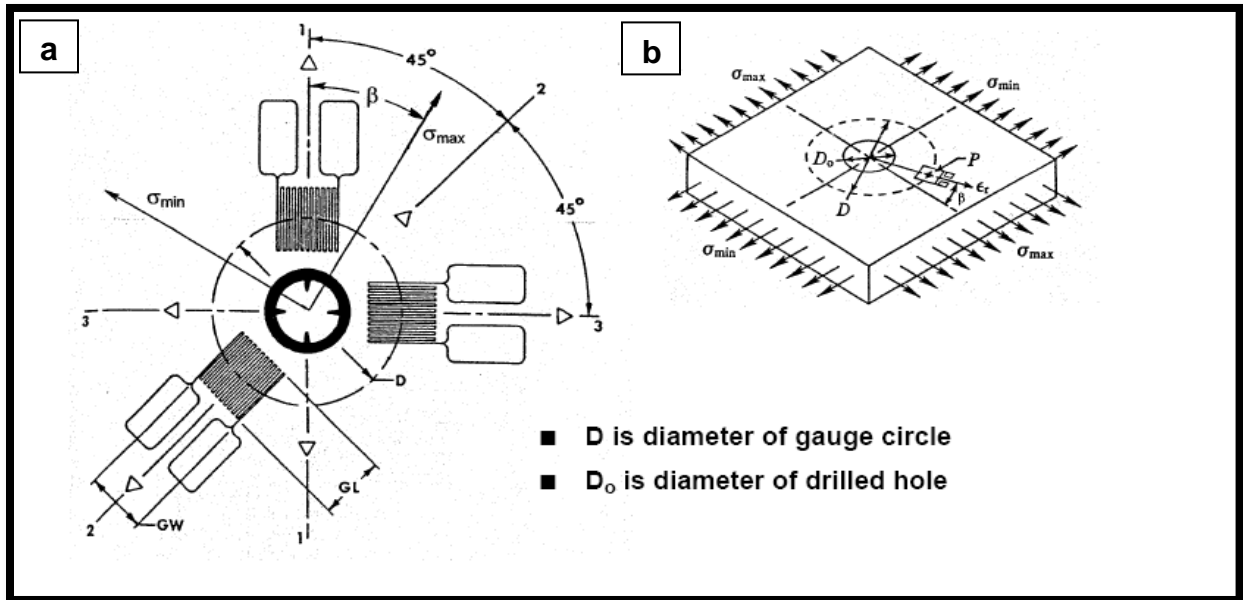


Figure 33 – Average Residual Stress Measured on Varying Coating Surface Preparations in the Circumferential (Hoop) X-direction

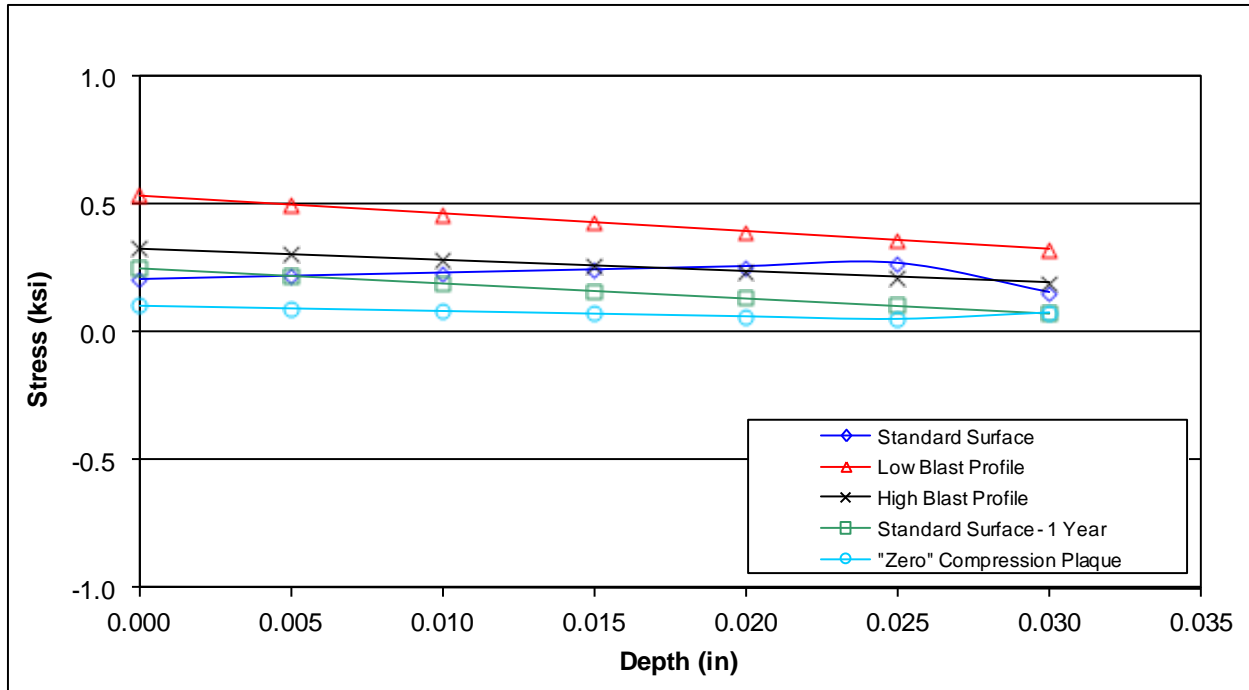


Figure 34 – Average Residual Stress Measured on Varying Coating Surface Preparations in the Longitudinal (Tangential) Y-direction

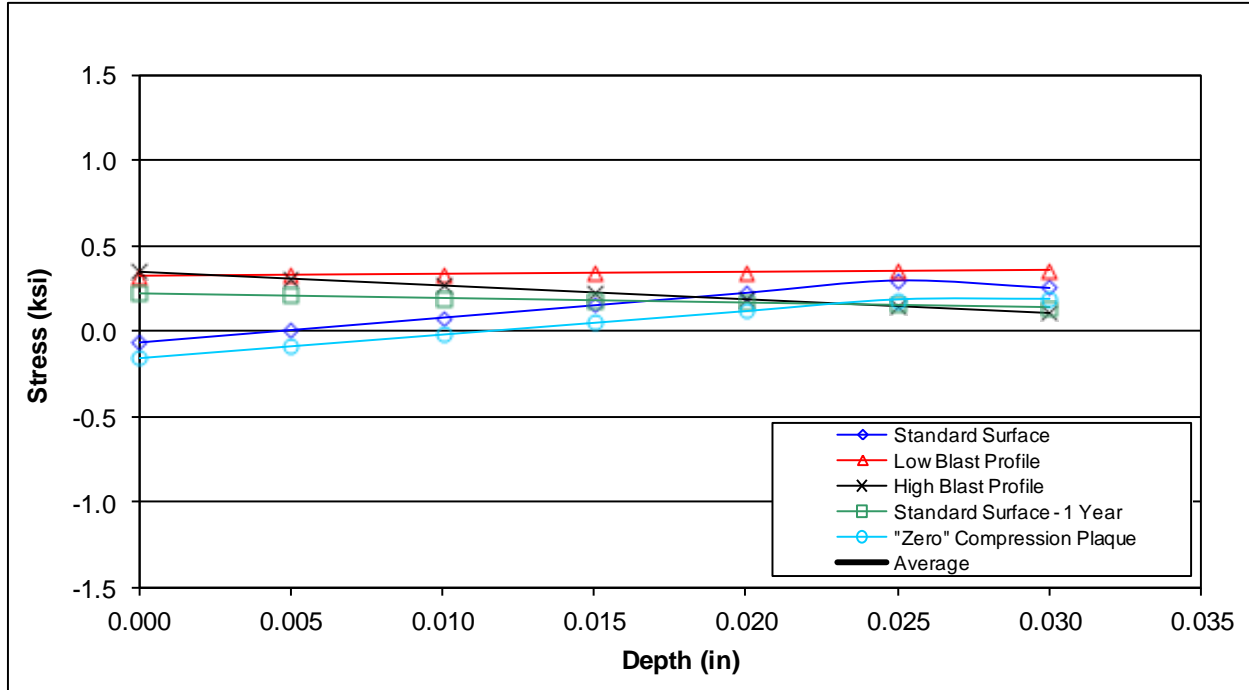
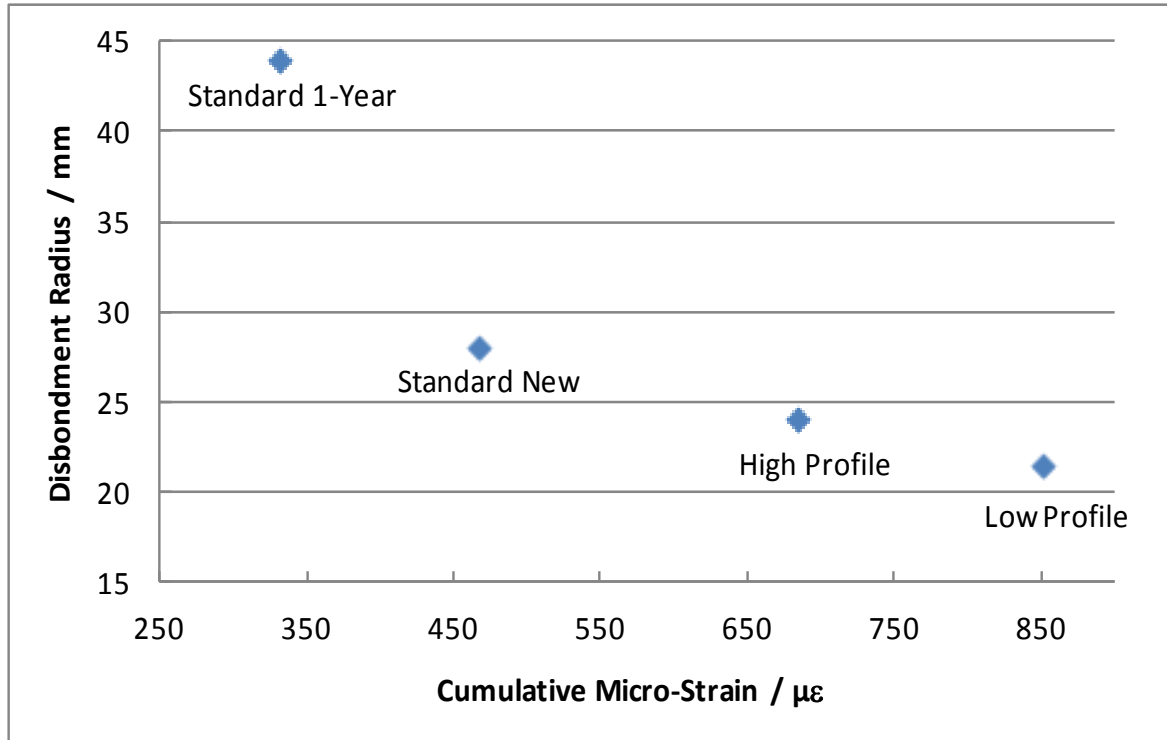


Figure 35 – Relationship between Coating Disbondment of No Pre-Treatment Samples and Magnitude of Cumulative Micro-Strain



14.0 APPENDIX

APPENDIX 1 – Residual Stress Measurement Database on HPCC Samples

STANDARD SURFACE

Ring 1 Uniform Stresses						
Location	Sx (ksi)	Sy (ksi)	Txy (ksi)	Smax (ksi)	Tmax (ksi)	beta (deg)
1	+0.232 ±0.008	+0.090 ±0.003	-0.026 ±0.001	+0.237 ±0.007	+0.076 ±0.002	+10 ±1
2	+0.034 ±0.001	+0.077 ±0.003	-0.077 ±0.003	+0.135 ±0.000	+0.080 ±0.003	+53 ±1
3	+0.378 ±0.012	-0.079 ±0.002	-0.262 ±0.008	+0.497 ±0.004	+0.347 ±0.003	+24 ±1
4	+0.380 ±0.012	+0.229 ±0.007	-0.208 ±0.007	+0.526 ±0.005	+0.221 ±0.006	+35 ±1
5	+0.067 ±0.002	+0.056 ±0.002	-0.666 ±0.021	+0.728 ±0.019	+0.666 ±0.021	+45 ±0
Average	+0.218 ±0.163	+0.075 ±0.126	-0.248 ±0.110	+0.425 ±0.193	+0.278 ±0.130	+33 ±0
Ring 1 Location 1 Power Series						
Depth (in)	Sx (ksi)	Sy (ksi)	Txy (ksi)	Smax (ksi)	Tmax (ksi)	beta (deg)
0.000	+0.347 ±0.013	+0.016 ±0.005	+0.009 ±0.003	+0.347 ±0.014	+0.166 ±0.004	-2 ±1
0.005	+0.294 ±0.010	+0.049 ±0.003	-0.007 ±0.001	+0.294 ±0.010	+0.122 ±0.004	+2 ±1
0.010	+0.240 ±0.008	+0.082 ±0.003	-0.023 ±0.001	+0.243 ±0.007	+0.082 ±0.002	+8 ±1
0.015	+0.186 ±0.007	+0.116 ±0.005	-0.039 ±0.002	+0.203 ±0.006	+0.052 ±0.001	+24 ±1
0.020	+0.133 ±0.008	+0.149 ±0.007	-0.055 ±0.003	+0.196 ±0.005	+0.055 ±0.003	+49 ±0
0.025	+0.079 ±0.011	+0.182 ±0.009	-0.071 ±0.004	+0.218 ±0.006	+0.087 ±0.004	+63 ±1
0.030	+0.025 ±0.014	+0.215 ±0.012	-0.086 ±0.006	+0.249 ±0.008	+0.128 ±0.005	+69 ±1
Ring 1 Location 2 Power Series						
Depth (in)	Sx (ksi)	Sy (ksi)	Txy (ksi)	Smax (ksi)	Tmax (ksi)	beta (deg)
0.000	-0.125 ±0.005	+0.040 ±0.004	-0.449 ±0.014	+0.414 ±0.010	+0.457 ±0.015	+50 ±0
0.005	-0.048 ±0.003	+0.061 ±0.003	-0.278 ±0.009	+0.289 ±0.006	+0.283 ±0.008	+51 ±1
0.010	+0.029 ±0.002	+0.082 ±0.003	-0.106 ±0.004	+0.165 ±0.002	+0.110 ±0.004	+52 ±0
0.015	+0.106 ±0.004	+0.103 ±0.004	+0.065 ±0.005	+0.170 ±0.009	+0.065 ±0.005	-44 ±0
0.020	+0.183 ±0.008	+0.125 ±0.005	+0.237 ±0.010	+0.393 ±0.017	+0.238 ±0.011	-41 ±1
0.025	+0.260 ±0.011	+0.146 ±0.007	+0.408 ±0.016	+0.615 ±0.025	+0.412 ±0.016	-41 ±0
0.030	+0.338 ±0.013	+0.167 ±0.009	+0.579 ±0.022	+0.838 ±0.033	+0.586 ±0.022	-41 ±0
Ring 1 Location 3 Power Series						
Depth (in)	Sx (ksi)	Sy (ksi)	Txy (ksi)	Smax (ksi)	Tmax (ksi)	beta (deg)
0.000	+0.751 ±0.026	-0.603 ±0.019	-0.449 ±0.016	+0.887 ±0.016	+0.813 ±0.006	+17 ±1
0.005	+0.583 ±0.019	-0.359 ±0.011	-0.363 ±0.012	+0.706 ±0.011	+0.594 ±0.005	+19 ±1
0.010	+0.414 ±0.013	-0.114 ±0.005	-0.276 ±0.009	+0.532 ±0.006	+0.383 ±0.004	+23 ±1
0.015	+0.246 ±0.010	+0.130 ±0.007	-0.190 ±0.007	+0.387 ±0.003	+0.199 ±0.006	+37 ±1
0.020	+0.077 ±0.011	+0.374 ±0.016	-0.104 ±0.007	+0.407 ±0.011	+0.182 ±0.002	+72 ±2
0.025	-0.092 ±0.016	+0.619 ±0.023	-0.018 ±0.010	+0.619 ±0.023	+0.356 ±0.003	+89 ±1
0.030	-0.260 ±0.023	+0.863 ±0.032	+0.068 ±0.013	+0.867 ±0.034	+0.566 ±0.006	-87 ±1

Ring 1 Location 4 Power Series											
Depth (in)	Sx (ksi)		Sy (ksi)		Txy (ksi)		Smax (ksi)		Tmax (ksi)		beta (deg)
0.000	+0.287	±0.017	+0.479	±0.017	-1.232	±0.039	+1.618	±0.022	+1.235	±0.039	+47 ±0
0.005	+0.327	±0.014	+0.361	±0.012	-0.761	±0.024	+1.105	±0.011	+0.761	±0.024	+46 ±0
0.010	+0.366	±0.012	+0.243	±0.008	-0.290	±0.010	+0.601	±0.001	+0.296	±0.010	+39 ±0
0.015	+0.406	±0.014	+0.124	±0.006	+0.181	±0.013	+0.494	±0.023	+0.229	±0.013	-26 ±1
0.020	+0.445	±0.019	+0.006	±0.008	+0.652	±0.028	+0.913	±0.042	+0.688	±0.028	-36 ±0
0.025	+0.485	±0.025	-0.112	±0.012	+1.123	±0.043	+1.348	±0.062	+1.162	±0.043	-38 ±1
0.030	+0.524	±0.031	-0.230	±0.017	+1.594	±0.059	+1.785	±0.083	+1.638	±0.059	-38 ±0
Ring 1 Location 5 Power Series											
Depth (in)	Sx (ksi)		Sy (ksi)		Txy (ksi)		Smax (ksi)		Tmax (ksi)		beta (deg)
0.000	-0.227	±0.012	-0.270	±0.013	-1.048	±0.042	+0.800	±0.030	+1.049	±0.042	+44 ±0
0.005	-0.059	±0.004	-0.085	±0.005	-0.846	±0.029	+0.774	±0.024	+0.846	±0.029	+45 ±0
0.010	+0.109	±0.005	+0.100	±0.005	-0.644	±0.020	+0.748	±0.015	+0.644	±0.020	+45 ±0
0.015	+0.276	±0.013	+0.284	±0.013	-0.441	±0.019	+0.721	±0.007	+0.441	±0.019	+45 ±0
0.020	+0.444	±0.020	+0.469	±0.021	-0.239	±0.029	+0.696	±0.008	+0.239	±0.029	+47 ±1
0.025	+0.611	±0.028	+0.654	±0.030	-0.036	±0.042	+0.675	±0.009	+0.042	±0.039	+60 ±1
0.030											
Ring 1 Average Power Series											
Depth (in)	Sx (ksi)		Sy (ksi)		Txy (ksi)		Smax (ksi)		Tmax (ksi)		beta (deg)
0.000	+0.207	±0.015	+0.068	±0.012	-0.634	±0.023	+0.813	±0.018	+0.744	±0.021	+31 ±0
0.005	+0.219	±0.010	+0.005	±0.007	-0.451	±0.015	+0.634	±0.012	+0.521	±0.014	+33 ±1
0.010	+0.232	±0.008	+0.079	±0.005	-0.268	±0.009	+0.458	±0.006	+0.303	±0.008	+33 ±0
0.015	+0.244	±0.010	+0.151	±0.007	-0.085	±0.009	+0.395	±0.010	+0.197	±0.009	+7 ±1
0.020	+0.256	±0.013	+0.225	±0.011	+0.098	±0.015	+0.521	±0.017	+0.280	±0.015	+18 ±1
0.025	+0.269	±0.018	+0.298	±0.016	+0.281	±0.023	+0.695	±0.025	+0.412	±0.021	+27 ±1
0.030	+0.157	±0.020	+0.254	±0.018	+0.539	±0.025	+0.935	±0.040	+0.730	±0.023	-24 ±1

LOW BLAST PROFILE

Ring 2 Uniform Stresses											
Location	Sx (ksi)		Sy (ksi)		Txy (ksi)		Smax (ksi)		Tmax (ksi)		beta (deg)
1	+0.362	±0.011	+0.288	±0.009	+0.105	±0.003	+0.437	±0.014	+0.111	±0.004	-35 ±0
2	+0.293	±0.010	+0.132	±0.005	-0.129	±0.004	+0.365	±0.005	+0.152	±0.002	+29 ±1
3	+0.373	±0.012	+0.299	±0.010	-0.047	±0.002	+0.396	±0.011	+0.060	±0.001	+26 ±1
4	+0.627	±0.020	+0.297	±0.010	-0.101	±0.004	+0.656	±0.018	+0.193	±0.003	+16 ±1
5	+0.649	±0.021	+0.656	±0.021	+0.004	±0.000	+0.658	±0.021	+0.005	±0.001	-66 ±1
Average	+0.461	±0.147	+0.334	±0.081	-0.034	±0.104	+0.502	±0.132	+0.104	±0.057	-6 ±0

Ring 2 Location 1 Power Series						
Depth (in)	Sx (ksi)	Sy (ksi)	Txy (ksi)	Smax (ksi)	Tmax (ksi)	beta (deg)
0.000	+0.438 ±0.019	+0.691 ±0.024	+0.414 ±0.013	+0.998 ±0.034	+0.433 ±0.013	-54 ±1
0.005	+0.393 ±0.015	+0.496 ±0.017	+0.272 ±0.008	+0.722 ±0.024	+0.277 ±0.009	-50 ±0
0.010	+0.349 ±0.012	+0.301 ±0.010	+0.130 ±0.004	+0.457 ±0.015	+0.132 ±0.004	-40 ±0
0.015	+0.304 ±0.011	+0.106 ±0.007	-0.012 ±0.004	+0.305 ±0.011	+0.100 ±0.002	+5 ±1
0.020	+0.259 ±0.014	-0.090 ±0.011	-0.155 ±0.008	+0.318 ±0.009	+0.233 ±0.004	+21 ±1
0.025	+0.214 ±0.019	-0.285 ±0.017	-0.297 ±0.012	+0.352 ±0.009	+0.388 ±0.009	+25 ±1
0.030	+0.170 ±0.024	-0.480 ±0.024	-0.439 ±0.017	+0.391 ±0.010	+0.546 ±0.014	+27 ±1
Ring 2 Location 2 Power Series						
Depth (in)	Sx (ksi)	Sy (ksi)	Txy (ksi)	Smax (ksi)	Tmax (ksi)	beta (deg)
0.000	+0.295 ±0.014	-0.161 ±0.010	+0.292 ±0.014	+0.437 ±0.024	+0.370 ±0.013	-26 ±1
0.005	+0.300 ±0.011	-0.020 ±0.004	+0.098 ±0.006	+0.328 ±0.014	+0.188 ±0.006	-16 ±1
0.010	+0.305 ±0.010	+0.120 ±0.004	-0.095 ±0.004	+0.346 ±0.006	+0.133 ±0.001	+23 ±1
0.015	+0.310 ±0.011	+0.261 ±0.010	-0.289 ±0.011	+0.576 ±0.001	+0.290 ±0.011	+43 ±1
0.020	+0.315 ±0.014	+0.401 ±0.015	-0.483 ±0.019	+0.843 ±0.004	+0.485 ±0.019	+48 ±1
0.025	+0.320 ±0.018	+0.541 ±0.022	-0.676 ±0.027	+1.116 ±0.007	+0.685 ±0.026	+50 ±1
0.030	+0.325 ±0.022	+0.682 ±0.027	-0.870 ±0.034	+1.392 ±0.009	+0.888 ±0.033	+51 ±1
Ring 2 Location 3 Power Series						
Depth (in)	Sx (ksi)	Sy (ksi)	Txy (ksi)	Smax (ksi)	Tmax (ksi)	beta (deg)
0.000	+0.057 ±0.017	+0.328 ±0.015	-0.006 ±0.003	+0.328 ±0.015	+0.136 ±0.001	+89 ±1
0.005	+0.208 ±0.011	+0.321 ±0.012	-0.025 ±0.002	+0.326 ±0.011	+0.061 ±0.001	+78 ±1
0.010	+0.360 ±0.012	+0.313 ±0.010	-0.044 ±0.001	+0.386 ±0.010	+0.050 ±0.001	+31 ±1
0.015	+0.511 ±0.018	+0.306 ±0.011	-0.063 ±0.002	+0.529 ±0.016	+0.120 ±0.002	+16 ±1
0.020	+0.663 ±0.026	+0.299 ±0.014	-0.082 ±0.004	+0.681 ±0.024	+0.200 ±0.004	+12 ±1
0.025	+0.814 ±0.035	+0.291 ±0.018	-0.102 ±0.005	+0.833 ±0.033	+0.281 ±0.006	+11 ±1
0.030	+0.966 ±0.043	+0.284 ±0.022	-0.121 ±0.007	+0.987 ±0.041	+0.362 ±0.008	+10 ±1
Ring 2 Location 4 Power Series						
Depth (in)	Sx (ksi)	Sy (ksi)	Txy (ksi)	Smax (ksi)	Tmax (ksi)	beta (deg)
0.000	+0.964 ±0.036	+0.131 ±0.014	-0.038 ±0.005	+0.965 ±0.036	+0.418 ±0.011	+3 ±1
0.005	+0.805 ±0.028	+0.204 ±0.010	-0.067 ±0.004	+0.813 ±0.026	+0.308 ±0.008	+6 ±1
0.010	+0.647 ±0.021	+0.277 ±0.009	-0.096 ±0.003	+0.670 ±0.019	+0.208 ±0.004	+14 ±1
0.015	+0.489 ±0.017	+0.350 ±0.013	-0.124 ±0.005	+0.562 ±0.013	+0.142 ±0.003	+30 ±1
0.020	+0.331 ±0.021	+0.423 ±0.018	-0.153 ±0.006	+0.537 ±0.013	+0.160 ±0.006	+53 ±0
0.025	+0.173 ±0.028	+0.496 ±0.024	-0.182 ±0.008	+0.578 ±0.018	+0.243 ±0.008	+66 ±1
0.030	+0.014 ±0.037	+0.569 ±0.030	-0.211 ±0.011	+0.640 ±0.024	+0.348 ±0.009	+71 ±1

Ring 2 Location 5 Power Series						
Depth (in)	Sx (ksi)	Sy (ksi)	Txy (ksi)	Smax (ksi)	Tmax (ksi)	beta (deg)
0.000	+0.922 ±0.036	+0.603 ±0.031	-0.282 ±0.010	+1.086 ±0.027	+0.324 ±0.008	+30 ±1
0.005	+0.792 ±0.028	+0.623 ±0.024	-0.150 ±0.005	+0.880 ±0.022	+0.172 ±0.004	+30 ±1
0.010	+0.662 ±0.021	+0.643 ±0.021	-0.019 ±0.002	+0.674 ±0.020	+0.021 ±0.002	+32 ±2
0.015	+0.532 ±0.019	+0.663 ±0.023	+0.113 ±0.005	+0.728 ±0.027	+0.130 ±0.006	-60 ±0
0.020	+0.402 ±0.023	+0.683 ±0.031	+0.244 ±0.010	+0.824 ±0.037	+0.282 ±0.011	-60 ±0
0.025	+0.272 ±0.031	+0.703 ±0.040	+0.375 ±0.015	+0.920 ±0.050	+0.433 ±0.015	-60 ±0
0.030	+0.142 ±0.040	+0.723 ±0.050	+0.507 ±0.019	+1.017 ±0.064	+0.584 ±0.019	-60 ±0
Ring 2 Average Power Series						
Depth (in)	Sx (ksi)	Sy (ksi)	Txy (ksi)	Smax (ksi)	Tmax (ksi)	beta (deg)
0.000	+0.535 ±0.024	+0.318 ±0.019	0.076 ±0.009	+0.763 ±0.027	+0.336 ±0.009	+8 ±1
0.005	+0.500 ±0.019	+0.325 ±0.013	0.026 ±0.005	+0.614 ±0.019	+0.201 ±0.006	+10 ±1
0.010	+0.465 ±0.015	+0.331 ±0.011	-0.025 ±0.003	+0.507 ±0.014	+0.109 ±0.002	+12 ±1
0.015	+0.429 ±0.015	+0.337 ±0.013	-0.075 ±0.005	+0.540 ±0.014	+0.156 ±0.005	7 ±1
0.020	+0.394 ±0.020	+0.343 ±0.018	-0.126 ±0.009	+0.641 ±0.017	+0.272 ±0.009	15 ±1
0.025	+0.359 ±0.026	+0.349 ±0.024	-0.176 ±0.013	+0.760 ±0.023	+0.406 ±0.013	18 ±1
0.030	+0.323 ±0.033	+0.356 ±0.031	-0.227 ±0.018	+0.885 ±0.030	+0.546 ±0.017	20 ±1

HIGH BLAST PROFILE

Ring 3 Uniform Stresses						
Location	Sx (ksi)	Sy (ksi)	Txy (ksi)	Smax (ksi)	Tmax (ksi)	beta (deg)
1	+0.126 ±0.004	+0.146 ±0.005	-0.134 ±0.004	+0.271 ±0.001	+0.135 ±0.004	+47 ±0
2	+0.275 ±0.009	+0.524 ±0.016	+0.102 ±0.003	+0.560 ±0.018	+0.161 ±0.005	-70 ±0
3	+0.402 ±0.013	+0.226 ±0.010	-0.122 ±0.004	+0.464 ±0.009	+0.151 ±0.002	+27 ±1
4	+0.454 ±0.014	+0.339 ±0.011	-0.137 ±0.004	+0.545 ±0.009	+0.149 ±0.003	+34 ±1
5	+0.172 ±0.006	+0.096 ±0.003	-0.082 ±0.003	+0.224 ±0.003	+0.090 ±0.002	+33 ±1
Average	+0.286 ±0.146	+0.266 ±0.164	-0.075 ±0.117	+0.413 ±0.133	+0.137 ±0.011	+14 ±1
Ring 3 Location 1 Power Series						
Depth (in)	Sx (ksi)	Sy (ksi)	Txy (ksi)	Smax (ksi)	Tmax (ksi)	beta (deg)
0.000	+0.071 ±0.006	+0.086 ±0.007	-0.633 ±0.020	+0.711 ±0.014	+0.633 ±0.020	+45 ±0
0.005	+0.099 ±0.004	+0.116 ±0.005	-0.403 ±0.014	+0.511 ±0.008	+0.404 ±0.012	+46 ±0
0.010	+0.127 ±0.004	+0.146 ±0.005	-0.174 ±0.006	+0.311 ±0.002	+0.174 ±0.006	+47 ±1
0.015	+0.155 ±0.006	+0.176 ±0.006	+0.056 ±0.006	+0.222 ±0.012	+0.057 ±0.006	-50 ±1
0.020	+0.183 ±0.008	+0.206 ±0.009	+0.285 ±0.013	+0.480 ±0.021	+0.285 ±0.013	-46 ±0
0.025	+0.211 ±0.010	+0.236 ±0.011	+0.515 ±0.020	+0.738 ±0.031	+0.515 ±0.020	-46 ±0
0.030	+0.239 ±0.013	+0.266 ±0.014	+0.744 ±0.028	+0.996 ±0.042	+0.744 ±0.028	-46 ±0

Ring 3 Location 2 Power Series						
Depth (in)	Sx (ksi)	Sy (ksi)	Txy (ksi)	Smax (ksi)	Tmax (ksi)	beta (deg)
0.000	+0.613 ±0.022	+1.121 ±0.038	+0.361 ±0.012	+1.308 ±0.045	+0.441 ±0.015	-63 ±1
0.005	+0.439 ±0.015	+0.827 ±0.027	+0.242 ±0.007	+0.943 ±0.031	+0.310 ±0.010	-64 ±0
0.010	+0.264 ±0.009	+0.534 ±0.018	+0.123 ±0.004	+0.581 ±0.019	+0.182 ±0.006	-69 ±0
0.015	+0.089 ±0.007	+0.240 ±0.012	+0.003 ±0.003	+0.240 ±0.012	+0.076 ±0.003	-89 ±1
0.020	-0.086 ±0.010	-0.054 ±0.016	-0.116 ±0.006	+0.047 ±0.008	+0.117 ±0.006	+49 ±1
0.025	-0.261 ±0.016	-0.347 ±0.026	-0.235 ±0.010	-0.065 ±0.010	+0.239 ±0.011	+40 ±1
0.030	-0.436 ±0.023	-0.641 ±0.036	-0.354 ±0.015	-0.169 ±0.015	+0.369 ±0.015	+37 ±0
Ring 3 Location 3 Power Series						
Depth (in)	Sx (ksi)	Sy (ksi)	Txy (ksi)	Smax (ksi)	Tmax (ksi)	beta (deg)
0.000	+0.644 ±0.024	+0.286 ±0.013	-0.421 ±0.013	+0.922 ±0.009	+0.457 ±0.010	+33 ±1
0.005	+0.527 ±0.018	+0.251 ±0.009	-0.283 ±0.009	+0.704 ±0.008	+0.315 ±0.006	+32 ±1
0.010	+0.409 ±0.013	+0.216 ±0.007	-0.146 ±0.005	+0.488 ±0.008	+0.175 ±0.002	+28 ±1
0.015	+0.292 ±0.011	+0.181 ±0.007	-0.008 ±0.004	+0.292 ±0.011	+0.056 ±0.002	+4 ±2
0.020	+0.174 ±0.013	+0.146 ±0.009	+0.129 ±0.007	+0.290 ±0.018	+0.130 ±0.007	-42 ±0
0.025	+0.057 ±0.018	+0.111 ±0.012	+0.266 ±0.012	+0.352 ±0.026	+0.268 ±0.011	-48 ±1
0.030	-0.061 ±0.024	+0.076 ±0.016	+0.404 ±0.016	+0.417 ±0.035	+0.410 ±0.015	-50 ±1
Ring 3 Location 4 Power Series						
Depth (in)	Sx (ksi)	Sy (ksi)	Txy (ksi)	Smax (ksi)	Tmax (ksi)	beta (deg)
0.000	+0.370 ±0.021	+0.237 ±0.016	-0.423 ±0.014	+0.732 ±0.005	+0.428 ±0.013	+41 ±1
0.005	+0.413 ±0.015	+0.288 ±0.012	-0.291 ±0.009	+0.648 ±0.006	+0.298 ±0.008	+39 ±0
0.010	+0.455 ±0.014	+0.339 ±0.010	-0.160 ±0.005	+0.567 ±0.008	+0.170 ±0.004	+35 ±1
0.015	+0.497 ±0.017	+0.389 ±0.014	-0.028 ±0.004	+0.504 ±0.015	+0.061 ±0.000	+14 ±2
0.020	+0.539 ±0.023	+0.440 ±0.019	+0.103 ±0.006	+0.604 ±0.027	+0.114 ±0.007	-32 ±0
0.025	+0.581 ±0.030	+0.491 ±0.024	+0.235 ±0.011	+0.775 ±0.037	+0.239 ±0.011	-40 ±1
0.030	+0.623 ±0.037	+0.542 ±0.030	+0.366 ±0.015	+0.951 ±0.048	+0.368 ±0.016	-42 ±0
Ring 3 Location 5 Power Series						
Depth (in)	Sx (ksi)	Sy (ksi)	Txy (ksi)	Smax (ksi)	Tmax (ksi)	beta (deg)
0.000	-0.055 ±0.010	+0.010 ±0.005	-0.381 ±0.012	+0.360 ±0.006	+0.383 ±0.013	+47 ±1
0.005	+0.055 ±0.005	+0.056 ±0.003	-0.244 ±0.008	+0.299 ±0.004	+0.244 ±0.008	+45 ±0
0.010	+0.166 ±0.006	+0.102 ±0.003	-0.106 ±0.004	+0.245 ±0.001	+0.111 ±0.003	+37 ±1
0.015	+0.277 ±0.010	+0.148 ±0.005	+0.032 ±0.004	+0.285 ±0.011	+0.072 ±0.004	-13 ±1
0.020	+0.388 ±0.015	+0.194 ±0.008	+0.169 ±0.008	+0.486 ±0.020	+0.195 ±0.008	-30 ±0
0.025	+0.499 ±0.020	+0.240 ±0.011	+0.307 ±0.014	+0.703 ±0.028	+0.333 ±0.013	-34 ±0
0.030	+0.610 ±0.026	+0.287 ±0.013	+0.444 ±0.017	+0.921 ±0.037	+0.473 ±0.018	-35 ±0

Ring 3 Average Power Series											
Depth (in)	Sx (ksi)		Sy (ksi)		Txy (ksi)		Smax (ksi)		Tmax (ksi)		beta (deg)
0.000	+0.329	±0.017	+0.348	±0.016	-0.299	±0.014	+0.807	±0.016	+0.468	±0.014	+21 ±1
0.005	+0.307	±0.011	+0.308	±0.011	-0.196	±0.009	+0.621	±0.011	+0.314	±0.009	+20 ±0
0.010	+0.284	±0.009	+0.267	±0.009	-0.093	±0.005	+0.438	±0.008	+0.162	±0.004	+16 ±1
0.015	+0.262	±0.010	+0.227	±0.009	+0.011	±0.004	+0.309	±0.012	+0.064	±0.003	-27 ±1
0.020	+0.240	±0.014	+0.186	±0.012	+0.114	±0.008	+0.381	±0.019	+0.168	±0.008	-20 ±0
0.025	+0.217	±0.019	+0.146	±0.017	+0.218	±0.013	+0.501	±0.026	+0.319	±0.013	-26 ±1
0.030	+0.195	±0.025	+0.106	±0.022	+0.321	±0.018	+0.623	±0.035	+0.473	±0.018	-27 ±0

STANDARD SURFACE - 1 Year Old

Big Ring 4 Uniform Stresses											
Depth (in)	Sx (ksi)		Sy (ksi)		Txy (ksi)		Smax (ksi)		Tmax (ksi)		beta (deg)
1	+0.288	±0.009	+0.238	±0.008	+0.085	±0.003	+0.352	±0.011	+0.089	±0.003	-37 ±0
2	+0.132	±0.004	+0.119	±0.004	-0.019	±0.001	+0.146	±0.003	+0.020	±0.001	+36 ±1
3	+0.052	±0.002	+0.128	±0.004	+0.036	±0.002	+0.142	±0.005	+0.052	±0.002	-68 ±0
4	+0.132	±0.004	+0.155	±0.005	+0.113	±0.004	+0.257	±0.008	+0.113	±0.004	-48 ±0
5	+0.355	±0.012	+0.337	±0.011	+0.106	±0.004	+0.453	±0.014	+0.107	±0.004	-43 ±0
Average	+0.160	±0.125	+0.163	±0.092	+0.054	±0.055	+0.225	±0.134	+0.064	±0.039	-32 ±0

Big Ring 4 Location 1 Power Series											
Depth (in)	Sx (ksi)		Sy (ksi)		Txy (ksi)		Smax (ksi)		Tmax (ksi)		beta (deg)
0.000	+0.587	±0.021	+0.407	±0.016	+0.253	±0.009	+0.766	±0.027	+0.269	±0.009	-35 ±0
0.005	+0.440	±0.015	+0.320	±0.011	+0.176	±0.006	+0.566	±0.019	+0.186	±0.006	-36 ±0
0.010	+0.293	±0.010	+0.233	±0.008	+0.098	±0.004	+0.366	±0.012	+0.103	±0.003	-37 ±0
0.015	+0.146	±0.007	+0.146	±0.006	+0.021	±0.002	+0.167	±0.008	+0.021	±0.002	-45 ±1
0.020	0.000	±0.009	+0.059	±0.008	-0.057	±0.004	+0.093	±0.005	+0.064	±0.004	+59 ±1
0.025	-0.147	±0.014	-0.028	±0.012	-0.134	±0.007	+0.059	±0.007	+0.147	±0.007	+57 ±0
0.030	-0.294	±0.020	-0.114	±0.016	-0.212	±0.009	+0.026	±0.009	+0.230	±0.009	+57 ±1

Big Ring 4 Location 2 Power Series											
Depth (in)	Sx (ksi)		Sy (ksi)		Txy (ksi)		Smax (ksi)		Tmax (ksi)		beta (deg)
0.000	-0.056	±0.008	-0.003	±0.006	-0.048	±0.003	+0.026	±0.004	+0.055	±0.003	+59 ±1
0.005	+0.037	±0.004	+0.060	±0.004	-0.035	±0.002	+0.085	±0.002	+0.037	±0.002	+54 ±0
0.010	+0.130	±0.004	+0.122	±0.004	-0.021	±0.001	+0.148	±0.003	+0.022	±0.001	+40 ±0
0.015	+0.223	±0.008	+0.185	±0.007	-0.008	±0.001	+0.224	±0.008	+0.021	±0.001	+12 ±2
0.020	+0.315	±0.012	+0.247	±0.010	+0.005	±0.002	+0.316	±0.012	+0.035	±0.002	-4 ±2
0.025	+0.408	±0.016	+0.309	±0.013	+0.019	±0.003	+0.411	±0.018	+0.053	±0.003	-10 ±1
0.030	+0.501	±0.021	+0.372	±0.016	+0.032	±0.004	+0.508	±0.022	+0.072	±0.004	-13 ±1

Big Ring 4 Location 3 Power Series						
Depth (in)	Sx (ksi)	Sy (ksi)	Txy (ksi)	Smax (ksi)	Tmax (ksi)	beta (deg)
0.000	-0.008 ±0.004	+0.117 ±0.007	+0.119 ±0.004	+0.188 ±0.009	+0.134 ±0.005	-59 ±0
0.005	+0.021 ±0.002	+0.123 ±0.005	+0.080 ±0.003	+0.167 ±0.007	+0.095 ±0.003	-61 ±0
0.010	+0.050 ±0.002	+0.130 ±0.004	+0.042 ±0.002	+0.148 ±0.005	+0.058 ±0.002	-67 ±0
0.015	+0.079 ±0.003	+0.137 ±0.005	+0.004 ±0.001	+0.137 ±0.005	+0.029 ±0.001	-86 ±1
0.020	+0.109 ±0.005	+0.144 ±0.007	-0.034 ±0.003	+0.165 ±0.004	+0.038 ±0.002	+59 ±2
0.025	+0.138 ±0.006	+0.150 ±0.009	-0.072 ±0.004	+0.217 ±0.004	+0.073 ±0.004	+47 ±1
0.030	+0.167 ±0.008	+0.157 ±0.011	-0.111 ±0.006	+0.273 ±0.004	+0.111 ±0.006	+44 ±1
Big Ring 4 Location 4 Power Series						
Depth (in)	Sx (ksi)	Sy (ksi)	Txy (ksi)	Smax (ksi)	Tmax (ksi)	beta (deg)
0.000	+0.272 ±0.010	+0.162 ±0.008	+0.343 ±0.011	+0.564 ±0.020	+0.347 ±0.011	-40 ±1
0.005	+0.204 ±0.007	+0.156 ±0.006	+0.237 ±0.007	+0.418 ±0.014	+0.238 ±0.008	-42 ±0
0.010	+0.137 ±0.005	+0.149 ±0.005	+0.131 ±0.004	+0.275 ±0.009	+0.131 ±0.004	-46 ±0
0.015	+0.070 ±0.004	+0.143 ±0.006	+0.025 ±0.003	+0.151 ±0.007	+0.044 ±0.003	-73 ±2
0.020	+0.003 ±0.005	+0.136 ±0.007	-0.081 ±0.006	+0.174 ±0.003	+0.104 ±0.004	+65 ±1
0.025	-0.064 ±0.007	+0.130 ±0.009	-0.186 ±0.009	+0.243 ±0.001	+0.210 ±0.007	+59 ±1
0.030	-0.131 ±0.010	+0.123 ±0.011	-0.292 ±0.012	+0.314 ±0.001	+0.319 ±0.011	+57 ±1
Big Ring 4 Location 5 Power Series						
Depth (in)	Sx (ksi)	Sy (ksi)	Txy (ksi)	Smax (ksi)	Tmax (ksi)	beta (deg)
0.000	+0.464 ±0.020	+0.430 ±0.018	+0.036 ±0.005	+0.487 ±0.023	+0.040 ±0.005	-32 ±1
0.005	+0.410 ±0.015	+0.383 ±0.014	+0.068 ±0.004	+0.466 ±0.018	+0.070 ±0.004	-39 ±1
0.010	+0.356 ±0.011	+0.337 ±0.010	+0.101 ±0.003	+0.447 ±0.015	+0.101 ±0.003	-42 ±0
0.015	+0.302 ±0.011	+0.290 ±0.011	+0.133 ±0.005	+0.429 ±0.015	+0.133 ±0.005	-44 ±0
0.020	+0.247 ±0.014	+0.244 ±0.013	+0.165 ±0.007	+0.411 ±0.020	+0.165 ±0.007	-45 ±0
0.025	+0.193 ±0.018	+0.197 ±0.017	+0.198 ±0.009	+0.393 ±0.026	+0.198 ±0.009	-45 ±0
0.030	+0.139 ±0.023	+0.151 ±0.022	+0.230 ±0.012	+0.375 ±0.034	+0.230 ±0.012	-46 ±0
Big Ring 4 Average Power Series						
Depth (in)	Sx (ksi)	Sy (ksi)	Txy (ksi)	Smax (ksi)	Tmax (ksi)	beta (deg)
0.000	+0.252 ±0.013	+0.223 ±0.011	+0.141 ±0.006	+0.406 ±0.017	+0.169 ±0.007	-21 ±1
0.005	+0.222 ±0.009	+0.208 ±0.008	+0.105 ±0.004	+0.340 ±0.012	+0.125 ±0.005	-25 ±0
0.010	+0.193 ±0.006	+0.194 ±0.006	+0.070 ±0.003	+0.277 ±0.009	+0.083 ±0.003	-30 ±0
0.015	+0.164 ±0.007	+0.180 ±0.007	+0.035 ±0.002	+0.222 ±0.009	+0.050 ±0.002	-47 ±1
0.020	+0.135 ±0.009	+0.166 ±0.009	+0.000 ±0.004	+0.232 ±0.009	+0.081 ±0.004	+27 ±1
0.025	+0.106 ±0.012	+0.152 ±0.012	-0.035 ±0.006	+0.265 ±0.011	+0.136 ±0.006	+22 ±1
0.030	+0.076 ±0.016	+0.138 ±0.015	-0.071 ±0.009	+0.299 ±0.014	+0.192 ±0.006	+20 ±1

"ZERO" COMPRESSION PLAQUE

Plaque Uniform Stresses						
Location	Sx (ksi)	Sy (ksi)	Txy (ksi)	Smax (ksi)	Tmax (ksi)	beta (deg)
1	+0.188 ±0.006	+0.115 ±0.004	+0.115 ±0.004	+0.272 ±0.009	+0.121 ±0.004	-36 ±0
2	+0.057 ±0.002	-0.200 ±0.006	-0.166 ±0.006	+0.139 ±0.002	+0.210 ±0.006	+26 ±0
3	-0.021 ±0.001	-0.116 ±0.004	+0.044 ±0.002	-0.004 ±0.002	+0.065 ±0.000	-21 ±1
4	+0.111 ±0.004	+0.043 ±0.002	-0.099 ±0.003	+0.181 ±0.001	+0.105 ±0.003	+35 ±1
5	+0.077 ±0.003	+0.041 ±0.002	+0.001 ±0.001	+0.077 ±0.003	+0.018 ±0.001	-2 ±1
Average	+0.069 ±0.106	-0.020 ±0.163	-0.018 ±0.146	+0.111 ±0.138	+0.087 ±0.073	0 ±1

Plaque Location 1 Power Series						
Depth (in)	Sx (ksi)	Sy (ksi)	Txy (ksi)	Smax (ksi)	Tmax (ksi)	beta (deg)
0.000	+0.377 ±0.015	+0.331 ±0.013	+0.165 ±0.008	+0.521 ±0.021	+0.167 ±0.008	-41 ±0
0.005	+0.269 ±0.010	+0.209 ±0.007	+0.139 ±0.005	+0.381 ±0.014	+0.142 ±0.005	-39 ±0
0.010	+0.161 ±0.005	+0.086 ±0.004	+0.112 ±0.004	+0.241 ±0.008	+0.118 ±0.004	-36 ±0
0.015	+0.053 ±0.005	-0.036 ±0.005	+0.085 ±0.004	+0.104 ±0.009	+0.096 ±0.003	-31 ±1
0.020	-0.055 ±0.010	-0.159 ±0.010	+0.058 ±0.006	-0.029 ±0.015	+0.078 ±0.005	-24 ±2
0.025	-0.163 ±0.015	-0.282 ±0.015	+0.032 ±0.009	-0.155 ±0.019	+0.067 ±0.005	-14 ±3
0.030						

Plaque Location 2 Power Series						
Depth (in)	Sx (ksi)	Sy (ksi)	Txy (ksi)	Smax (ksi)	Tmax (ksi)	beta (deg)
0.000	+0.001 ±0.005	-0.765 ±0.027	-0.515 ±0.018	+0.261 ±0.005	+0.642 ±0.021	+27 ±0
0.005	+0.043 ±0.002	-0.453 ±0.015	-0.331 ±0.011	+0.208 ±0.004	+0.413 ±0.013	+27 ±1
0.010	+0.084 ±0.003	-0.142 ±0.006	-0.146 ±0.005	+0.156 ±0.001	+0.184 ±0.005	+26 ±0
0.015	+0.126 ±0.005	+0.169 ±0.012	+0.039 ±0.007	+0.192 ±0.016	+0.045 ±0.007	-59 ±0
0.020	+0.167 ±0.009	+0.480 ±0.024	+0.224 ±0.013	+0.597 ±0.031	+0.273 ±0.015	-62 ±1
0.025	+0.209 ±0.011	+0.791 ±0.036	+0.409 ±0.020	+1.002 ±0.047	+0.502 ±0.023	-63 ±0
0.030						

Plaque Location 3 Power Series						
Depth (in)	Sx (ksi)	Sy (ksi)	Txy (ksi)	Smax (ksi)	Tmax (ksi)	beta (deg)
0.000	-0.211 ±0.008	-0.495 ±0.016	+0.026 ±0.003	-0.209 ±0.009	+0.144 ±0.004	-5 ±1
0.005	-0.112 ±0.004	-0.309 ±0.010	+0.035 ±0.002	-0.106 ±0.005	+0.104 ±0.002	-10 ±1
0.010	-0.013 ±0.002	-0.123 ±0.005	+0.043 ±0.002	+0.001 ±0.003	+0.070 ±0.001	-19 ±1
0.015	+0.085 ±0.004	+0.062 ±0.005	+0.051 ±0.002	+0.126 ±0.006	+0.052 ±0.002	-39 ±1
0.020	+0.184 ±0.007	+0.248 ±0.011	+0.059 ±0.003	+0.283 ±0.012	+0.067 ±0.004	-59 ±0
0.025	+0.283 ±0.011	+0.434 ±0.017	+0.067 ±0.004	+0.459 ±0.019	+0.101 ±0.005	-69 ±0
0.030	+0.382 ±0.014	+0.619 ±0.023	+0.075 ±0.006	+0.641 ±0.025	+0.141 ±0.007	-74 ±1

Plaque Location 4 Power Series						
Depth (in)	Sx (ksi)	Sy (ksi)	Txy (ksi)	Smax (ksi)	Tmax (ksi)	beta (deg)
0.000	+0.228 ±0.008	+0.001 ±0.003	-0.335 ±0.011	+0.468 ±0.004	+0.353 ±0.010	+36 ±1
0.005	+0.172 ±0.006	+0.019 ±0.002	-0.226 ±0.009	+0.334 ±0.003	+0.239 ±0.006	+36 ±1
0.010	+0.117 ±0.004	+0.036 ±0.002	-0.118 ±0.004	+0.201 ±0.001	+0.124 ±0.004	+35 ±1
0.015	+0.062 ±0.003	+0.054 ±0.003	-0.009 ±0.003	+0.068 ±0.000	+0.010 ±0.003	+33 ±5
0.020	+0.007 ±0.004	+0.071 ±0.004	+0.099 ±0.006	+0.143 ±0.009	+0.104 ±0.005	-54 ±0
0.025	-0.048 ±0.006	+0.088 ±0.005	+0.208 ±0.009	+0.239 ±0.014	+0.219 ±0.009	-54 ±1
0.030	-0.104 ±0.008	+0.106 ±0.006	+0.316 ±0.013	+0.334 ±0.019	+0.333 ±0.012	-54 ±1
Plaque Location 5 Power Series						
Depth (in)	Sx (ksi)	Sy (ksi)	Txy (ksi)	Smax (ksi)	Tmax (ksi)	beta (deg)
0.000	+0.132 ±0.005	+0.147 ±0.006	+0.086 ±0.004	+0.226 ±0.009	+0.086 ±0.004	-48 ±1
0.005	+0.103 ±0.004	+0.095 ±0.004	+0.047 ±0.002	+0.146 ±0.006	+0.047 ±0.002	-43 ±0
0.010	+0.075 ±0.003	+0.043 ±0.002	+0.008 ±0.001	+0.077 ±0.003	+0.018 ±0.001	-13 ±1
0.015	+0.046 ±0.002	-0.009 ±0.002	-0.031 ±0.002	+0.060 ±0.001	+0.041 ±0.001	+24 ±1
0.020	+0.017 ±0.003	-0.061 ±0.004	-0.070 ±0.003	+0.058 ±0.000	+0.080 ±0.003	+30 ±1
0.025	-0.011 ±0.005	-0.113 ±0.006	-0.109 ±0.005	+0.058 ±0.001	+0.120 ±0.005	+32 ±1
0.030	-0.040 ±0.006	-0.165 ±0.008	-0.147 ±0.007	+0.057 ±0.001	+0.160 ±0.006	+34 ±1
Plaque Average Power Series						
Depth (in)	Sx (ksi)	Sy (ksi)	Txy (ksi)	Smax (ksi)	Tmax (ksi)	beta (deg)
0.000	+0.105 ±0.008	-0.156 ±0.013	-0.115 ±0.009	+0.253 ±0.010	+0.278 ±0.009	-6 ±1
0.005	+0.095 ±0.005	-0.088 ±0.008	-0.067 ±0.006	+0.193 ±0.006	+0.189 ±0.006	-6 ±1
0.010	+0.085 ±0.003	-0.020 ±0.004	-0.020 ±0.003	+0.135 ±0.003	+0.103 ±0.003	-1 ±1
0.015	+0.074 ±0.004	+0.048 ±0.005	+0.027 ±0.004	+0.110 ±0.006	+0.049 ±0.003	-14 ±2
0.020	+0.064 ±0.007	+0.116 ±0.011	+0.074 ±0.006	+0.210 ±0.013	+0.120 ±0.006	-34 ±1
0.025	+0.054 ±0.010	+0.184 ±0.016	+0.121 ±0.009	+0.321 ±0.020	+0.202 ±0.009	-34 ±1
0.030	+0.079 ±0.009	+0.187 ±0.012	+0.081 ±0.009	+0.344 ±0.015	+0.211 ±0.008	-31 ±1

APPENDIX 2 – Shaw FBE Product Data Sheet

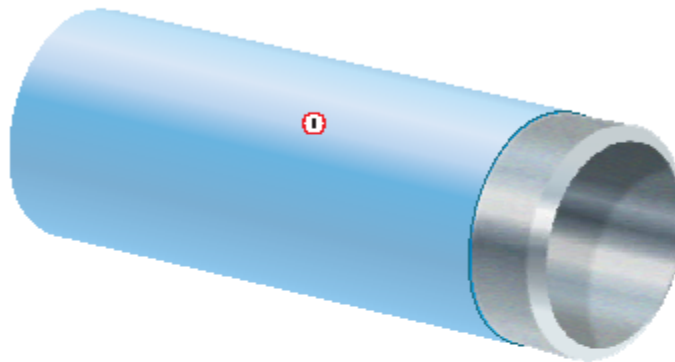


the
**GLOBAL
LEADER**
in pipe coating solutions.

FBE

PRODUCT DATA SHEET

Fusion Bonded Epoxy Powder Coating



 Fusion Bonded Epoxy



Oil & Gas pipelines



Large diameter pipelines



Small diameter pipelines



Waterworks pipelines

PRODUCT DESCRIPTION

Bredero Shaw is the world's leading provider of Fusion Bonded Epoxy (FBE) coatings. FBE is a high performance anti-corrosion coating that provides excellent protection for small and large diameter pipelines with moderate operating temperatures.

FEATURES AND BENEFITS

Long Term Corrosion Protection

FBE's excellent adhesion to steel provides superior long term corrosion resistance and protection of pipelines operating at moderate temperatures for the designed life. The superior adhesion properties of FBE also provides excellent resistance to cathodic disbondment which reduces the total cost of cathodic protection during the operation of the pipeline.

Engineered Solutions

Advanced manufacturing techniques allow FBE to be customized to your specific project. The system can be applied to various pipe diameters from 90 mm (3.5") to over 1220 mm (48"). FBE can also be applied in a wide range of thicknesses to cost effectively meet unique project specifications and performance requirements.

Good Mechanical and Chemical Protection

FBE can be applied as a dual layer product which provides tough physical properties that minimize damage during handling, transportation, installation and operation. FBE has also been designed for good chemical resistance under most soil conditions.

Global Availability

Bredero Shaw has a network of 27 coating plants strategically located across 6 continents to minimize pipe transportation costs. FBE can be manufactured in a single plant or in multiple coating plants to improve project logistics. High capacity within the Bredero Shaw plant network allows the client to benefit from single source advantages, ultimately providing more cost effective management of pipe coating needs.



www.brederoshaw.com



FBE



Americas
 Brodero Shaw
 A ShawCor Company
 3638 N. Sam Houston Pkwy E.
 Suite 300
 Houston, Texas
 77033-3400, USA
 Telephone: +1-281-886-2350
 Fax: +1-281-886-2353

Shaw Pipe
 A ShawCor Company
 Two Executive Plaza
 1824 Crowchild Trail, N.W.,
 Calgary, Alberta
 T2M 3T7, Canada
 Telephone: +1-403-263-2255
 Fax: +1-403-264-3649

Europe/Africa/Russia
 Brodero Shaw
 A ShawCor Company
 Imperial Dock
 Leith, Edinburgh, EH6 7DT
 Scotland, UK
 Telephone: +44-131-533-9600
 Fax: +44-131-533-9699

Brodero Shaw Norway
 A ShawCor Company
 PO. Box 214
 N-7301 Oranger
 Norway
 Telephone: +47-72-46-60-60
 Fax: +47-72-46-60-70

Middle East
 Brodero Shaw
 A ShawCor Company
 PO. Box 1789,
 Suite 402, Al Raam Plaza
 Bahrain Corniche, Sharjah, U.A.E
 Telephone: +971-6-573-7374
 Fax: +971-6-573-7379

Asia Pacific
 Brodero Shaw
 A ShawCor Company
 101 Thomson Road
 #17-01/02 United Square
 Singapore 307591
 Telephone: +65-6732-2355
 Fax: +65-6732-9073

www.brederoshaw.com

PCS_AC_FBE_rev020

TYPICAL PRODUCT PROPERTIES

PROPERTY	FBE
Minimum Pipe Diameter	90 mm (3.5")
Maximum Pipe Diameter	1220 mm + (48" +)
Minimum Pipe Length	5.5 m (18')
Maximum Pipe Length	24.4 m (80')
Minimum Recommended Operating Temperature	-40°C (-40°F)
Maximum Recommended Operating Temperature	85°C (185°F)

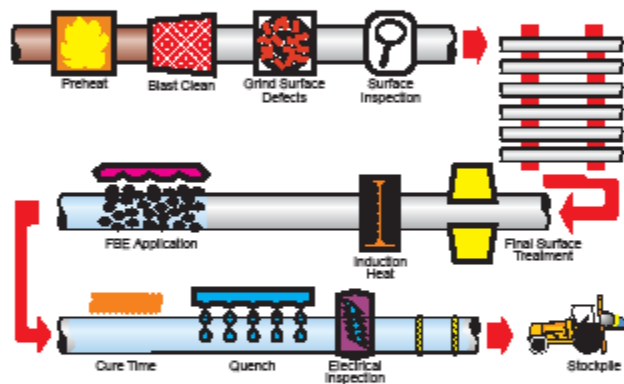
Values shown are typical and may vary from plant to plant. Consult Brodero Shaw for special requirements.

APPROVALS

- CSA Z245.20
- AWWA C 213
- AS3862:2002
- GAZ de France R 09
- GBE/CW 6
- NACE RP 0394
- NF A 49 706
- ISO 10080
- ISO 9001:2000



PRODUCT APPLICATION PROCESS



PLANTS

Camrose I, Camrose, Alberta	Montemey, Mexico	Ras Al Khaimah, UAE
Camrose II, Camrose, Alberta	Veracruz, Mexico	Rayong, Thailand
Regina, Saskatchewan	Belo Horizonte, Brazil	Kuantan, Malaysia
Portland, Oregon	Ellon, Scotland	Kabil, Batam Island, Indonesia
Fonsara, California	Leith, Scotland	Kembla Grange, Australia
Vineyard, Utah	Oranger, Norway	
Pearland, Texas	Jubail, Saudi Arabia	

BREDERO SHAW: THE GLOBAL LEADER IN PIPE COATING SOLUTIONS

Brodero Shaw is the world leader in pipe coating solutions, with more than 75 years of experience, over 27 pipe coating facilities on 6 continents and the largest team of technical and service specialists in the business. Brodero Shaw offers technologically advanced solutions for anti-corrosion coatings, protective and weight coatings, thermal flow assurance coatings, internal coatings, custom coatings and field joints for both onshore and offshore applications. This broad range of products and services provides Brodero Shaw with the unique capability to service the full spectrum of pipeline protection and flow assurance requirements. Consult your Brodero Shaw representative for your unique project requirements.

The information contained herein is indicative of the types of coatings provided by Brodero Shaw and is not intended to be a guarantee that a particular coating will be suitable for a given application. Since many unique environmental, operating, and design conditions must be considered, the user shall determine the suitability of the coating for the intended use and assume all the risks and liabilities in connection therewith. Brodero Shaw's liability is stated in our standard conditions of sale.

APPENDIX 3 – Shaw HPCC Product Data Sheet

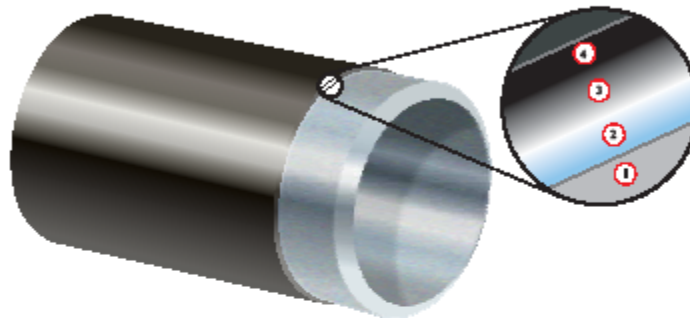


the
GLOBAL LEADER
 in pipe coating solutions.

HPCC

PRODUCT DATA SHEET

High Performance Composite Coating



1 Steel 2 FBE 3 FBE/Adhesive Interface 4 Polyethylene

- Small diameter pipe
- Large diameter pipe
- Wet Environments

PRODUCT DESCRIPTION

High Performance Composite Coating (HPCC) is an advanced composite system that represents the latest development in anti-corrosion systems. The product consists of fusion bonded epoxy, polyolefin adhesive and tough polyethylene.

HPCC is designed to protect buried oil and gas pipelines in environments where superior mechanical protection, moisture and corrosion resistance and high operating performance characteristics are required.

FEATURES AND BENEFITS

Long Term Corrosion Protection

The FBE component of HPCC provides excellent adhesion to steel, thereby providing superior long term corrosion resistance and protection of pipelines operating up to 85°C. The superior adhesion properties of the FBE also provides excellent resistance to cathodic disbondment which reduces the cost of cathodic protection during the operation of the pipeline.

Fused Monolithic Coating System

The unique application process of HPCC provides a fused, monolithic profile that prevents delamination and loss of adhesion. During construction, the system demonstrates excellent field handling and flexibility characteristics, thus minimizing construction installation costs.

Very Good Mechanical Protection

HPCC provides excellent uniform coverage of the weld bead profile, thus preventing "tenting" and weaknesses in the coating cross-section. The polyethylene component protects the

pipeline during transportation, thereby, reducing costly repairs while also providing added in-ground protection against shear forces, chemicals and abrasive soil conditions.

Flexible Solutions

Advanced manufacturing techniques allow the HPCC System to be customized to your specific project. The system can be applied to various pipe diameters from 400 mm (16") to over 1220 mm (48"). HPCC Systems can also be applied in a wide range of thicknesses to cost effectively meet unique project specifications and performance requirements.

Global Availability

Bredero Shaw has a network of 27 coating plants strategically located across 6 continents to minimize pipe transportation costs. HPCC can be manufactured in a single plant or in multiple coating plants to improve project logistics. High capacity within the Bredero Shaw plant network allows the client to benefit from single source advantages, ultimately providing more cost effective management of pipe coating needs.



www.brederoshaw.com



HPCC



Americas
 Bredero Shaw
 A ShawCor Company
 3838 N. Sam Houston Pkwy E.
 Suite 300
 Houston, Texas
 77032-3400 USA
 Telephone: +1-281-886-2350
 Fax: +1-281-886-2353

Shaw Pipe
 A ShawCor Company
 Two Executive Plaza
 1824 Crowchild Trail, N.W.,
 Calgary, Alberta
 T2M 3T7, Canada
 Telephone: +1-403-263-2255
 Fax: +1-403-264-3649

Europe/Africa/Russia
 Bredero Shaw
 A ShawCor Company
 Imperial Dock
 Leith, Edinburgh, EH6 7DT
 Scotland, UK
 Telephone: +44-131-553-9600
 Fax: +44-131-553-9699

Bredero Shaw Norway
 A ShawCor Company
 PO Box 214
 N-7301 Oranger
 Norway
 Telephone: +47-72-46-60-60
 Fax: +47-72-46-60-70

Middle East
 Bredero Shaw
 A ShawCor Company
 PO Box 1789
 Suite 402, Al Reem Plaza
 Bahrain Corniche, Sheikh, U.A.E
 Telephone: +971-6-573-7371
 Fax: +971-6-573-7379

Asia Pacific
 Bredero Shaw
 A ShawCor Company
 101 Thomson Road
 #17-01/02 United Square
 Singapore 307591
 Telephone: +65-6-732-2355
 Fax: +65-6-732-9073

www.brederoshaw.com

PCS_AC_HPCC_rev017

TYPICAL PRODUCT PROPERTIES

PROPERTY	HPCC
Minimum Pipe Diameter	400 mm (16")
Maximum Pipe Diameter	1220 mm + (48"+)
Minimum Pipe Length	18.3 m (60')
Maximum Pipe Length	24.4 m (80')
Minimum Recommended Operating Temperature	-40°C (-40°F)
Maximum Recommended Operating Temperature	85°C (185°F)

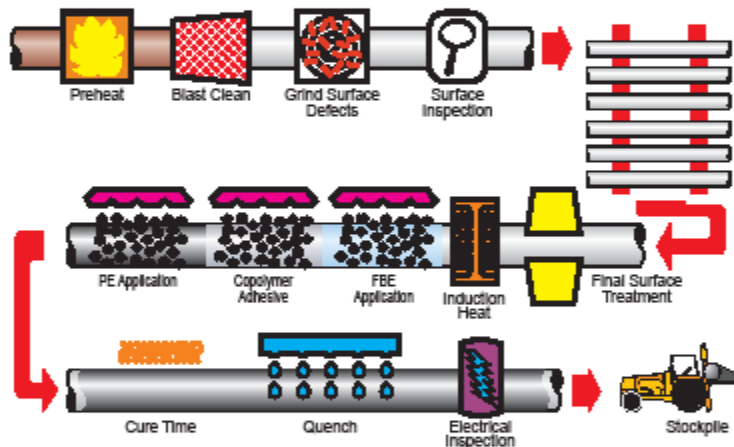
Values shown are typical and may vary from plant to plant. Consult Bredero Shaw for special requirements.

APPROVALS & QUALITY ASSURANCE



- CSA Z245.21-02 (System B2)

PRODUCT APPLICATION PROCESS



PLANTS

Camrose I, Camrose, Alberta	Jubail, Saudi Arabia (planned)
Regina, Saskatchewan	

BREDERO SHAW: THE GLOBAL LEADER IN PIPE COATING SOLUTIONS

Bredero Shaw is the world leader in pipe coating solutions, with more than 75 years of experience, over 27 pipe coating facilities on 6 continents and the largest team of technical and service specialists in the business. Bredero Shaw offers technologically advanced solutions for anti-corrosion coatings, protective and weight coatings, thermal flow assurance coatings, internal coatings, custom coatings and field joints for both onshore and offshore applications. This broad range of products and services provides Bredero Shaw with the unique capability to service the full spectrum of pipeline protection and flow assurance requirements. Consult your Bredero Shaw representative for your unique project requirements.

The information contained herein is indicative of the type of coating provided by Bredero Shaw and is not intended to be a guarantee that a particular coating will be suitable for a given application. Since many unique environmental, operating, and design conditions must be considered, the user shall determine the suitability of the coating for the intended use and assume all the risks and liabilities in connection therewith. Bredero Shaw's liability is stated in our standard conditions of sale.